UNIVERSITY OF CALIFORNIA SAN DIEGO

Investigation of *Para*-Substituted Benzoylferrocene Compounds as Photodynamic Anticancer Agents Through a Proposed Mechanism of Ferroptosis

A dissertation submitted in satisfaction of the
requirements for the degree Doctor of Philosophy

in

Chemistry

by

Pauline Michelle Olsen

Committee in charge:

Professor Joseph M. O'Connor
Professor Guy Bertrand
Professor William Fenical
Professor Charles Perrin
Professor Michael Sailor

2019

The Dissertation of Pauline Michelle Olsen is approved, and it is acceptable in quality and form for publication on microfilm and electronically:

_____

_____

_____

_____

_____
Chair

University of California San Diego

2019

DEDICATION

I would like to first and foremost thank my advisor Professor Joseph M. O'Connor. He has always had his doors open to talk about research and to welcoming to expanding my project past the scope of the lab. He has been a tremendous help for my research and success as a graduate student. I am incredibly thankful for all his support. I would also like my advisor for my master's work, Professor Guy Bertrand. I had an incredible experience in his lab. His lab grew my knowledge exponentially for synthetic chemistry and I enjoyed learning how to think about science from his perspective. I would also like to thank the rest of my committee Professors Charles Perrin, William Fenical, and Michael Sailor whose advice was invaluable during my time here. Additionally, I would like to thank my collaboration labs: Professors Robert Tukey and Kamil Godula. Without their support and incredible lab members I would have not been able to perform my research. I would especially like to thank Dr. Mia Huang who took the time to teach me all I know flow cytometry procedures. She continued to challenge and expand my knowledge of chemical biology and was essential in my success as a graduate student. I would also like to warmly thank Dr. Eva Rettenmeier and Dr. Elvira Mennillo of the Tukey lab their patience, knowledge and assistance were indispensable with all RT-qPCR and western blot data. I appreciated all their time and knowledge through-out my experience. They have been fantastic mentors and friends.

I would also like to thank my coworkers in the O'Connor lab both past and present in no particular order: Kate Veccharelli, Marissa Aubrey, Christina Huang, Pengjin Qin, Yifan Li, Han Steger, Li A Wang and Ryan Holland. I would also like to thank all my coworkers from the Bertrand lab for all their help. I would like to give a warm thank you to all my undergraduates I had the pleasure to mentor in research and all their hard work: Nargis Kiyam, Polin Ivanova, Andrea Gonzalez, Roberto Lean Baxin, and Jose Rizo. I would also like to thank the Figuroa and the Bertrand labs for all the support throughout graduate school, you are all fantastic scientists and people and appreciate for all our science discussions over coffee and lunch breaks.

I would also like to give a warm thank you and appreciation to all my friends I have made in graduate school. Without all your support and push I would not be where I am today. Last but not least I would like to thank my family for all their support through in my life and in graduate school.

EPIGRAPH

“I have not failed. I've just found 10,000 ways that won't work.”
- Thomas A. Edison**.**

“Progress is made by trial and failure; the failures are generally a hundred times more numerous than the successes ; yet they are usually left unchronicled.”
-William Ramsay

TABLE OF CONTENTS

LIST OF FIGURES

LIST OF SCHEMES

ACKNOWLEDGEMENTS

I would like to acknowledge Professor Joseph M. O'Connor for his support as the chair of my committee. I would also like to acknowledge the Tukey and Godula labs, without whom my research would have not been plausible to complete.

Chapter 2, in full, is currently being prepared for submission for publication of the material. Olsen, Pauline; Huang, Christina; Aubrey, Marissa; Chen, Wenfan; Melaimi, Mohand; O'Connor, Joseph. Dr. Christina and Dr. Marissa both completed some synthesis and characterization for this chapter. Dr. Mohammad completed the Cyclic Voltammetry of the compounds and Wenfan completed the two-photon laser setup and excitation. The dissertation author was the primary investigator and author of this material.

Chapter 5, in full, is currently being prepared for submission for publication of the material. Olsen, Pauline; Braddock, Alexander; O'Connor, Joseph. Alexander Braddock synthesized the material for the studies completed. The dissertation author was the primary investigator and author of this material.

Chapter 6, in full, is currently being prepared for submission for publication of the material. Olsen, Pauline; Qin, Pengjin; O'Connor, Joseph. Pengjin synthesized and characterized the material for the biological studies. The dissertation author was the primary investigator and author of this material.

Chapter 7, in full, is a reprint of the material as it appears in Angewandte Chemie International Edition 2017. Romero, Erik A.; Jazzar, Rodolphe; Solieilhavoup, Michele; Gembicky, Milan; Bertrand, Guy. Volume 56, page 4024-4027. The dissertation author was the secondary investigator and author of this paper.

VITA

2019 **PhD.** Chemistry. University of California, San Diego. La Jolla, California

2016 **M.S.** Chemistry. University of California, San Diego. La Jolla, California

2014 **B.S.** Biochemistry-Chemistry, University of California, Riverside. Riverside, California

Research

Professor Joseph O'Connor 2017-19

Synthesis and Cytotoxicity Mechanism of Photoactivated Metallocenes

Professor Guy Bertrand 2014-16

Synthesis and Activity of Carbene Stabilized Copper Hydride

Professor Jack F. Eichler 2011-14

Anticancer Activity of Gold (III) 2,9 Substituted Phenanthroline

Professor Catherine Larsen 2012-14

Gold (III) Pyridyl Quinoline Complexes and Binding Studies

Publications

Erik A. Romero, **Pauline M. Olsen**, Rodolphe Jazzar, Michele Soleilhavoup, Milan Gembicky, and Guy Bertrand. " Spectroscopic Evidence for a Monomeric Copper(I) Hydride and Crystallographic Characterization of a Monomeric Silver(I) Hydride" *Angew. Chem. Int. Ed.* **2017**, *56*, 4024-4027.

Edward M. Laguna, **Pauline M. Olsen**, Michael D. Sterling, Jack F. Eichler, Arnold L. Rheingold, and Catharine H. Larsen. "Structure and properties of neutral and cationic gold(III) complexes from substituted 2-(2'-pyridyl)quinoline ligands" *Inorg. Chem.,* **2014**, *53*, 12231-12233.

Pauline M. Olsen, Charles Ruiz, Daniel Lussier, Brian Khoa Le, Noah Angel, Michelle Smith, Chihyun (Brian) Hwang, Raneen Khatib, Julia Jenkins, Kaitlyn Adam, Jonathan Getcher, Fook Tham, Zhou (Georgia) Chen, Emma H. Wilson, Jack F. Eichler, "Synthesis, characterization, and anti tumor activity of unusual pseudo five coordinate gold(III) complexes: Distinct cytotoxic mechanism or expensive ligand delivery systems?" *J. Inorg. Biochem.*, **2014**, *141*, 121-131.

Chinar D. Sanghvi[1], **Pauline M. Olsen[1]**, Catherine Elix, Shifang Peng, Dongsheng Wang, Zhuo Chen, Dong M. Shin, Kenneth I. Hardcastle, Cora E. MacBetha, Jack F. Eichler, "Antitumor Properties of Five-Coordinate Gold (III) Complexes Bearing Substituted Polypyridyl Ligands" *J. Inorg. Biochem.*, **2013**, 128, 68-7

Teaching Experience

Teaching Assistant Positions

General Chemistry 6A	Fall	2014
General Chemistry Laboratory 7L	Winter	2015
General Chemistry 6C	Spring	2015
Biochemistry Laboratory 109	Winter	2016
General Chemistry 6C	Spring	2016
Organic Chemistry 140C	Summer	2016
General Chemistry Laboratory 7L	Winter	2017
Periodic Table– Head TA	Spring	2017
General Chemistry Laboratory 7L	Summer	2017
Periodic Table Chem 11	Fall	2017
Biochemistry Laboratory 109	Winter	2018
General Chemistry 6C	Spring	2018
General Chemistry Laboratory 7L	Summer	2018
General Chemistry 6B	Summer	2018
Periodic Table	Fall	2018
General Chemistry 6C	Summer	2019
Biochemical Structure and Function	Summer	2019

Teaching Associate

General Chemistry 6B	Winter	2019
General Chemistry 6B	Spring	2019

ABSTRACT OF THE DISSERTATION

Investigation of *Para*-Substituted Benzoylferrocene Compounds as Photodynamic Anticancer Agents Through a Proposed Mechanism of Ferroptosis

by

Pauline Michelle Olsen

Doctor of Philosophy in Chemistry

University of California San Diego, 2019

Professor Joseph M. O'Connor, Chair

Cisplatin, the first successful metallotherapy, has been utilized over the past four decades as chemotherapy treatment of a wide range of tumors. However, due to persistent side-effects and a buildup of platinum resistance in cancer cells, alternative metallotherapies have been sought after. Ferrocene is a promising scaffold alternative due to advantages such as cost, biologically stability, and as iron is a biologically relevant metal. Ferrocene compound Ferroquine, has been successful clinically as an anti-malarial compound, currently going through the third phase of clinical trial.

We have synthesized *para*-substituted benzoyferrocene derivatives that photochemically release free iron(II). Through the group of derivatives, we have optimized highly specific photodynamic therapy (PDT) compounds that induce no cytotoxicity in the dark but do after irradiation. It is hypothesized that the

observed cytotoxicity is due to the release of iron(II), which catalyzes the Fenton reaction, leading to the formation of toxic reactive oxygen species (ROS) in the cell. Through a series of *in vitro* experiments, we have reported that photolysis in cells incubated with 1,1`-bis(4-*n*-pentylbenzoyl)ferrocene leads to a dose-dependent increase in lipid peroxidation, suggesting ferroptosis as a mechanism of cell death. Additionally, we found that ferroptosis GPx4, SOD1, and VDAC are overexpressed after irradiation. Overall this work reports ferrocene derivatives function as highly specific PDT anti-cancer agents.

Chapter 1 Metals, Iron and Cancer First Generation of Metallotherapies

Cisplatin was discovered to be a potent anti-cancer therapy in the 1960s and has been clinically used as a chemotherapy for an overwhelming variety of cancer types. Because of this, other platinum metallotherapies were sought, including Carboplatin and Oxaliplatin.[1-4] They proved to be potent anticancer therapies.[3] Unfortunately, these compounds have decreased potency in some cancer cell lines due to platinum resistance and exhibit serious side effects due to heavy metal cytotoxicity. Because of this, other metals, such as iron due to its natural bioavailability, were sought as alternatives. [1]

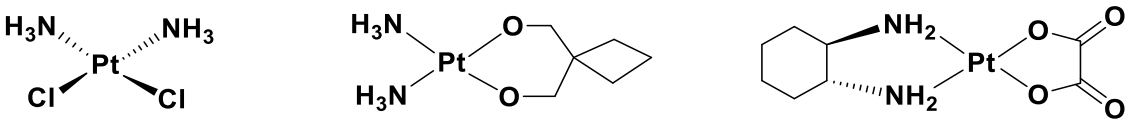

Cisplatin 1.1 **Carboplatin 1.2** **Oxaliplatin 1.3**

Figure 1.1: Successful cytotoxic platinum compounds

1.1 Iron homeostasis

Iron homeostasis is a highly regulated process in mammalian cells and when perturbed induces the formation of destructive radical species in the cell.[2, 3] The redox chemistry of iron is crucial for cell metabolism, proliferation, and growth.[4] However, iron's ability to gain and lose electrons can initiate a deadly positive-feedback loop from the generation of free radicals by the Fenton reaction (Figure 1.2). In this process, iron(II) is oxidized to iron(III) upon reacting with endogenous H_2O_2 to form reactive oxygen species (ROS) such as hydroxyl radical (•OH). These radicals can cause damage to lipids, proteins, and DNA and ultimately induce cell death.[5] The beneficial and deleterious effects of iron have given rise to increased research in an attempt to discover new metallotherapies to replace platinum-based drugs.[6]

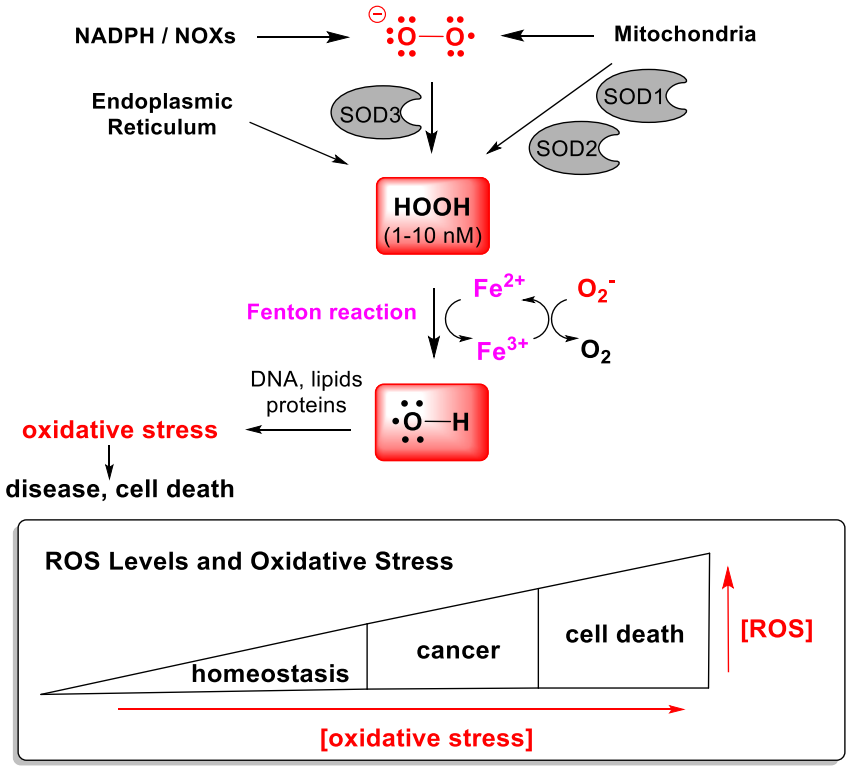

Figure 1.2: Iron disrupts cell homeostasis by increasing ROS concentration thereby inducing cell death via a positive feedback system. Adapted from Sies and Glasauer [7, 8]

1.2 Nanoparticle iron delivery systems

Iron encapsulated and iron oxide nanoparticles have been widely studied, with limited success, as potential drugs that may overload the cell with iron.[9-14] These agents induced the formation of ROS in both *in vitro* and *in vivo* studies. The Overholtzer group studied a ferroptosis-inducing nanoparticle whose potency resides in nutrient-deprived melanoma cancer cells that accumulate within the lysosomes.[12] Although both *in vitro* and *in vivo* studies showed promise, limitations include having to starve the cells and incubate with high concentrations of nanoparticles compared to concentrations used in previous clinically studied silica nanoparticles.[15] This process could be reversed through application of the ferroptosis inhibitor, liproxstatin-1, but to further become a drug candidate, modifications are needed in order to increase potency and induce cell death.

1.3 Brief background on photodynamic therapies

Photodynamic therapies began with Lipson and Baldes in the 1960s. [16] They reported a porphyrin mixture that would initiate fluorescence under ultraviolet light irradiation.[16] The Schwartz group studied a porphyrin mixture that had a higher affinity for tumors and more potent phototoxicity than crude hematoporphyrin.[17] Further optimization of the porphyrin system led to the first photodynamic therapy to be approved by the FDA, Photofrin® (**1.4**).[17-23] Photofrin® is the only PDT anticancer drug currently used today. It has been approved for esophageal cancer in the United States and is currently undergoing clinical trials for lung, head, and neck cancers.[24] It is activated at wavelengths 515 and 630 nm and has a cytotoxicity of 12.5 μM in HeLa cells.[25]

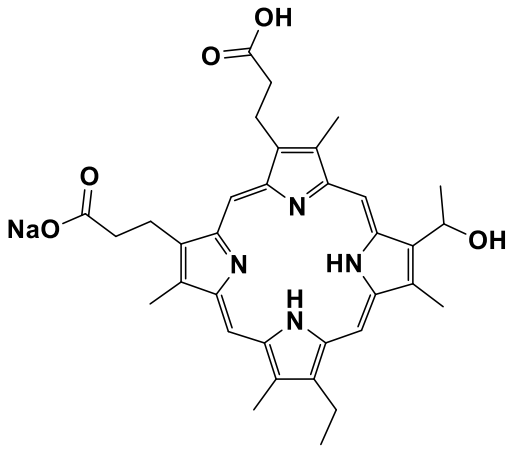

Photofrin® (Porfimer sodium)
1.4

Figure 1.3: Photofrin® is the first anticancer PDT used clinically

1.4 Previously Reported Biological Activity of Ferrocene and Ferricenium

1.4.1 Ferrocene and ferricenium toxicity.

Ferrocene (**1.5**) and ferricenium (**1.6**) anti-cancer cytotoxicity was studied in Ehrlich ascites tumor cells in 1984.[26] Ferricenium proved to be the more potent derivative for inducing DNA oxidation damage,

specifically as a DNA target from initiation of guanine oxidation, through the production of hydroxyl radicals under physiological conditions.[27, 28] However, ferricenium's Achilles heel as a potential therapy was its relative insolubility.[29] Investigations of ROS production in breast cancer cells, MCF7 and MCF10, found that ferricenium was cytotoxic. It was stated to be a great scaffold due to its stability and positive charge which would have improved specificity for cancer's negatively charged surface. [30, 31] Ferrocene did not display an inhibitory effect but did show potential because of its high lipophilicity which improved membrane permeability.[27, 28] Additionally, it was proposed that if the cell conditions were oxidizing due to a high concentration of H_2O_2, ferrocene could oxidize in the cell to produce cytotoxic ferricenium. Both ferrocene and ferrocenium have been reported to produced highly reactive oxygen species (ROS) that would exceed the capacity of the cellular antioxidant system and would be an excellent scaffold for drug design. [30]

1.4.2 Previously reported medicinal applications of ferrocene derivatives

Ferrocene has been widely used as an iron scaffold in drug design, due to its biological stability, electrochemical properties, and ease of membrane permeability due to its high lipophilic nature. [32-35] Because of this, a variety of medicinal applications have been reported, such as for potential treatment of human immunodeficiency virus (HIV), malaria, bacterial, and antifungal activity.[36-41]. Previously, it was observed that ferrocene and ferrocenyl moieties function as antitumor agents via disruption of iron homeostasis.[42, 43] To increase uptake, ferrocene derivatives of carbohydrates, proteins, nucleic acids, hormones, and selective endocrine modulators were tested as cancer targets.[31, 44, 45]

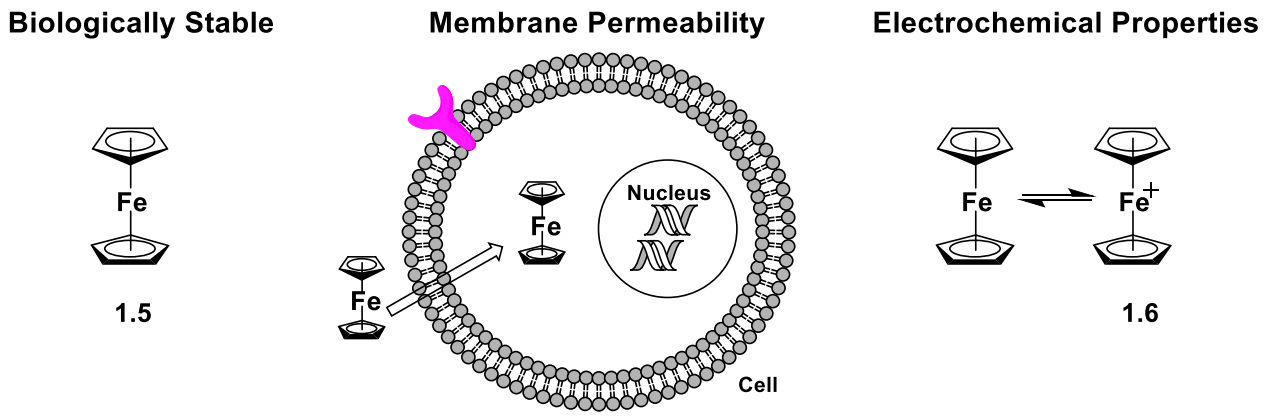

Figure 1.4: Ferrocene scaffold benefits for medicinal application

1.4.3 Ferrocene derivatives' toxicity

In 1997, the known antimalarial drug Chloroquine® was modified as a ferrocene derivative for potential antimalarial applications (Figure 1.5). [38, 39] A variety of substitutions and changes have shown success, which has led to the compound ferroquine (**1.7**) [46, 47]. Ferroquine displayed significant activity against chloroquine-resistant strains and was demonstrated to reduced the negative side effects of chloroquine.[37, 38, 48, 49] It was hypothesized that the introduction of lipophilic ferrocene would reduce the limited potency due to the basic properties of chloroquine which leds to the engulfment in acid food vacuoles of the plasmodia. This modification contributed to significant anti-plasmodia activity.[50] The addition of ferrous iron was proposed to reduce chloroquine resistance.[38] It is currently in Stage 3 as a therapy alone and additionally is being studied in a dual multi-drug stage 2 trial.[24]

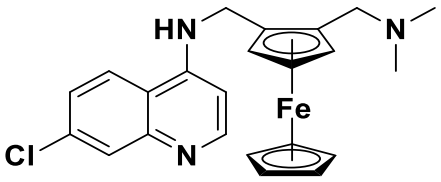

1.7

Figure 1.5: Ferroquine compound

1.4.4 Previously Reported Ferrocene PDT Studies

Photoactivated ferrocene derivatives have shown promise as anticancer drug candidates. The first generation of compounds incorporated phenanthroline (**1.8**) and polydentate terpyridine (**1.9** – **1.12**) ligands, as shown in Figure 1.6.[51, 52] Both types of compounds exhibited some efficacy as photodynamic therapies, as demonstrated by a difference in light and dark cytotoxicity. The phenanthroline derivative is activated by irradiation at 476 nm to 532 nm, and has dark and light cytotoxicity values of 33 μM and 13 μM, respectively, resulting in an efficacy (the difference of dark and light cytotoxicity) of 2.53. [51] Terpyridine derivatives were also reported to have limited success in cytotoxicity studies. Both the iron and cobalt derivatives proved to have no significant cytotoxicity up to 50 μM, while the copper derivative had light and dark cytotoxicities of 3.1 μM and 6.7 μM, respectively. The best cytotoxicity was with the zinc version which had 7.5 μM (light) and 49.1 μM (dark) cytotoxicity values, for an efficacy of 6.54.[52] All of the first generation complexes were reported to bind or cleave DNA through photoactivation.

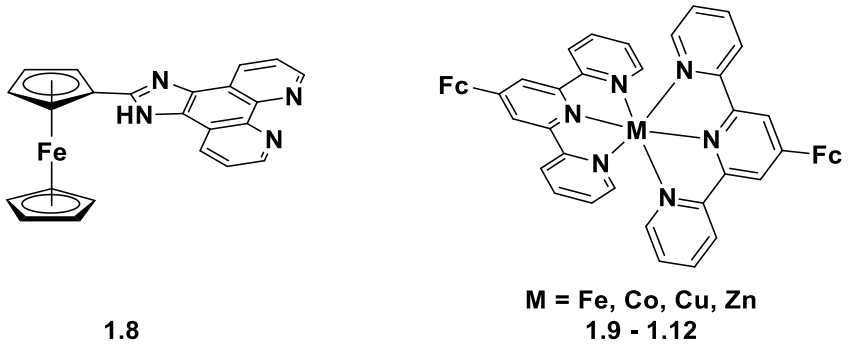

Figure 1.6: The first generation of photoactivated ferrocene compound

The second-generation of ferrocene PDT was an altered terpyridine derivative with a platinum addition (**1.13**; Figure 1.7).[53] It has displayed PDT cytotoxicity in BT474, invasive ductal carcinoma of the breast, with a light cytotoxicity of 7.7 μM and dark cytotoxicity higher than tested at 50 μM, which is improved from the first generation of terpyridine complexes with efficacy greater than 6.50. The complex was additionally tested in the HBL-100 cell line and reported to have limited irradiation cytotoxicity of 45.2 μM in the dark and again over 50 μM. Unsurprisingly, with platinum and the polydentate terpyridine ligand,

it was reported to bind DNA binding and cleavage and increase cytosolic ROS. This derivative proved to have promise as a PDT therapy with increase specificity but limited cell line cytotoxic versatility.

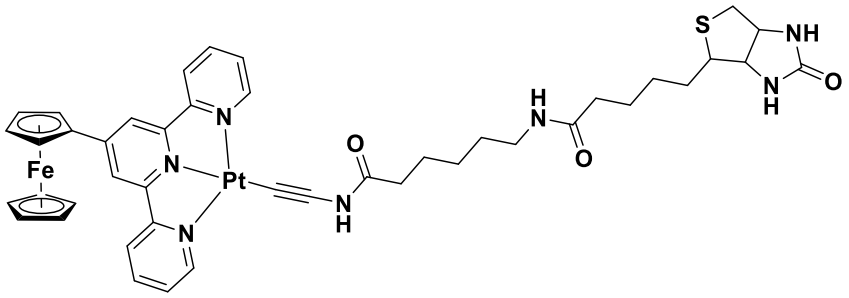

1.13

Figure 1.7: The second generation of a photodynamic platinum ferrocene derivative

Both ferrocene generations displayed promise and anticancer compounds. Due to the success of these future generations of ferrocene compounds should be synthesized. The next generation of ferrocene anticancer compounds should shift cell death induction to induction of ROS chemistry rather than DNA damage as this is differing the mechanism from platinum drugs.

1.5 Chapter 1 References

1. Cleare, M.J., *Transition meta* Cleare, M. J., Transition metal complexes in cancer chemotherapy. *Coordination Chemistry Reviews* **1974,** *12* (4), 349-405.

2. Conrad, M. E.; Umbreit, J. N.; Moore, E. G., Iron Absorption and Transport. *The American Journal of the Medical Sciences* **1999,** *318* (4), 213-229.

3. Philpott, C. C.; Ryu, M.-S., Special delivery: distributing iron in the cytosol of mammalian cells. *Frontiers in Pharmacology* **2014,** *5* (173).

4. Torti, S. V.; Torti, F. M., Iron and cancer: more ore to be mined. *Nature reviews. Cancer* **2013,** *13* (5), 342-355.

5. Halliwell, B.; Clement, M. V.; Long, L. H., Hydrogen peroxide in the human body. *FEBS Letters* **2000,** *486* (1), 10-13.

6. Shen, D.-W.; Pouliot, L. M.; Hall, M. D.; Gottesman, M. M., Cisplatin resistance: a cellular self-defense mechanism resulting from multiple epigenetic and genetic changes. *Pharmacological reviews* **2012,** *64* (3), 706-721.

7. Glasauer, A.; Chandel, N. S., Targeting antioxidants for cancer therapy. *Biochem Pharmacol* **2014,** *92* (1), 90-101.

8. Sies, H., Hydrogen peroxide as a central redox signaling molecule in physiological oxidative stress: Oxidative eustress. *Redox Biol* **2017,** *11*, 613-619.

9. Gonzales, M.; Mitsumori, L. M.; Kushleika, J. V.; Rosenfeld, M. E.; Krishnan, K. M., Cytotoxicity of iron oxide nanoparticles made from the thermal decomposition of organometallics and aqueous phase transfer with Pluronic F127. *Contrast Media Mol Imaging* **2010,** *5* (5), 286-293.

10. Wu, Y.-N.; Yang, L.-X.; Shi, X.-Y.; Li, I. C.; Biazik, J. M.; Ratinac, K. R.; Chen, D.-H.; Thordarson, P.; Shieh, D.-B.; Braet, F., The selective growth inhibition of oral cancer by iron core-gold shell nanoparticles through mitochondria-mediated autophagy. *Biomaterials* **2011,** *32* (20), 4565-4573.

11. Khan, M. I.; Mohammad, A.; Patil, G.; Naqvi, S. A.; Chauhan, L. K.; Ahmad, I., Induction of ROS, mitochondrial damage and autophagy in lung epithelial cancer cells by iron oxide nanoparticles. *Biomaterials* **2012,** *33* (5), 1477-88.

12. Kim, S. E.; Zhang, L.; Ma, K.; Riegman, M.; Chen, F.; Ingold, I.; Conrad, M.; Turker, M. Z.; Gao, M.; Jiang, X.; Monette, S.; Pauliah, M.; Gonen, M.; Zanzonico, P.; Quinn, T.; Wiesner, U.; Bradbury, M. S.; Overholtzer, M., Ultrasmall nanoparticles induce ferroptosis in nutrient-deprived cancer cells and suppress tumour growth. *Nat Nanotechnol* **2016,** *11* (11), 977-985.

13. Wei, Y.; Zhao, M.; Yang, F.; Mao, Y.; Xie, H.; Zhou, Q., Iron overload by Superparamagnetic Iron Oxide Nanoparticles is a High Risk Factor in Cirrhosis by a Systems Toxicology Assessment. *Scientific reports* **2016,** *6*, 29110-29110.

14. Ding, Y.; Wan, J.; Zhang, Z.; Wang, F.; Guo, J.; Wang, C., Localized Fe(II)-Induced Cytotoxic Reactive Oxygen Species Generating Nanosystem for Enhanced Anticancer Therapy. *ACS Appl Mater Interfaces* **2018,** *10* (5), 4439-4449.

15. Phillips, E.; Penate-Medina, O.; Zanzonico, P. B.; Carvajal, R. D.; Mohan, P.; Ye, Y.; Humm, J.; Gönen, M.; Kalaigian, H.; Schöder, H.; Strauss, H. W.; Larson, S. M.; Wiesner, U.; Bradbury, M. S., Clinical translation of an ultrasmall inorganic optical-PET imaging nanoparticle probe. *Science Translational Medicine* **2014,** *6* (260), 260ra149-260ra149.

16. Lipson, R. L.; Baldes, E. J.; Olsen, A. M., Hematoporphyrin derivative: a new aid for endoscopic detection of malignant disease. *J Thorac Cardiovasc Surg* **1961,** *42*, 623-629.

17. Dougherty, T.; Henderson, B.; Schwartz, S.; Winkelman, J.; Lipson, R., Historical perspective in photodynamic therapy. *Photodynamic Therapy* **1992**, 1-18.

18. Dougherty, T. J.; Gomer, C. J.; Henderson, B. W.; Jori, G.; Kessel, D.; Korbelik, M.; Moan, J.; Peng, Q., Photodynamic therapy. *JNCI: Journal of the national cancer institute* **1998,** *90* (12), 889-905.

19. Dougherty, T. J.; Lawrence, G.; Kaufman, J. H.; Boyle, D.; Weishaupt, K. R.; Goldfarb, A., Photoradiation in the treatment of recurrent breast carcinoma. *Journal of the National Cancer Institute* **1979,** *62* (2), 231-237.

20. Dougherty, T. J.; Kaufman, J. E.; Goldfarb, A.; Weishaupt, K. R.; Boyle, D.; Mittleman, A., Photoradiation therapy for the treatment of malignant 9. Kelly, JF, and Snell, ME Hematoporphyrin Derivative: a Possible Aid in tumors. *Cancer Res* **1978,** *38*, 2628-2635.

21. Dougherty, T. J.; Grindey, G.; Fiel, R.; Weishaupt, K. R.; Boyle, D., Photoradiation therapy. II. Cure of animal tumors with hematoporphyrin and light. *Journal of the National Cancer Institute* **1975,** *55* (1), 115-121.

22. Dougherty, T. J.; Grindey, G. B.; Fiel, R.; Weishaupt, K. R.; Boyle, D. G., Photoradiation Therapy. II. Cure of Animal Tumors With Hematoporphyrin and Light23. *JNCI: Journal of the National Cancer Institute* **1975,** *55* (1), 115-121.

23. Dougherty, T. J., A brief history of clinical photodynamic therapy development at Roswell Park Cancer Institute. *J Clin Laser Med* **1996,** *14*, 219-21.

24. Medicine, N. U. S. N. L. o. ClinicalTrials.gov. https://clinicaltrials.gov/ct2/home.

25. Yuichi Miyamoto, Y. Y. a. H. T., Effects of Photofrin-mediated photodynamic treatment on sensitivity to cisplatin in HeLa cells and the resistant subline. *The 16th International Conference on Biomedical Engineering* **2017,** *61*, 13-15.

26. Köpf-Maier, P.; Köpf, H.; Neuse, E. W., Ferricenium complexes: A new type of water-soluble antitumor agent. *Journal of Cancer Research and Clinical Oncology* **1984,** *108* (3), 336-340.

27. Tabbi, G.; Cassino, C.; Cavigiolio, G.; Colangelo, D.; Ghiglia, A.; Viano, I.; Osella, D., Water stability and cytotoxic activity relationship of a series of ferrocenium derivatives. ESR insights on the radical production during the degradation process. *J Med Chem* **2002,** *45* (26), 5786-96.

28. Osella, D.; Mahboobi, H.; Colangelo, D.; Cavigiolio, G.; Vessières, A.; Jaouen, G., FACS analysis of oxidative stress induced on tumour cells by SERMs. *Inorganica Chimica Acta* **2005,** *358* (6), 1993-1998.

29. Osella, D.; Ferrali, M.; Zanello, P.; Laschi, F.; Fontani, M.; Nervi, C.; Cavigiolio, G., On the mechanism of the antitumor activity of ferrocenium derivatives. *Inorganica Chimica Acta* **2000,** *306* (1), 42-48.

30. Acevedo-Morantes, C. Y.; Melendez, E.; Singh, S. P.; Ramirez-Vik, J. E., Cytotoxicity and Reactive Oxygen Species Generated by Ferrocenium and Ferrocene on MCF7 and MCF10A Cell Lines. *J Cancer Sci Ther* **2012,** *04* (09), 271-275.

31. Wang T; Wan P; L, M., Synthesis and Characterization of Alkoxy and Phenoxy-substituted Ferrocenium Salt Cationic Photoinitiators. *Chinese J Chem Eng* **2006,** *14*, 806-9.

32. Hansch, C.; Leo, A., *Substitution Constants for Correlation Analysis in Chemistry and Biology*. New York, 1979.

33. Hanzlik, R. P.; Soine, W. H., Enzymic hydroxylation of ferrocene. *Journal of the American Chemical Society* **1978,** *100* (4), 1290-1291.

34. Nielsen, P.; Heinrich, H. C., Metabolism of iron from (3,5,5-trimethylhexanoyl) ferrocene in rats: A dietary model for severe iron overload. *Biochemical Pharmacology* **1993,** *45* (2), 385-391.

35. Swarts, J. C.; Neuse, E. W.; Lamprecht, G. J., Synthesis and characterization of water-soluble polyaspartamide-ferrocene conjugates for biomedical applications. *Journal of Inorganic and Organometallic Polymers* **1994,** *4* (2), 143-153.

36. Fouda, M. F. R.; Abd-Elzaher, M. M.; Abdelsamaia, R. A.; Labib, A. A., On the medicinal chemistry of ferrocene. *Applied Organometallic Chemistry* **2007,** *21* (8), 613-625.

37. Biot, C.; Glorian, G.; Maciejewski, L. A.; Brocard, J. S.; Domarle, O.; Blampain, G.; Millet, P.; Georges, A. J.; Abessolo, H.; Dive, D.; Lebibi, J., Synthesis and Antimalarial Activity in Vitro and in Vivo of a New Ferrocene−Chloroquine Analogue. *Journal of Medicinal Chemistry* **1997,** *40* (23), 3715-3718.

38. Domarle, O.; Blampain, G.; Agnaniet, H.; Nzadiyabi, T.; Lebibi, J.; Brocard, J.; Maciejewski, L.; Biot, C.; Georges, A. J.; Millet, P., In vitro antimalarial activity of a new organometallic analog, ferrocene-chloroquine. *Antimicrobial agents and chemotherapy* **1998,** *42* (3), 540-544.

39. Dive, D.; Biot, C., Ferrocene conjugates of chloroquine and other antimalarials: the development of ferroquine, a new antimalarial. *ChemMedChem* **2008,** *3* (3), 383-91.

40. Biot, C.; François, N.; Maciejewski, L.; Brocard, J.; Poulain, D., Synthesis and antifungal activity of a ferrocene–fluconazole analogue. *Bioorganic & Medicinal Chemistry Letters* **2000,** *10* (8), 839-841.

41. Zhang, J., Preparation, characterization, crystal structure and bioactivity determination of ferrocenyl–thiazoleacylhydrazones. *Applied Organometallic Chemistry* **2008,** *22* (1), 6-11.

42. Ornelas, C., Application of ferrocene and its derivatives in cancer research. *New Journal of Chemistry* **2011,** *35* (10).

43. Kinski, E.; Marzenell, P.; Hofer, W.; Hagen, H.; Raskatov, J. A.; Knaup, K. X.; Zolnhofer, E. M.; Meyer, K.; Mokhir, A., 4-Azidobenzyl ferrocenylcarbamate as an anticancer prodrug activated under reductive conditions. *J Inorg Biochem* **2016,** *160*, 218-24.

44. Top, S.; Vessières, A.; Leclercq, G.; Quivy, J.; Tang, J.; Vaissermann, J.; Huché, M.; Jaouen, G., Synthesis, Biochemical Properties and Molecular Modelling Studies of Organometallic Specific Estrogen Receptor Modulators (SERMs), the Ferrocifens and Hydroxyferrocifens: Evidence for an Antiproliferative Effect of Hydroxyferrocifens on both Hormone-Dependent and Hormone-Independent Breast Cancer Cell Lines. *Chemistry – A European Journal* **2003,** *9* (21), 5223-5236.

45. Gao, L. M.; Hernández, R.; Matta, J.; Meléndez, E., Synthesis, structure, electrochemistry, and cytotoxic properties of ferrocenyl ester derivatives. *Met Based Drugs* **2009,** *2009*, 420784-420784.

46. Biot, C.; Delhaes, L.; N'Diaye, C. M.; Maciejewski, L. A.; Camus, D.; Dive, D.; Brocard, J. S., Synthesis and antimalarial activity in vitro of potential metabolites of ferrochloroquine and related compounds. *Bioorganic & Medicinal Chemistry* **1999,** *7* (12), 2843-2847.

47. Wani, W. A.; Jameel, E.; Baig, U.; Mumtazuddin, S.; Hun, L. T., Ferroquine and its derivatives: New generation of antimalarial agents. *European Journal of Medicinal Chemistry* **2015,** *101*, 534-551.

48. Delhaes, L.; Abessolo, H.; Biot, C.; Berry, L.; Delcourt, P.; Maciejewski, L.; Brocard, J.; Camus, D.; Dive, D., In vitro and in vivo antimalarial activity of ferrochloroquine, a ferrocenyl analogue of chloroquine against chloroquine-resistant malaria parasites. *Parasitology Research* **2001,** *87* (3), 239-244.

49. Atteke, C.; Ndong, J. M. M.; Aubouy, A.; Maciejewski, L.; Brocard, J.; Lébibi, J.; Deloron, P., In vitro susceptibility to a new antimalarial organometallic analogue, ferroquine, of Plasmodium falciparum isolates from the Haut-Ogooué region of Gabon. *Journal of Antimicrobial Chemotherapy* **2003,** *51* (4), 1021-1024.

50. Tilley, L.; Loria, P.; Foley, M., *Chloroquine and other quinoline antimalarials, in Antimalarial Chemotherapy: Mechanism of Action, Resistance and New Directions in Drug Discovery*. Humana Press: NJ, 2001.

51. Maity, B.; Chakravarthi, B. V. S. K.; Roy, M.; Karande, A. A.; Chakravarty, A. R., DNA Photocleavage and Cytotoxic Properties of Ferrocene Conjugates. *European Journal of Inorganic Chemistry* **2011,** *2011* (9), 1379-1386.

52. Maity, B.; Sudarshan Gadadhar; Tridib K. Goswami; Karande, A. A.; Chakravarty, A. R., Impact of metal on the DNA photocleavage activity and cytotoxicity of ferrocenyl terpyridine 3d metal complexes. *Dalton Trans.* **2011,** *40*, 11904.

53. Mitra, K.; Shettar, A.; Kondaiah, P.; Chakravarty, A. R., Biotinylated Platinum(II) Ferrocenylterpyridine Complexes for Targeted Photoinduced Cytotoxicity. *Inorg Chem* **2016,** *55* (11), 5612-22.

Chapter 2 Photochemical Studies on Synthetic and Photochemical Studies on Benzoylferrocene Derivatives

2.1 Synthesis of 1-benzoylferrocene and 1,1′-dibenzoylferrocene derivatives

The first synthesis of benzoylferrocene, published in 1956 by German chemists Hiemsehneider and Helm, involved a Friedel-Crafts acylation of ferrocene.[54] The Friedel-Crafts acylation involved electrophilic aromatic substitution of the cyclopentadienyl ligand with benzoyl chloride in the presence of $AlCl_3$. Soon after, a related synthesis of 1,1′-dibenzoylferrocene was reported by Vogel and Rosenburg. [55, 56]

Utilized the Friedel-Crafts acylation approach for the synthesis of new 1-benzoylferrocene derivatives, as shown in Scheme 2.1. This synthesis had successfully created a variety of *para*-substituted benzoylferrocene complexes, as shown in Figure 2.1. To add to the library, the mono-substituted benzoylferrocene phosphonium derivative **2.3** was synthesized from a Finkelstein reaction with compound **2.2** and NaI in acetone, followed by reaction with triphenylphosphine to produce **2.7 (**Scheme 2.2).

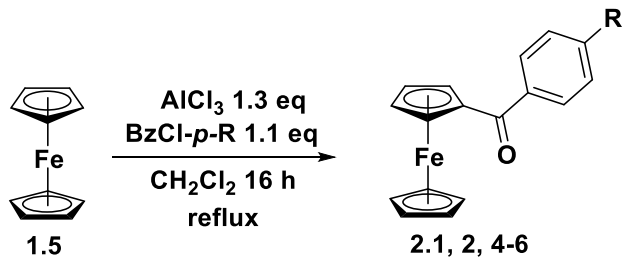

R = H, methyl, chloromethyl, ethyl, *n*-butyl, *n*-pentyl

Scheme 2.1: Friedel-Crafts acylation of ferrocene to synthesize benzoylferrocene derivatives

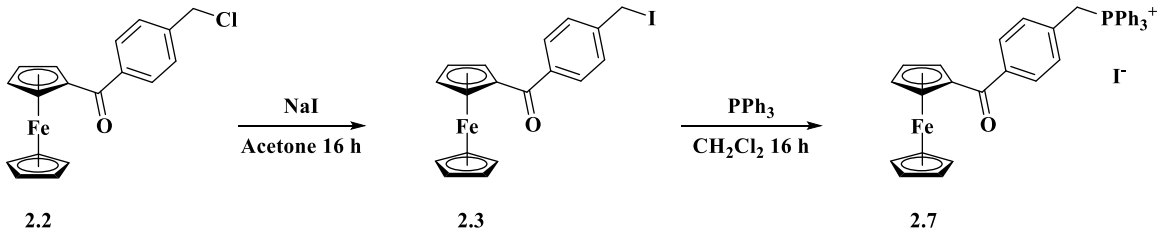

2.2 2.3 2.7

Scheme 2.2: Finkelstein or Halex reaction for the generation of 2.3 and proceeding reaction for synthesis of complex 2.7

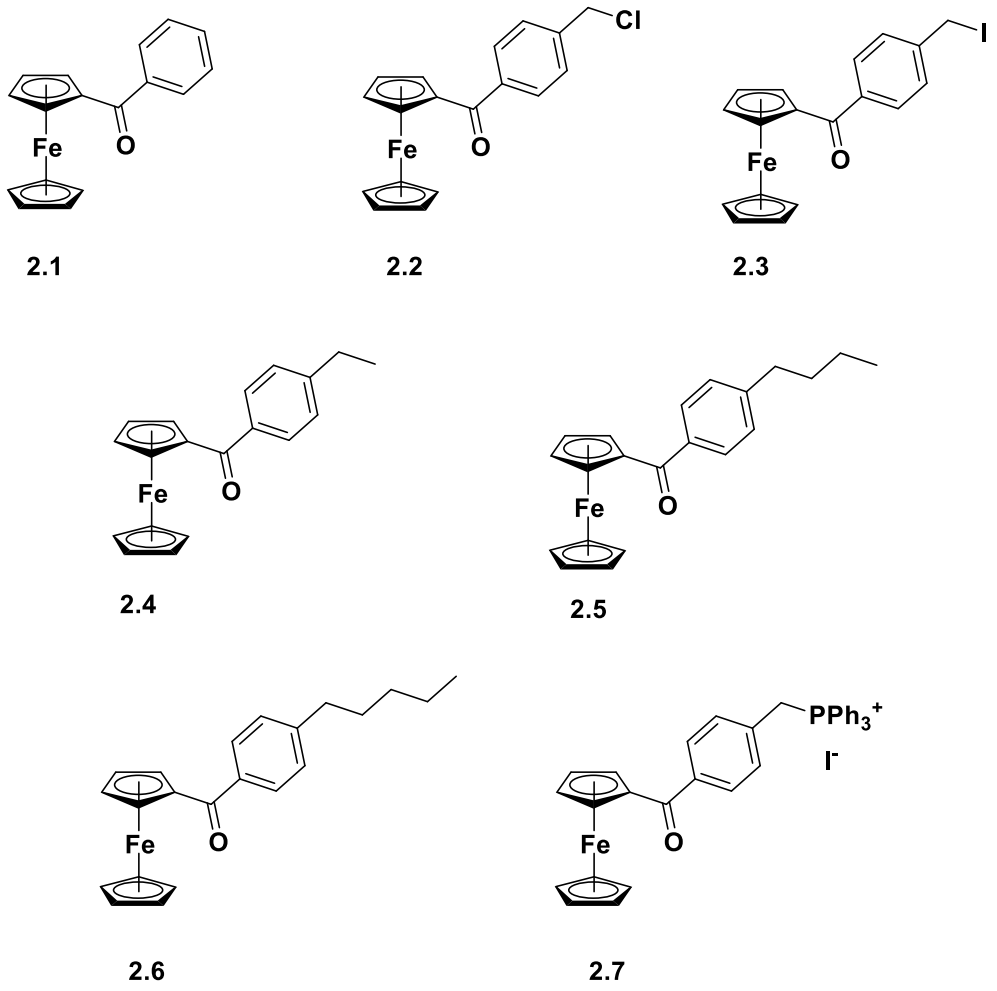

2.1 2.2 2.3

2.4 2.5

2.6 2.7

Figure 2.1: New and previously reported mono-substituted derivatives utilized in the studies described herein

Similar approaches were used to synthesize 1,1′-dibenzoylferrocene derivatives. Differences include heating the Friedel-Crafts reaction to reflux for 72 hours (Scheme 2.3). Both mono-substituted and di-substituted derivatives were synthesized successfully, Figure 2.2. These compounds were synthesized to

study *in vitro* as potential anticancer compounds. *Para*-substituents of variable lipophilicity and a phosphonium ion targeting group were prepared in order to increase potency and localization (Scheme 2.4).

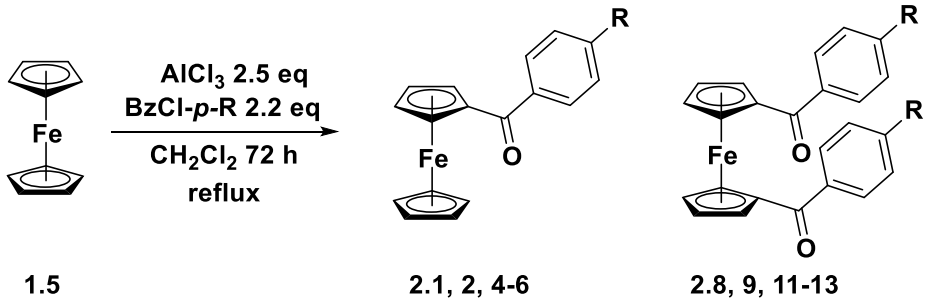

Scheme 2.3: Synthesis of benzoylferrocene and 1,1′-dibenzoylferrocene by Friedal Craft Acylation

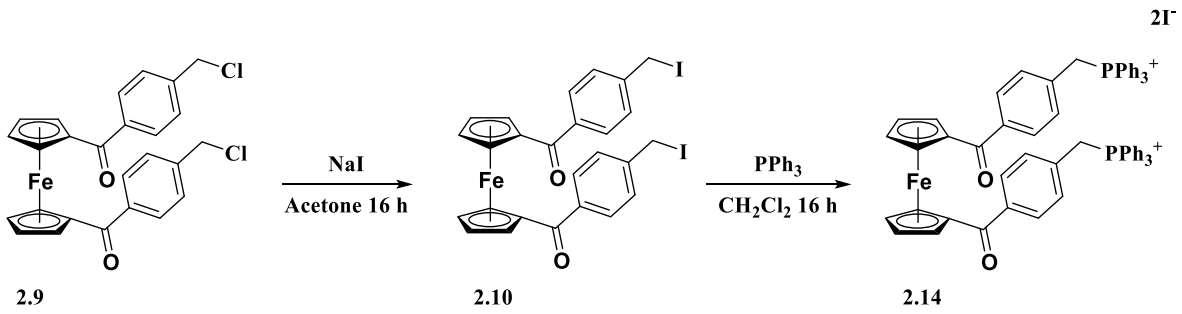

Scheme 2.4: Finkelstein or Halex reaction for the generation of 2.10 and proceeding reaction for synthesis of complex 2.14

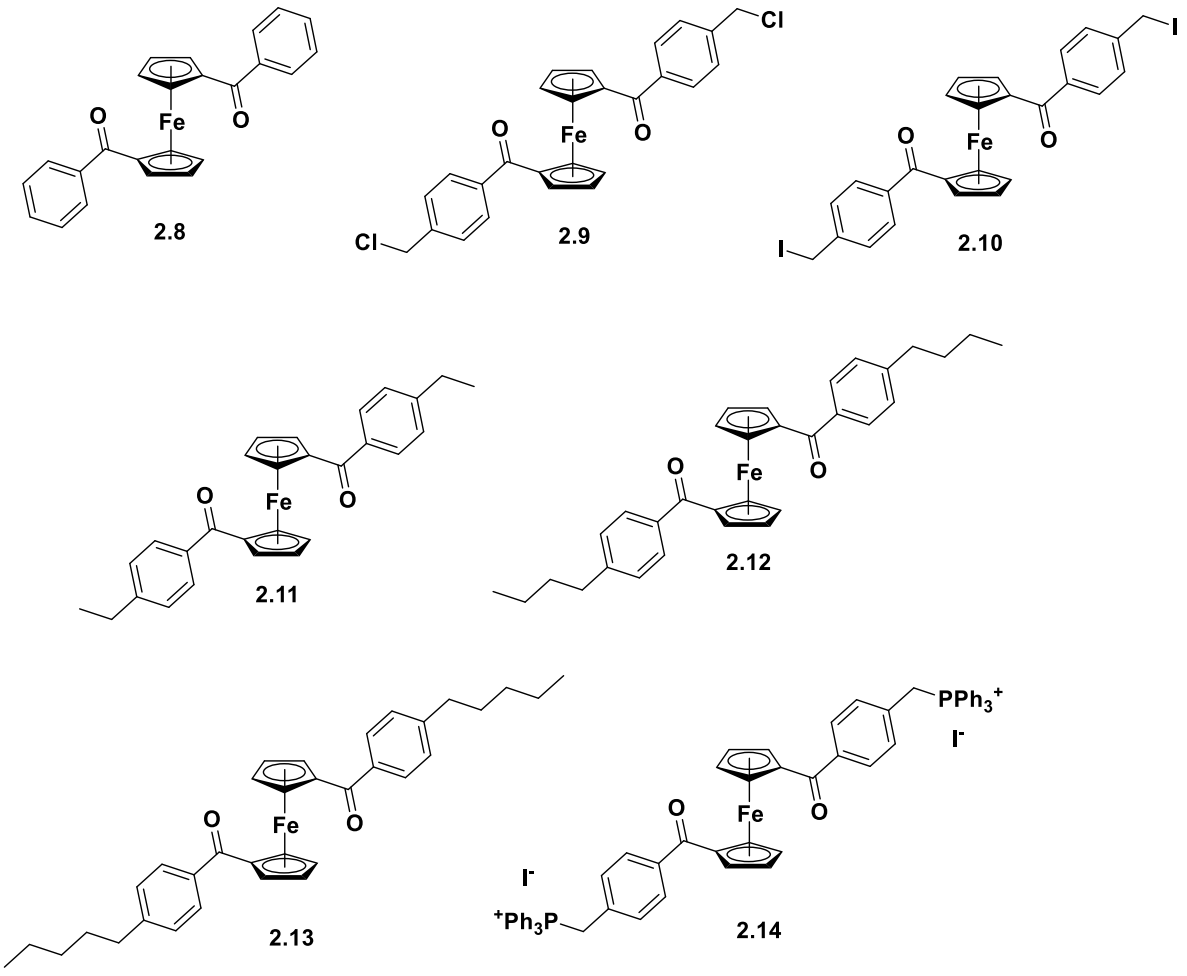

Figure 2.2: New and previously reported bis-substituted derivatives in the studies described herein

2.2 Cyclic Voltammetry of ferrocene derivatives

In a continued collaboration with Dr. Mohand Melaimi of the Bertrand lab at University of California San Diego, cyclic voltammetry (CV) data was collected. These studies were completed to fully characterized these 1-benzoylferrocenes and 1,1′-dibenzoyl ferrocenes derivatives for comparison to previous literature and future biological studies (*vide infra*, chapters 3 and 4). The scans were done in acetonitrile with added tetrabutylammonium hexafluorophosphate (0.1 M) as the electrolyte, with the scan initiated in the positive potential direction. Potentials were then calibrated to ferrocene versus ferricenium as an internal standard. Only one chemically reversible wave was detected for each complex.

Compound	$E_{1/2}$ (V)
2.6	0.251
2.5	0.299
2.4	0.300
2.1	0.250
2.13	0.441
2.11	0.502
2.9	0.474
2.8	0.462

Figure 2.3: Cyclic voltammetry of benzoylferrocene and 1,1′-dibenzoylferrocene derivatives

The positive potentials of the mono-substituted benzoyl ferrocenes was around half that of the 1,1`-dibenzoyl ferrocene derivatives. The higher difference of the bis-substituted ferrocenes is suggested due to the increased oxidative stability of the iron(II) center from the addition of two electron withdrawing benzoylferrocene functional groups. This is hypothesized to be an essential to describe the differences in the cytotoxicity behavior of the assortment of derivatives. The more robust the compounds in oxidative behavior could provide more stability in the cell environments that has oxidative and reductive potentials. This could be essential for reducing the dark cytotoxicity in the cell and provide a more specific and effective anticancer compound.

2.3 Previously Reported Studies on Benzoylferrocene Photoactivity

Since late 1960, benzoylferrocene derivatives have been known to release free iron(II) upon exposure to visible light.[57-59] Ferrocene itself is photo-inert upon exposure to either ultraviolet or sunlight in methanol for up to 15 hours.[59, 60] However, derivatives with a carbonyl group conjugated to the ferrocene ring rapidly decompose upon exposure to visible light.[57] At the time, the reactivity was attributed to metal to ligand charge transfer, followed by solvent-assisted oxidation of the sandwich complex. Isolation of the primary photoproduct proved to be difficult due to its reactivity toward oxygen, light, and heat in wet DMSO. An IR spectrum (solvent) obtained on the crude reaction mixture that resulted from photolysis of benzoylferrocene, exhibited absorption bands at 1538 and 1350 cm^{-1}, leading the authors to suggest the initial solvation of the carbonyl followed by cyclopentadienyl iron ring cleavage. The isolation of both

benzoic acid and cyclopentadiene adducts from the crude reaction mixture further supported this conclusion.[58]

More recently, ESI-MS analysis of a photolyzed benzoylferrocene reaction mixture provided evidence for free cyclopentadiene and benzoylcyclopentadiene.[61] Treatment of an irradiated solution of benzoylferrecene with 2,2′-bipyridine produced a red solution of $Fe(biby)_3^{2+}$.[61]Free iron(II) was detected by colorimetric analysis of the reaction of benzoylferrocene with 2,2′-bipyridine (bipy) to form a $Fe(biby)_3^{2+}$ complex.[59] The photodecomposition of benzoylferrocene was attributed to a low-lying metal to ligand charge transfer (MLCT) excited state where the benzoylcyclopentadienyl is labial by the substituted cyclopentadiene ring slipping η^5 to η^4, leaving an open coordination site and a formal positive charge on the iron, making the metal center susceptible to nucleophilic attack by the solvent. This intermediate can expel solvent to re-form the sandwich complex or continue ligand substitutions to ultimately give free iron(II) by the mechanism shown in Scheme 2.4. Kutal and coworkers proposed that 2-*H* goes to excited state III-η^4. We propose this could also go through a III- η^6 excited state. Kutal subsequently proposed intermediate IV- η^3-A forming in one of his latest papers. It may well be IV- η^3-B instead, since the non-coordinated double bond is conjugated and therefore stabilized. The following of the ring slippage we proposed is due to the complete solubilaztion of iron(II).

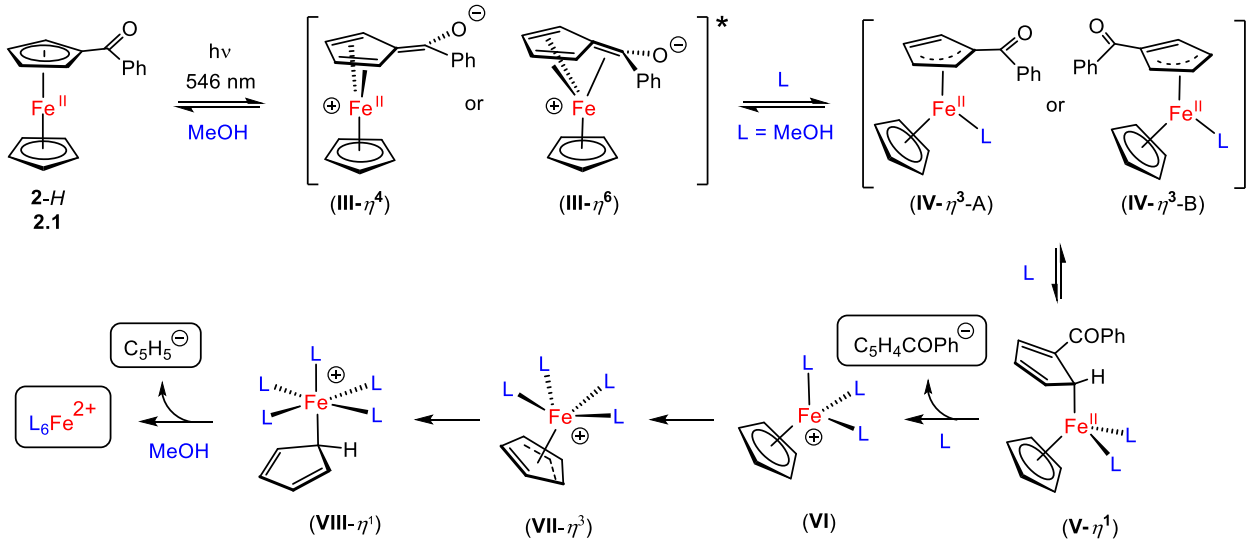

Scheme 2.5: Proposed mechanism of photochemical dissociation by Kutal

As the 1-benzoylferrocene and 1,1′-dibenzoylferrocene have been studied extensively and demonstrated to readily release iron(II) into the solution, it was hypothesized that these compounds could be photoactivated for release of iron(II) in a cell. This could lead to a new and promising mechanism for inducing iron overload in biological environments, with a degree of specificity in cases where targeting groups are present in the organoiron agent.

2.4 1-Benzoylferrocene and 1,1′-Dibenzoylferrocene Photoactivity Studies in Aqueous Solutions

2.4.1 Photoactivation of compound $CpFe(C_5H_4(C{=}O)C_6H_5C_5H_{11})$ 2.6 and $Fe(C_5H_4(C{=}OC_6H_5)C_5H_{11})_2$ 2.13

Photolysis reactions of 1-benzoylferrocenes and 1,1′-dibenzoylferrocenes have never been reported from a solution that would mimic that of the cell, as ferrocene is not readily soluble in water. By studying these compounds in solutions that would most mimic what would be introduced and incubated to the cell, there could be a better understanding of its reactivity in these conditions. To overcome solubility, the benzoylferrocene derivatives were dissolved in DMSO followed by dilution with water. To understand the

influence of the cell environment, photolyses of **2.6** and **2.13** were performed in the presence of 2,2′-bipyridine and the reaction progress was followed by UV-Vis spectroscopy, as previously reported. [59, 62] The solution was composed of $CpFe(C_5H_4(C{=}O)C_6H_5C_5H_{11})$ **2.6** (0.25 mM, H_2O/DMSO) with the addition of 2,2′-bipyridine (bipy, 3 equiv.) in a deoxygenated Millipore water and 0.75% DMSO solution. The solution was photolyzed (> 450 nm) in a quartz cuvette in the absence of oxygen and data was collected at intervals of 10 seconds. Results are presented in **Figures 2.4** and **2.5**. The solution quickly lost its characteristic orange color, forming a red solution with no precipitate, which is characteristic of $Fe(biby)_3^{2+}$. Analysis of UV-Vis spectroscopic data allows the determination of a reaction rate**.**

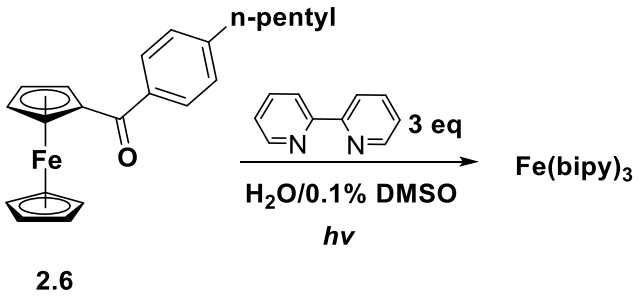

Scheme 2.7: Photoactivation iron(II) reaction of 2.6 and bipy followed by UV-Vis spectroscopy

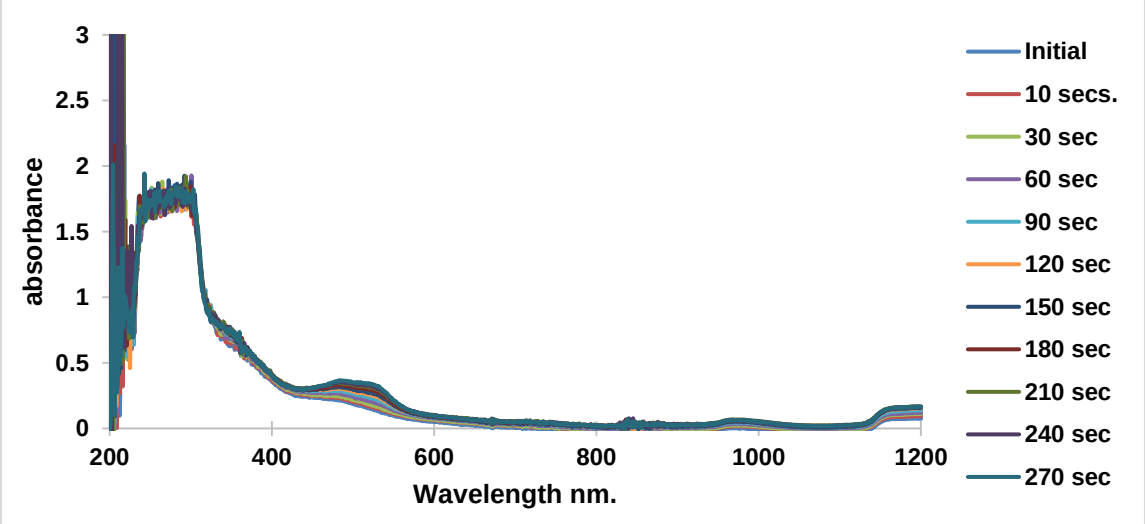

Figure 2.4: The graph over time of photolysis of 2.6 followed by UV-Vis

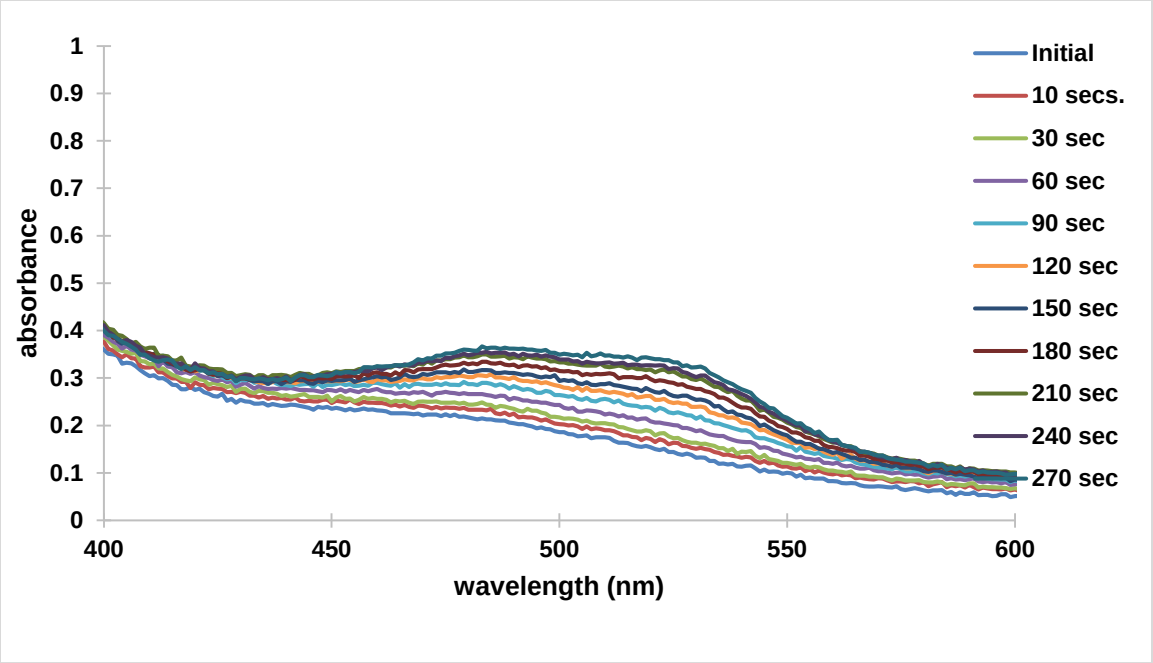

Figure 2.5: Absorbance characteristic of $Fe(biby)_3^{2+}$ λ_{max} at 522 nm

A rate of the photorelease of cyclopentadiene rings was determined the characteristic λ_{max} for $Fe(biby)_3^{2+}$ at 522 nm. The solution proved to complete the release of iron(II) after 5 minutes of photolysis. This determined a rate of production at 0.9 μM $Fe(biby)_3^{2+}$/s (Figure 2.6

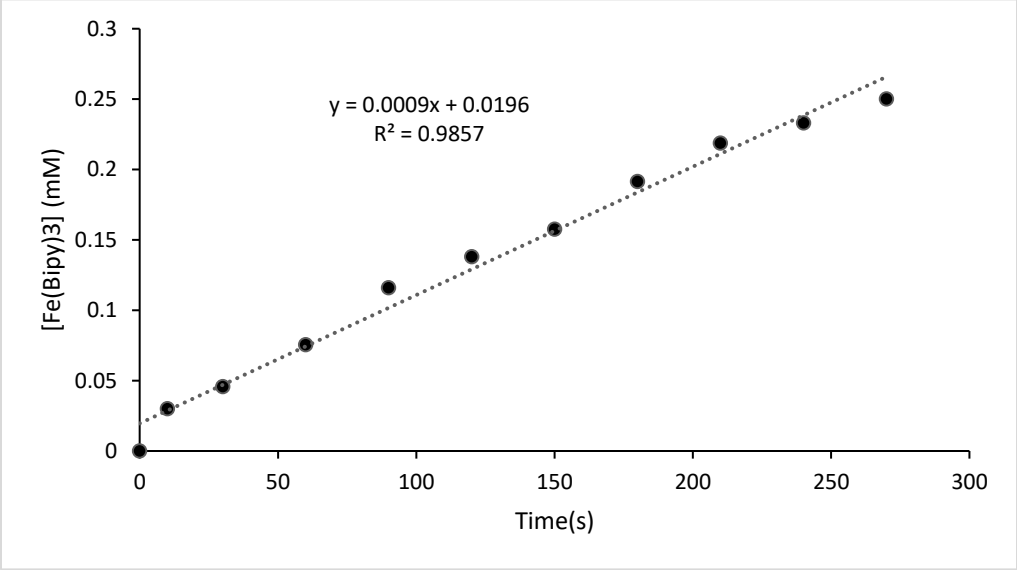

Figure 2.6: Rate of photochemical iron release from $Fe(C_5H_4(C{=}OC_6H_5)C_5H_{11})_2$ (2.6).

Photoactivation of $Fe(C_5H_4(C{=}OC_6H_5)C_5H_{11})_2$ **2.13** was completed similarly to $CpFe(C_5H_4(C{=}OC_6H_5)C_5H_{11})$**2.6**, **2.13** (0.25 mM, H_2O/DMSO) and of 2,2′-bipyridine (bipy, 3 equiv.) was dissolved in deoxygenated millipore water containing 0.75% DMSO. The solution was photolyzed (> 450 nm) in a quartz cuvette in the absence of oxygen for intervals of 10 seconds and analyzed by UV-Vis to detect the generation of $Fe(biby)_3^{2+}$. The results are presented in **Figures 2.8** and **2.9**.

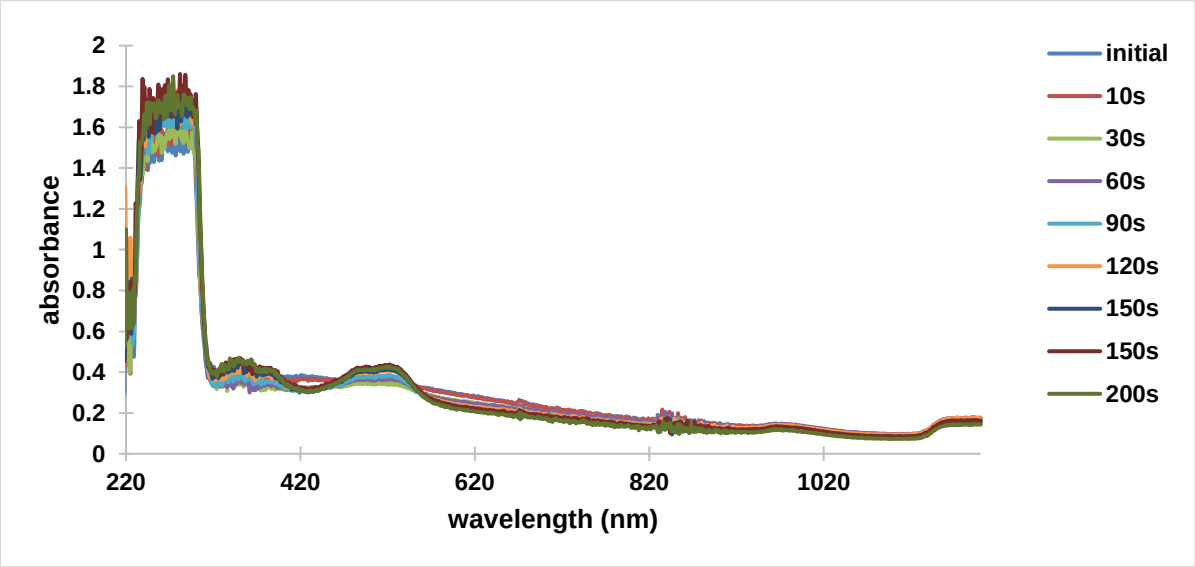

Figure 2.7: The graph over time of photolysis of 2.13 followed by UV-Vis

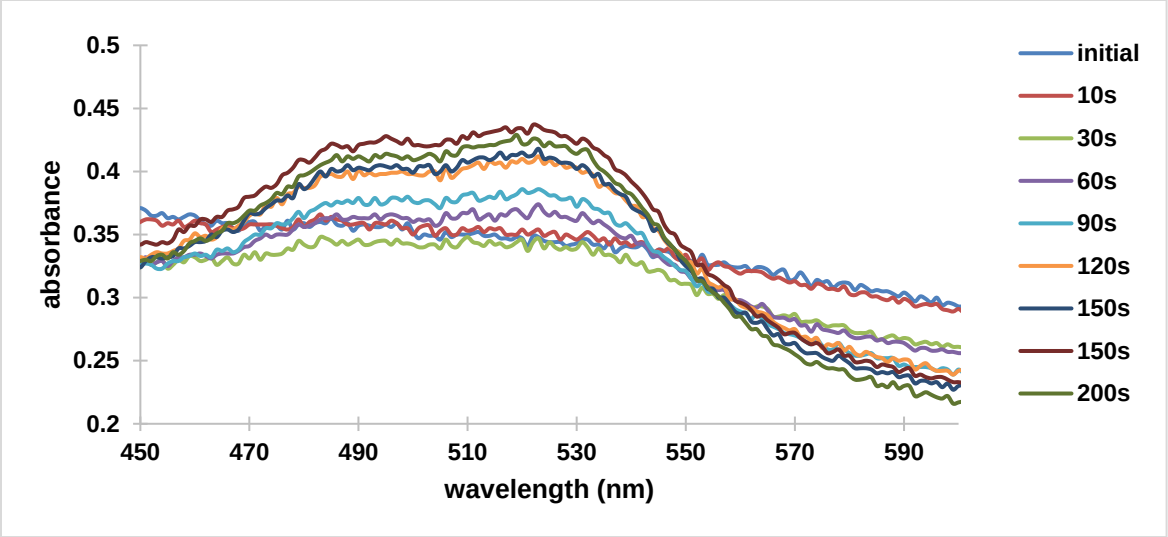

Figure 2.8: $Fe(bipy)_3^{2+}$ absorption of 2.13

Unfortunately, the rate of **2.13** was not able to be determined because the absorbance of **2.13** interferes with the absorbance of $Fe(biby)_3^{2+}$. No further studies were completed to determine the rate of photorelease and iron(II) reaction with bipy for **2.13**. It should be noted though that **2.13** was qualitatively faster than **2.6** at the 200 second time point.

2.5 2-photon photoactivation

2.5.1 Two-photon activation background

Two-photon excitation may occur when two photons at the same energy simultaneously excite an electron to an energy state corresponding to the summation of the two photons' energies, as depicted in **Figure 2.9.** [63] Two-photon excitation has been used for biological fluorescence to determine multiple channels for analyzing tissue. Excitation of small molecules has been minimally utilized as an absorbance source.

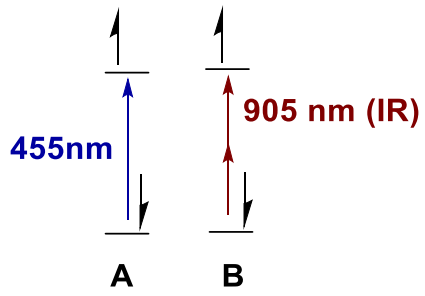

Figure 2.9: Two-photon excitation diagram

2.5.2 Two-photon activation of $CpFe(C_5H_4(C=O)C_6H_5C_5H_{11})$ 2.6 and $Fe(C_5H_4(C=OC_6H_5)C_5H_{11})_2$ 2.13

A process to perform photolysis on **2.6** and **2.13** utilizing two-photon activation was developed in order to increase the wavelength and decrease the energy required to activate the release of iron(II). This was studied to reduce the energy needed for the release of iron(II) from benzoylferrocene. This increase in wavelength would be optimal for clinical use to reduce negative side effect of a photodynamic therapy. Additionally, this would be interesting fundamental study of efficacy of a photodynamic therapy with 2-photon induction. To generate the energy comparable to that of a 452 nm wavelength source, the light was generated from a 1811 nm source and doubled with a crystal. Compounds **2.6** and **2.13** were irradiated for 30 minutes in the presence of excess bipy and analyzed for the generation of $Fe(bipy)_3^{2+}$ (Figures 2.11 and 2.12). For both **2.6** and **2.13**, the results indicate the generation of $Fe(bipy)_3^{2+}$.

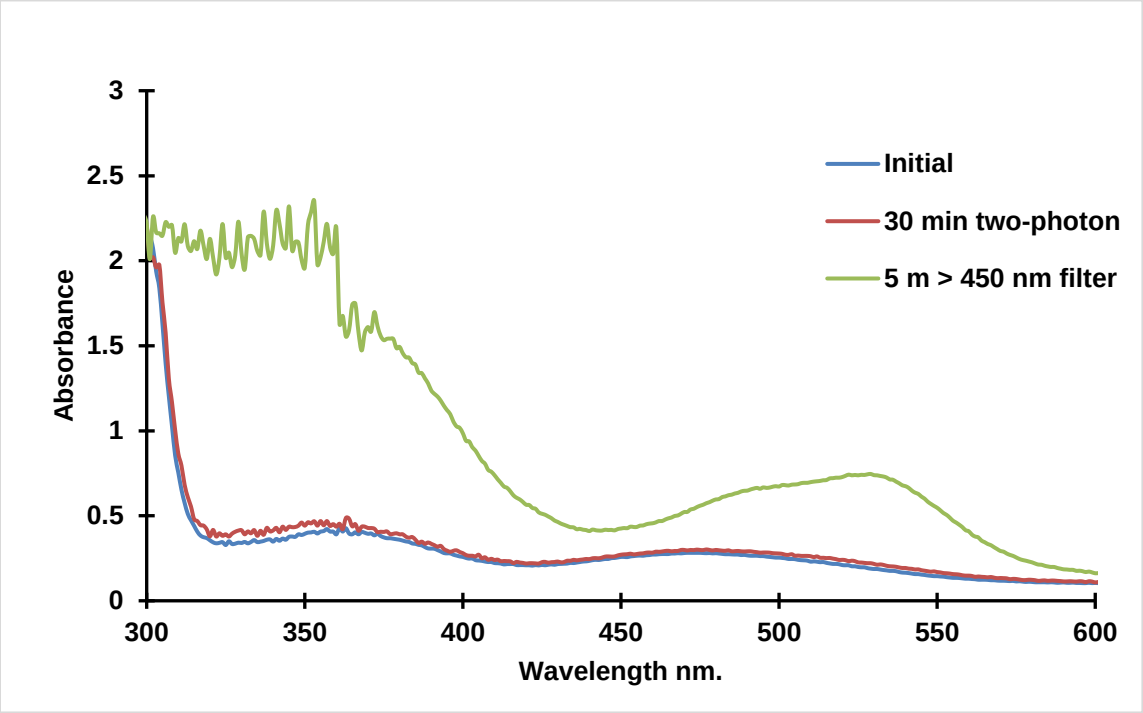

Figure 2.10: UV-Vis spectrum following 2-photon excitation of 2.6 after 30 minutes

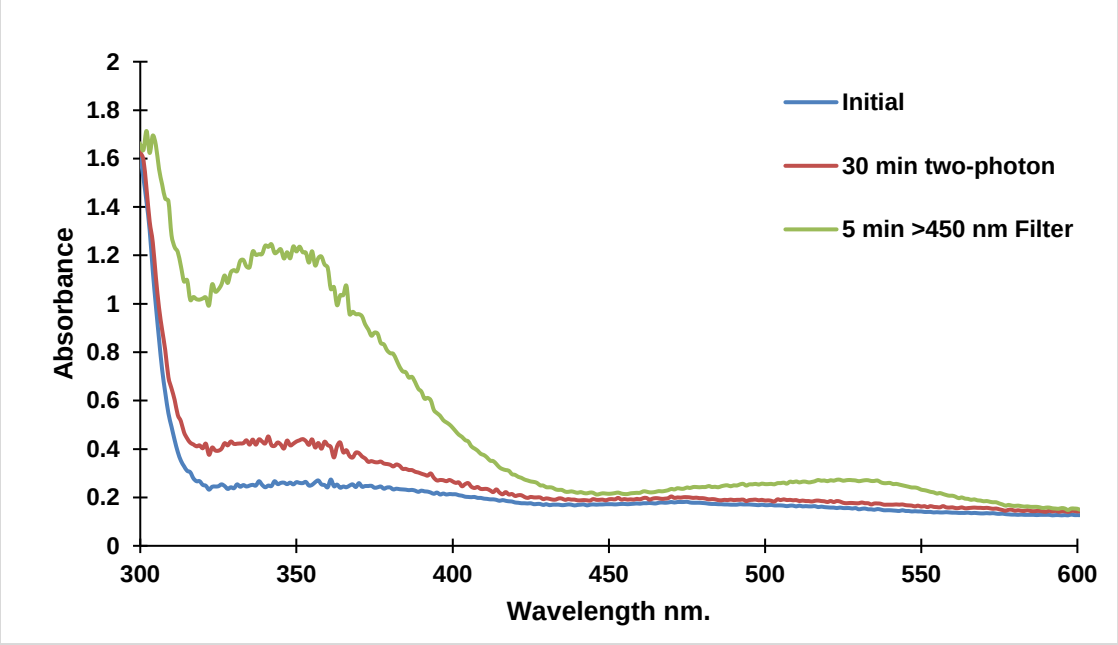

Figure 2.11: UV-Vis spectrum following 2-photon excitation of 2.13 for 30 min followed by 5 min 450 nm photolysis

To further the reaction, compound **2.6** was photolyzed with two-photon excitation for three hours at an energy equivalent to 452 nm similar to previous studies. It was shown that only around 30% of the photolysis reaction was completed through this time.

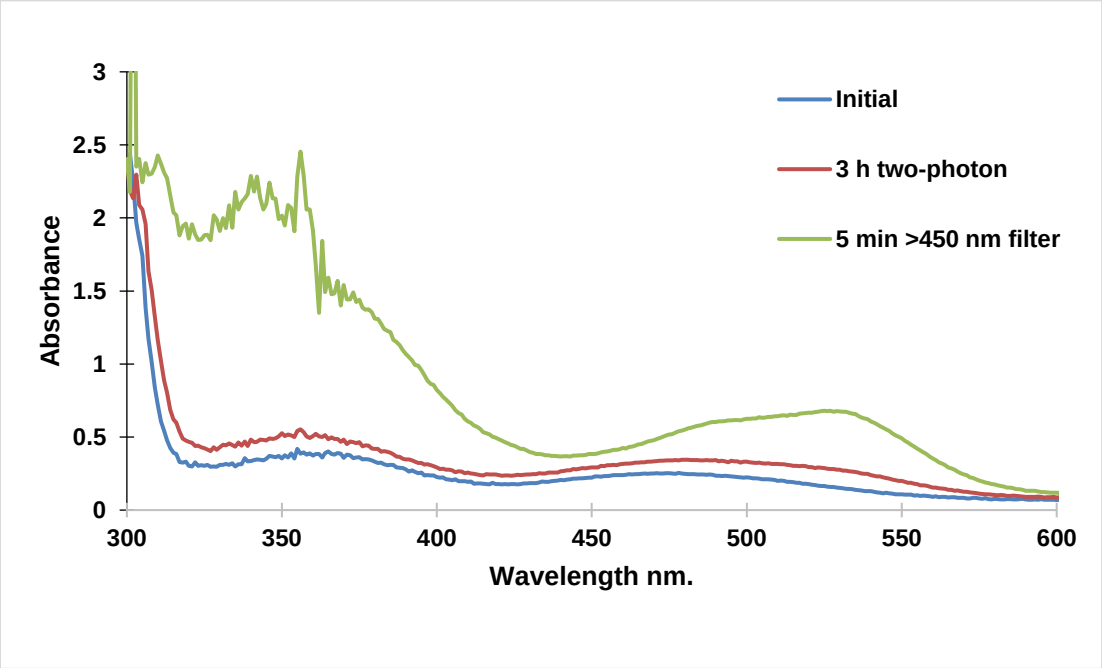

Figure 2.12: UV-Vis spectrum following 2-photon excitation of 2.6 photoactivations for 3 h

As a fundamental study, this proved the be successful, as $Fe(biby)_3^{2+}$ was produced upon two-photon activation. Unfortunately, two-photon irradation was not as dynamic of an activator as the light source used to study the rate of photoactiation of benzoylferrocenes as shown in section 2.4. Because of this two-photon activation will not be utilized in cell studies as a PDT light source. This difference in rate could be due to the surface area of the photon activation, as the all light source has a much higher surface area for a light source.

2.6 Experimental Methods

General Procedure of 1-benzoylferrocene acylation. Anhydrous $AlCl_3$ (0.98 g, 7.0 mmol, 1.3 equiv) and acid chloride (5.9 mmol, 1.1 eqiuv) were allowed to react for 5 min in anhydrous dichloromethane (16.4 mL). Slowly, ferrocene in dichloromethane (1.00 g, 5.4 mmol, 1 equiv, 5.0 mL) was added dropwise via syringe for a 0.25 M final concentration of ferrocene. The dark blue solution was stirred overnight at ambient temperature. The reaction mixture was quenched in ice water, extracted into 100 mL of CH_2Cl_2, then washed successively with 75 mL of 10% NaOH solution, water, and brine. The organic layer was dried over anhydrous $MgSO_4$, filtered, and the solvent removed under reduced pressure. Chromatography on silica gel with hexanes/ethyl acetate (90/10) as eluent led to isolation of the pure 1-benzoylferrocenes.

General Procedure for 1-benzoylferroence and 1,1′-dibenzoylferrocene acylation. Anhydrous $AlCl_3$ (0.98 g, 14.0 mmol, 2.5 equiv) and acid chloride (11.9 mmol, 2.2 eqiuv) were allowed to react for 5 min in anhydrous dichloromethane (30 mL). Ferrocene dissolved in dichloromethane (1.00 g, 5.4 mmol, 1 equiv, 10.0 mL) was slowly added dropwise via syringe and the mixture was then heated to reflux. The dark blue solution was allowed to stir for 72 h. The reaction mixture was poured into a flask of ice water, extracted into 100 mL of CH_2Cl_2, then washed successively with 10% NaOH solution, water, and brine. The organic layer was dried over $MgSO_4$, filtered, and the solvent removed under reduced pressure. Unless other wise stated chromatography on SiO_2 gel with hexanes/ethyl acetate (80/20) for the elution order of transparent acid chloride, secondly unreacted yellow ferrocene and subsequent of isolation of the orange 1-benzoylferrocene and final elution orange-red of 1,1′-dibenzoylferrocene.

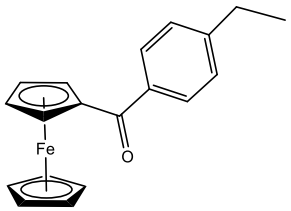

Compound 2.4 Prepared according to general procedure of 1-benzoylferrocene acylation using commercially available 4-ethyl benzoyl chloride. 78% yield. ^{1}H NMR (500 MHz, $CDCl_3$) δ 7.85 (d, J = 8.1 Hz, 2H), 7.29 (d, J = 8.0 Hz, 2H), 4.91 (t, J = 1.9 Hz, 2H), 4.57 (t, J = 1.9 Hz, 2H), 4.21 (s, 5H), 2.73 (d, J = 7.6 Hz, 2H), 1.29 (t, J = 7.6 Hz, 3H); ^{13}C NMR (126 MHz, $CDCl_3$) δ 198.93, 148.41, 137.40, 128.54, 127.86, 77.41, 77.16, 76.91, 72.51, 71.68, 70.34, 29.06, 15.49. IR ($CDCl_3$, cm^{-1}) 1104, 1384.2, 1474, 1568, 1803, 2252, 2851, 2915, 2989, 3154. HRMS (ESI-TOFMS) *m/z* calcd for $[C_{19}H_{19}FeO]^+$ 319.0779; found, 319.0780

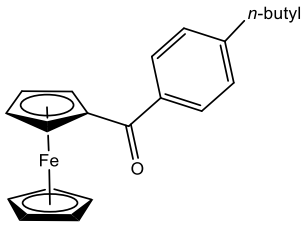

Compound 2.5. Prepared according to the general procedure of 1-benzoylferrocene acylation using commercially available 4-butylbenzoyl chloride. 71% Yield ^{1}H NMR (300 MHz, $CDCl_3$) δ 7.84 (d, J = 8.1 Hz, 2H), 7.27 (d, J = 6.9 Hz, 3H), 4.94 – 4.87 (m, 2H), 4.59 – 4.53 (m, 2H), 4.21 (s, 4H), 2.74 – 2.62 (m, 2H), 1.64 (d, J = 7.5 Hz, 2H), 1.39 (d, J = 7.5 Hz, 2H), 0.95 (t, J = 7.3 Hz, 3H); ^{13}C NMR (126 MHz, $CDCl_3$) δ 198.97, 147.13, 128.43, 128.38, 72.68, 71.80, 70.47, 35.78, 33.48, 22.49, 14.09.; IR ($CDCl_3$, cm^{-1}) 1174, 1279, 1440, 1635, 1792, 2253, 2866, 2932. HRMS (ESI-TOFMS) *m/z* calcd for $[C_{21}H_{23}FeO]^+$ 347.1093; found, 347.1093

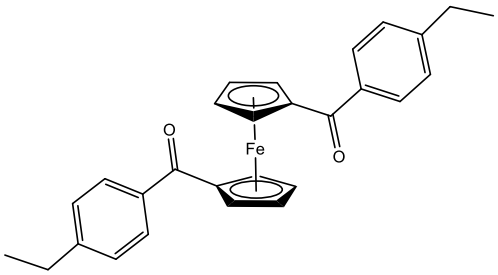

Compound 2.11. Prepared according to general procedure of 1-benzoylferrocene and 1,1`-dibenzoylferrocene acylation using commercially available 4-ethyl benzoyl chloride. 63% Yield ^{1}H NMR (300 MHz, $CDCl_3$) δ 7.75 (d, J = 8.1 Hz, 4H), 7.24 (s, 4H), 4.95 – 4.87 (m, 4H), 4.59 – 4.51 (m, 4H), 2.72 (q, J = 7.6 Hz, 4H), 1.29 (t, J = 7.6 Hz, 6H); ^{13}C NMR (126 MHz, $cdcl_3$) δ 197.81, 148.87, 136.74, 128.60, 127.95, 79.80, 77.41, 77.16, 76.91, 76.70, 74.71, 73.20, 29.85, 29.07, 15.44. IR ($CDCl_3$, cm^{-1}) 1168, 1280, 1444, 1602, 1641, 2879, 2969. HRMS (ESI-TOFMS) *m/z* calcd for $[C_{28}H_{27}FeO_2]^+$, 451.1359; found, 451.1355

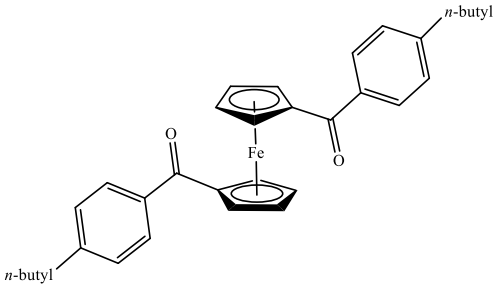

Compound 2.12. Prepared according to the General Procedure of 1-benzoylferrocene and 1,1`-dibenzoylferrocene acylation using commercially available 4-butyl benzoyl chloride. 21% yield .^{1}H NMR (300 MHz, $CDCl_3$) δ 7.77 (d, J = 8.2 Hz, 2H), 7.25 (d, J = 8.2 Hz, 2H), 4.98 – 4.92 (m, 2H), 4.61 – 4.54 (m, 2H), 2.74 – 2.67 (m, 2H), 1.67 (t, J = 7.7 Hz, 2H), 1.42 (dd, J = 15.0, 7.3 Hz, 2H), 0.98 (t, J = 7.3 Hz, 3H); ^{13}C NMR (126 MHz, $CDCl_3$) δ 197.69, 153.99, 148.74, 136.63, 128.47, 127.81, 77.28, 77.02, 76.77, 74.57, 73.08, 28.94, 15.29.; ($CDCl_3$, cm^{-1}) 1096, 1280, 1389, 1467, 1643, 1799, 2261, 2849 2979. HRMS (ESI-TOFMS) *m/z* calcd for $[C_{32}H_{35}FeO_2]^+$ 507.1983; found, 507.1981

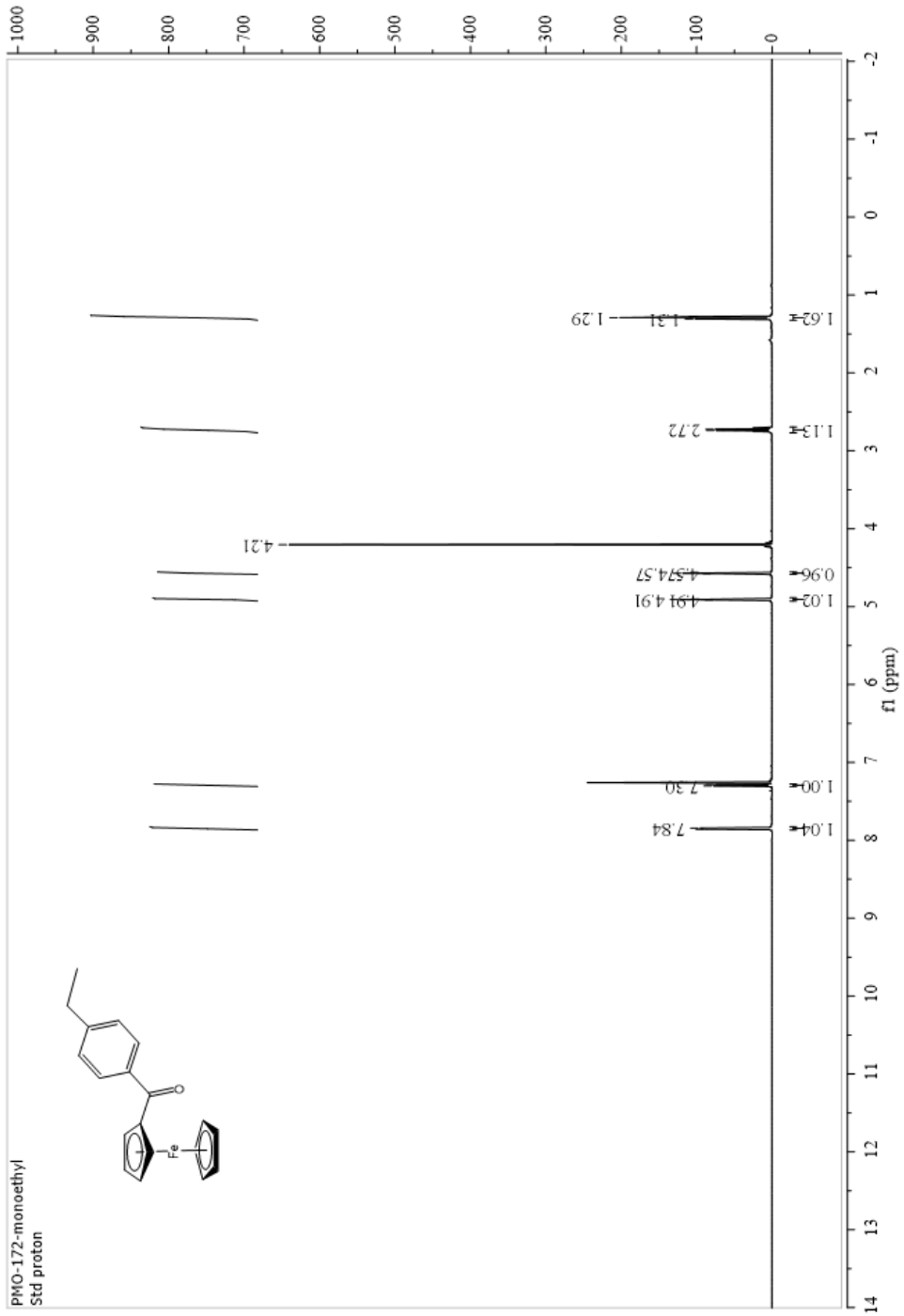

Figure 2.13: Reported ^{1}H NMR of compound 2.4 in $CDCl_3$

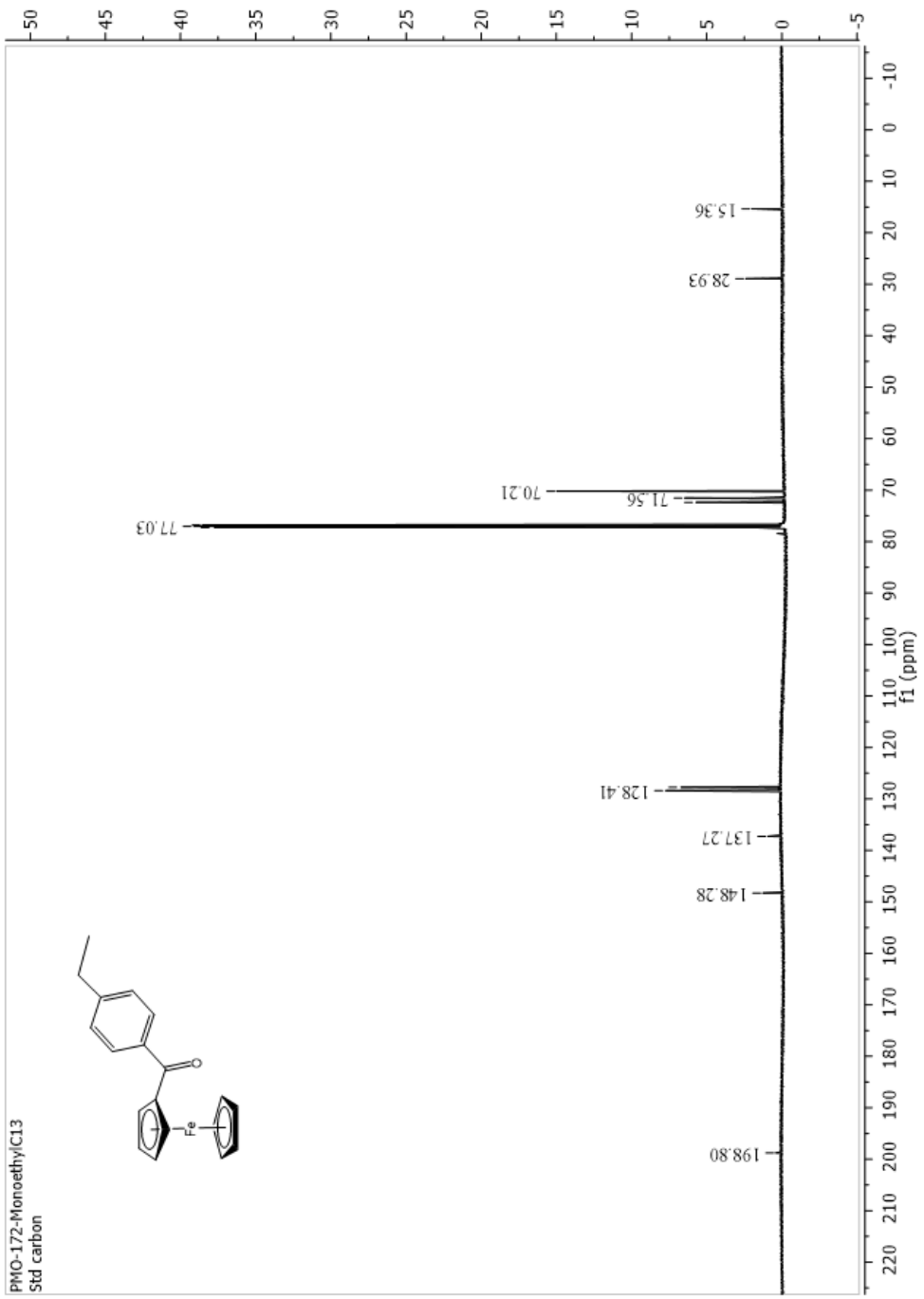

Figure 2.14: Reported ^{13}C NMR of compound 2.4 in $CDCl_3$

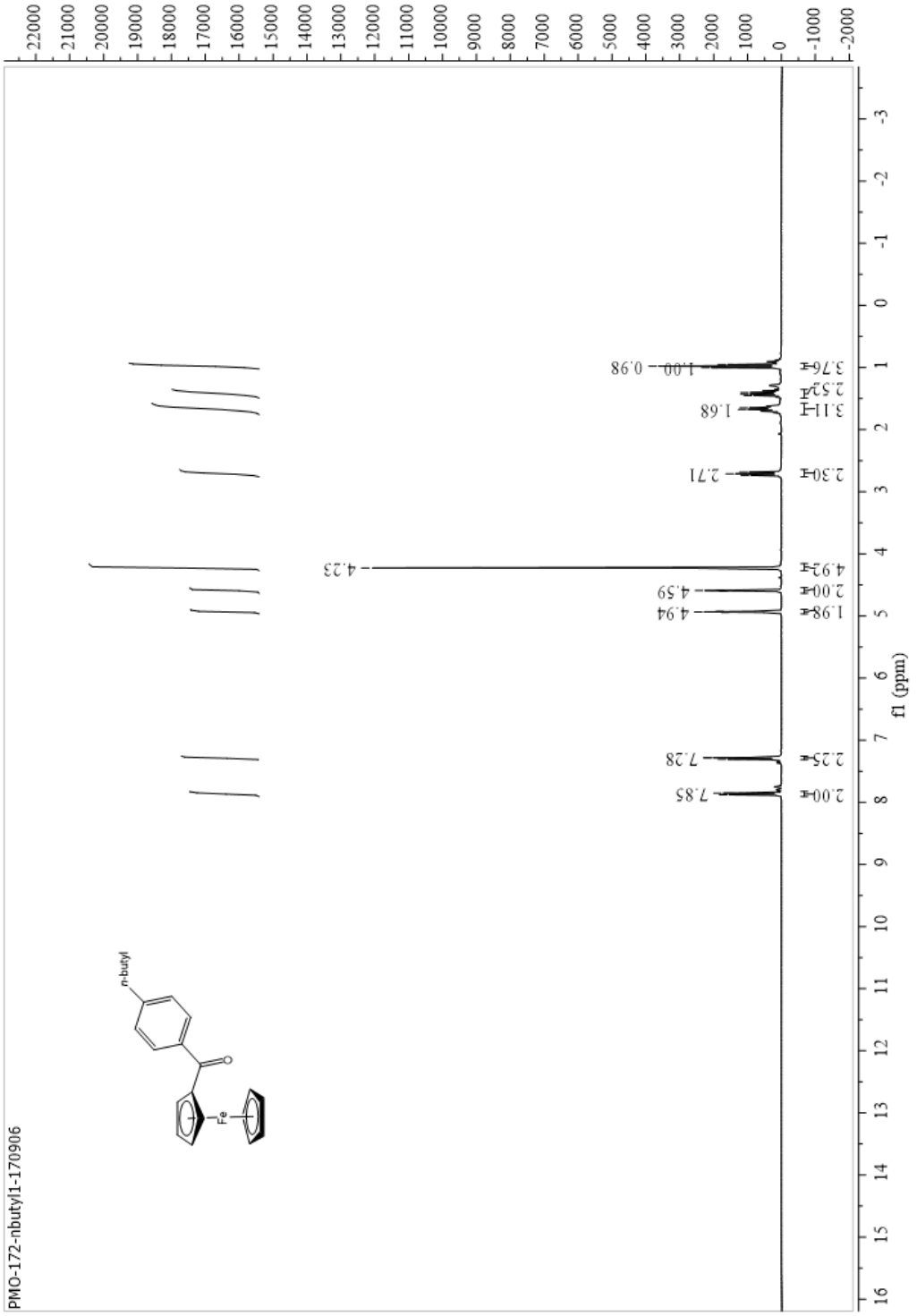

Figure 2.15: Reported ^{1}H NMR of compound 2.5 in $CDCl_3$

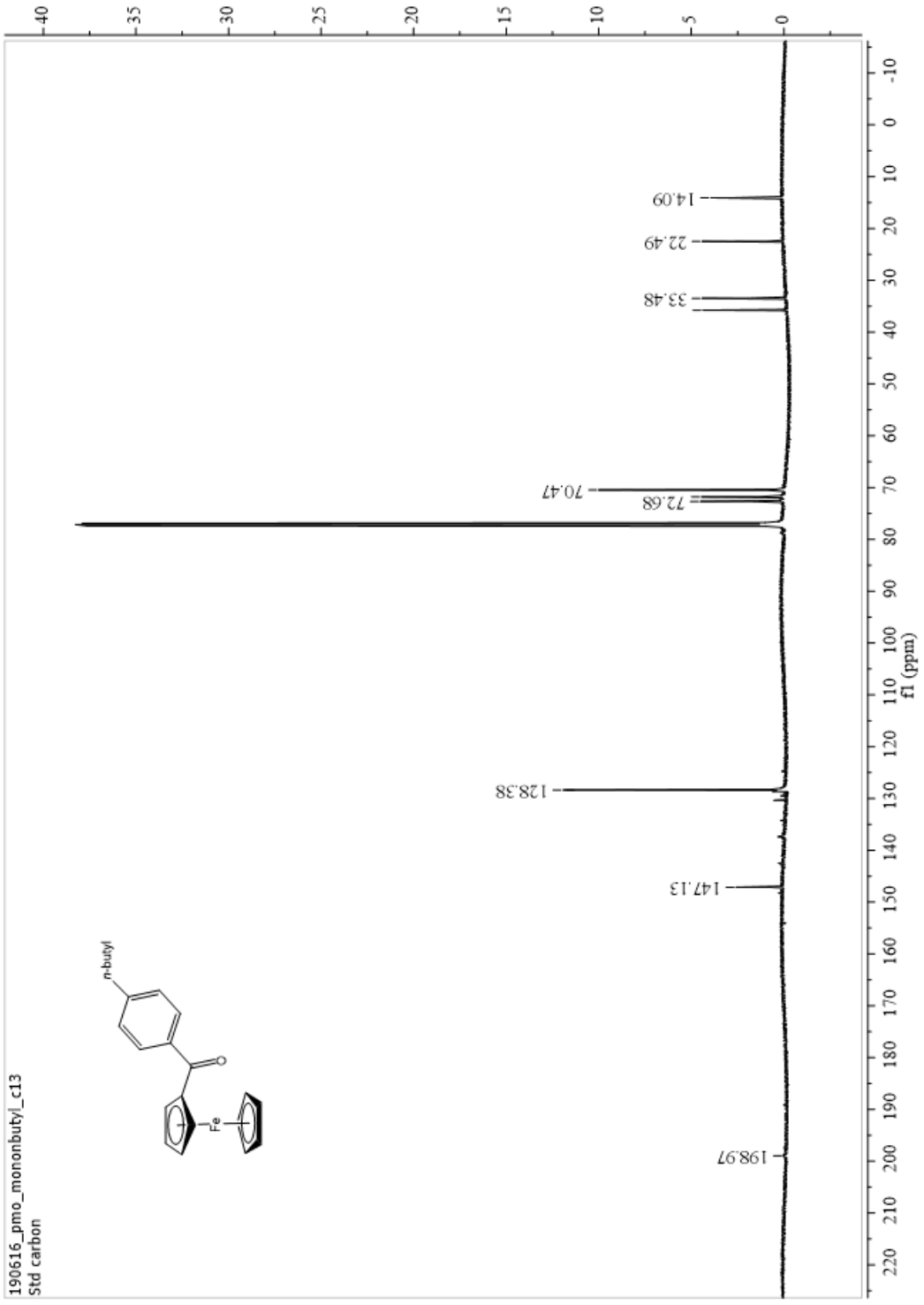

Figure 2.16: Reported ^{13}C NMR of compound 2.5 in $CDCl_3$

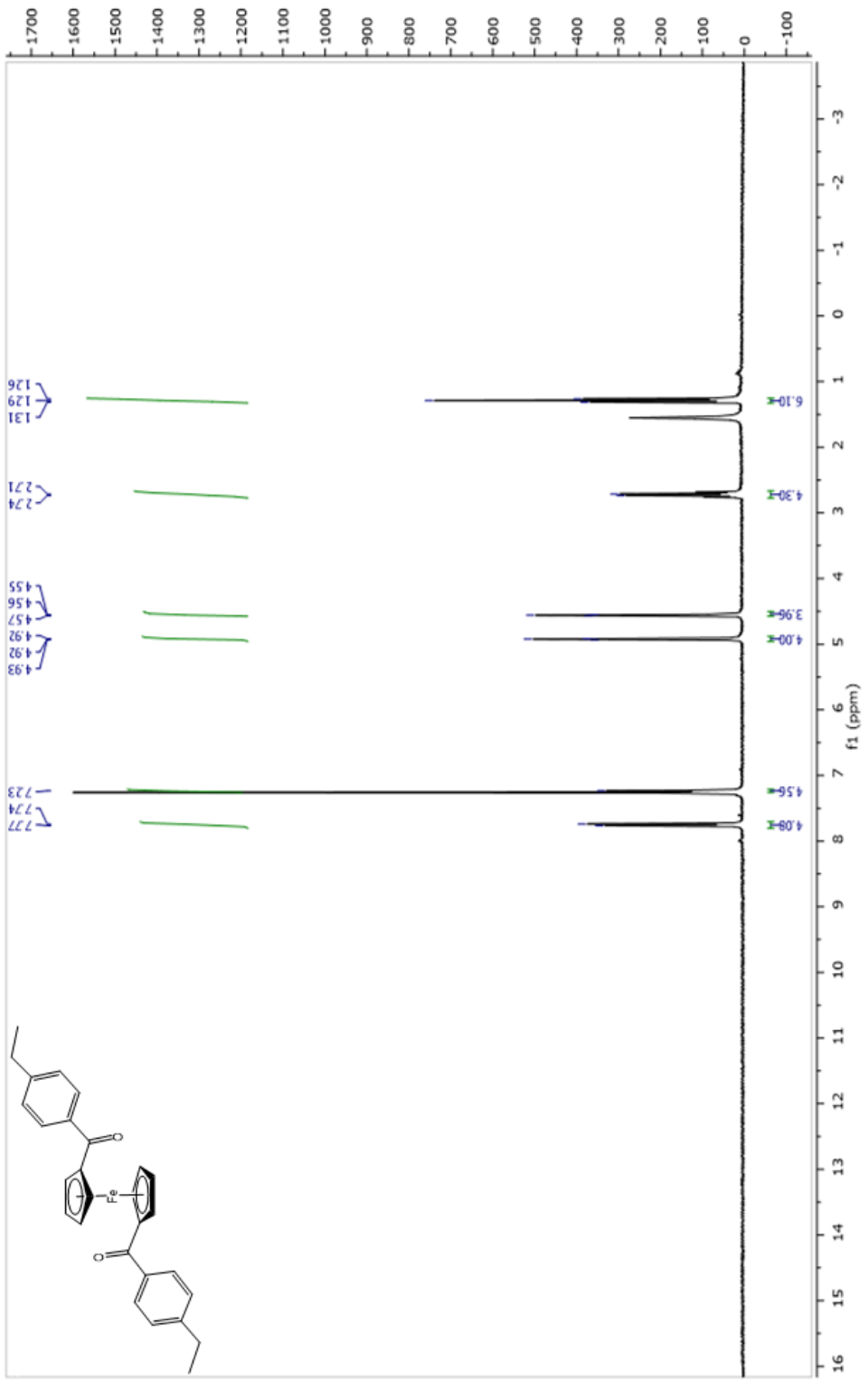

Figure 2.17: Reported ^{1}H NMR of compound 2.11 in $CDCl_3$

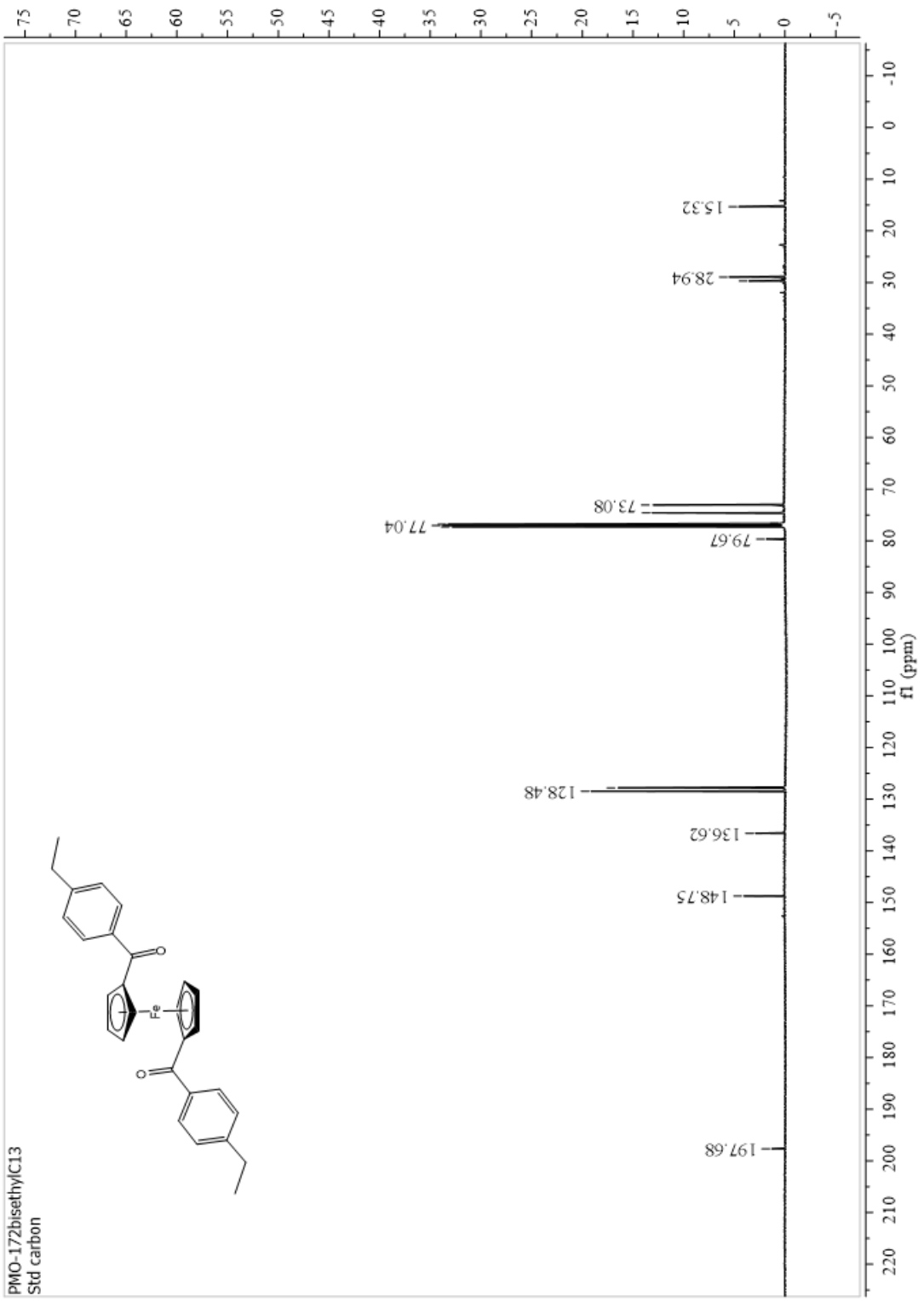

Figure 2.18: Reported ^{13}C NMR of compound 2.11 in $CDCl_3$

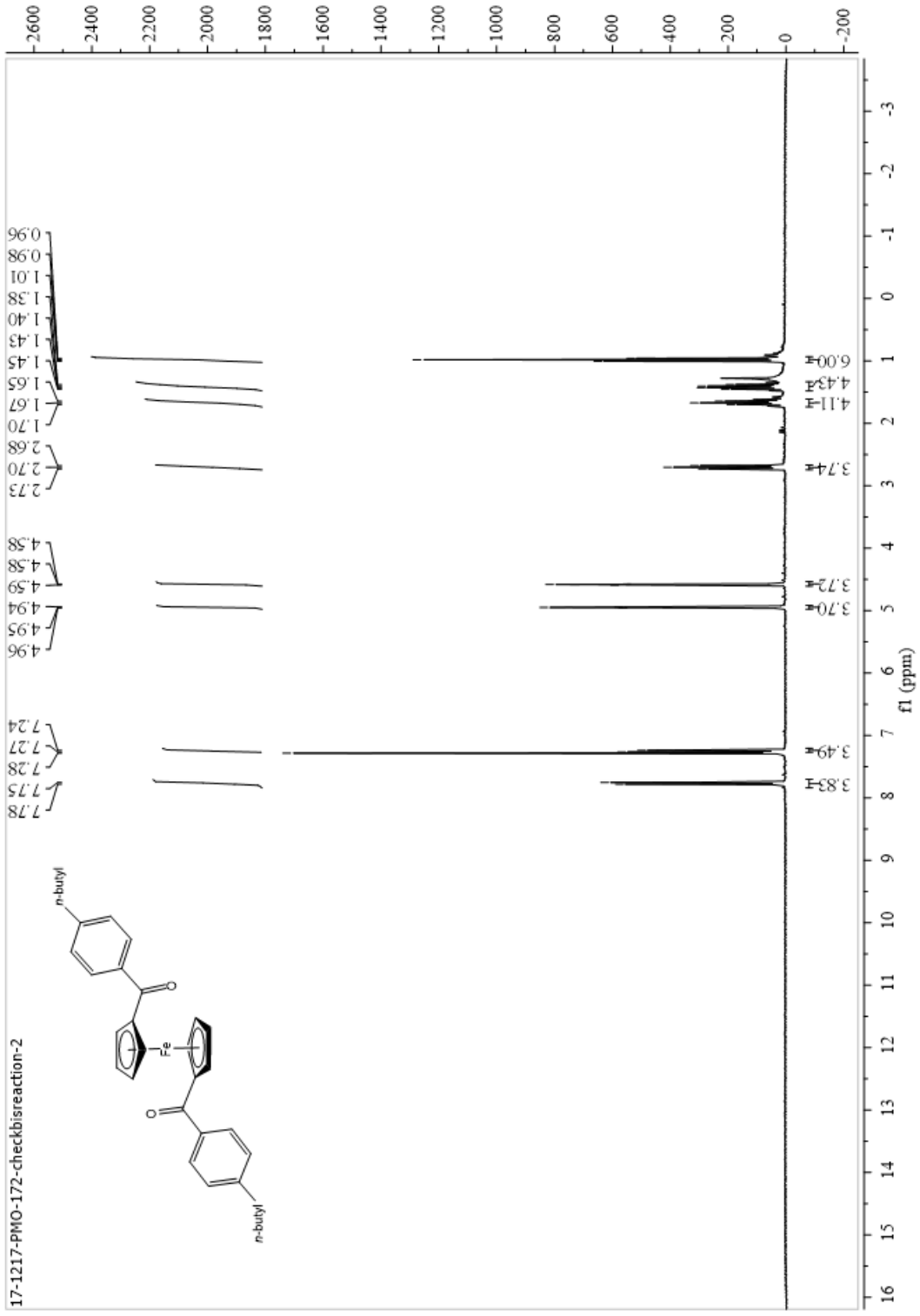

Figure 2.19: Reported ^{1}H NMR of compound 2.12

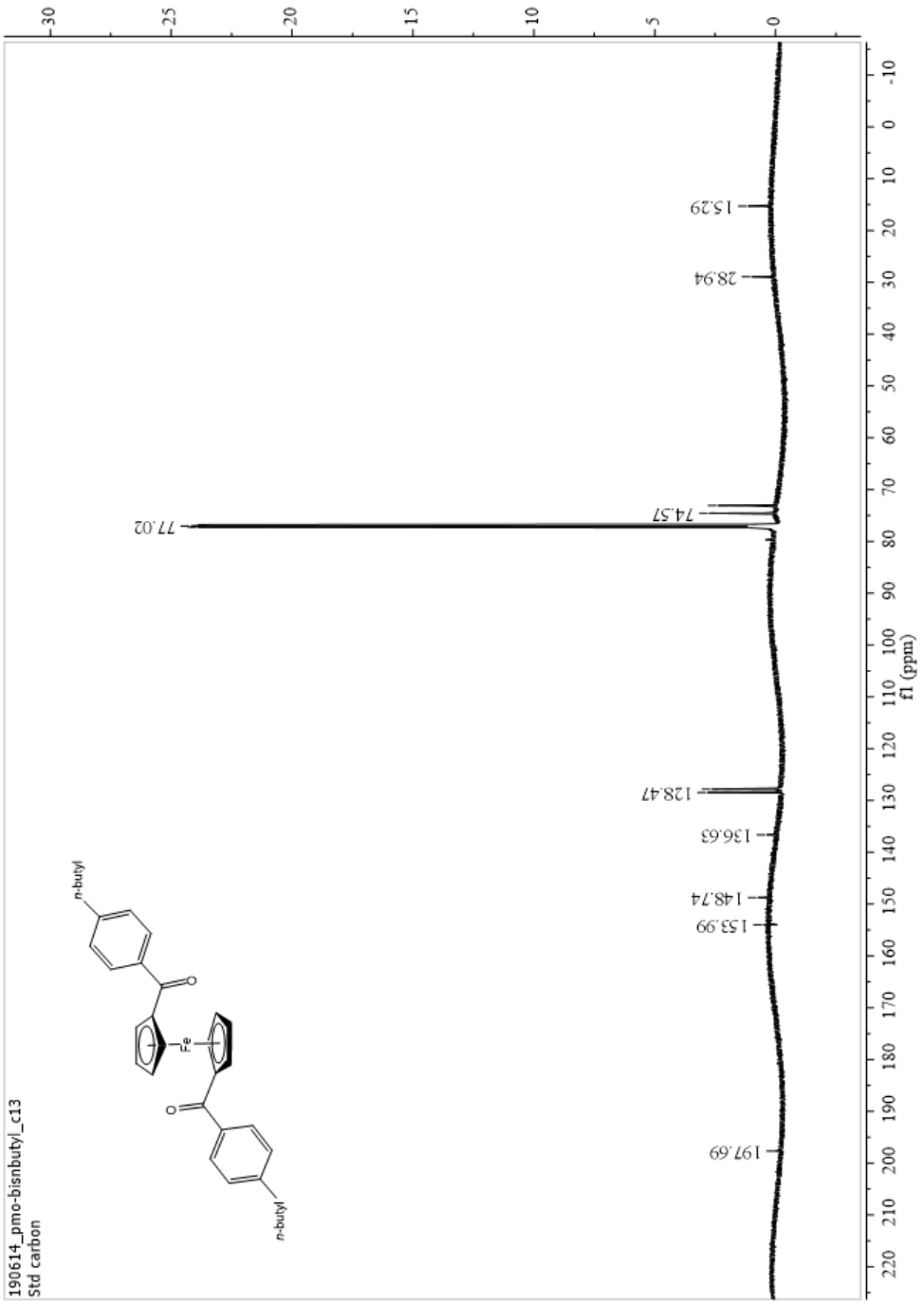

Figure 2.20: Reported ^{13}C NMR of compound 2.12 in CDCl

2.7 Acknowledgments

Olsen, Pauline; Huang, Christina; Aubrey, Marissa; Chen, Wenfan; Melaimi, Mohand; O'Connor, Joseph. Dr. Christina and Dr. Marissa both completed some synthesis and characterization for this chapter. Dr. Mohammad completed the Cyclic Voltammetry of the compounds and Wenfan completed the two-photon laser setup and excitation. The dissertation author was the primary investigator and author of this material.

2.8 Chapter 2 References

54. Riemschneider, R.; Helm, D., Über einige 1.1′-Disubstitutionsprodukte des Ferrocens. *Chemische Berichte* **1956,** *89* (1), 155-161.

55. MARVIN RAUSCH, M. V., and HAROLD ROSENBERG, Derivatives of Ferrocene. II. Some Reduction Products of Benzoylferrocene and 1,1'-Dibenzoylferrocene. *The Journal of Organic Chemistry* **1957,** *22* (8), 3.

56. Vol'kenau, A. N. N. a. N. A., *Dok lady Akad. Tauk SSSR* **1956,** *107*, 262.

57. Tarr, A. M.; Wiles, D. M., Electronic absorption spectra and photodecomposition of some substituted ferrocenes. *Can J Chem* **1968**, 2725-2731.

58. Ali, L. H.; Cox, A.; Kemp, T. J., Photochemistry of a-Carbonylferrocenes and Related Compounds. *J Chem Soc Chem Comm* **1972**, 265-266.

59. Yamaguchi, Y.; Kutal, C., Efficient Photodissociation of Anions from Benzoyl-Functionalized Ferrocene Complexes. *Inorg Chem* **1999,** *38*, 4861-4867.

60. Yamaguchi, Y.; Kutal, C., Benzoyl-Substituted Ferrocenes: An Attractive New Class of Anionic Photoinitiators. *Macromolecules* **2000,** *33*, 1152-1156.

61. Ding, W.; Sanderson, C. T.; Conover, R. C.; Johnson, M. K.; Amster, J.; Kutal, C., Characterization of the Low-Energy Electronic Excited States of Benzoyl-Substituted Ferrocenes. *Inorg Chem* **2003,** *42*, 1532-1537.

62. W. E. Siri Siri, J. H. L. a. C. A. T., *The Gross Composition of the Body. Advances in biological and medical physics.* 1956; p 41.

63. Ustione, A.; Piston, D. W., A simple introduction to multiphoton microscopy. *J Microsc* **2011,** *243* (3), 221-6.

Chapter 3 Cytotoxicity Studies of 1-Benzoylferrocene Derivatives and Proposed Cytotoxicity Mechanism

3.1 Proposed catalytic initiation of Fenton and the Haber-Weiss for 1-benzoylferrocene derivatives

After studying the photoactivated release of free iron(II) from benzoylferrocene derivatives, *in vitro* studies were completed to determine the therapeutic potential of these compounds against cancer. We hypothesized that the photo-release of free iron(II) from benzoyl ferrocene derivatives can elevate levels of reactive oxygen species (ROS), from iron-catalyzed cycling of the Fenton and Haber Weiss reactions as shown in Scheme 3.1 leading to cancer cell death.[64-66]

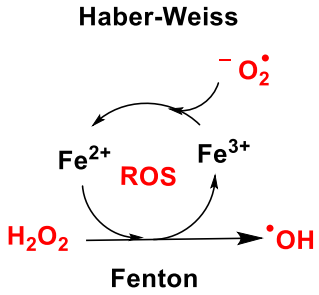

Scheme 3.1 Fenton and Haber-Weiss reaction scheme

Cancer was sought as a target for our benzoylferrocene derivatives due to the previous literature describing the concentration of hydrogen peroxide as compared to healthy cells and sensitive to ROS shifts in concentrations. [4-9] We hypothesize that benzoylferrocenes have the potential to be a potent anti-cancer therapy due to the cells naturally occuring high levels of hydrogen peroxide and irons ability to increase ROS production resulting in cancer cell death (Figure 3.2).

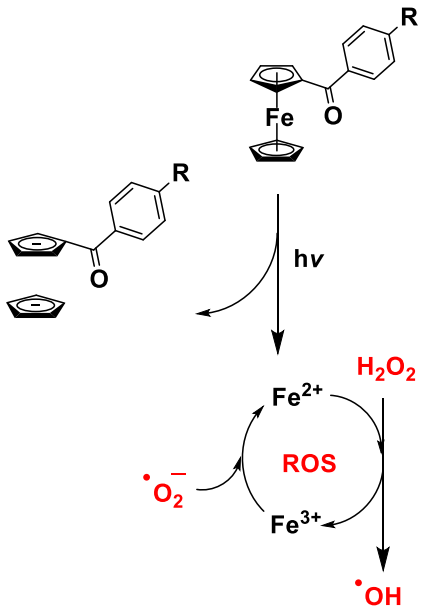

R = H, chloromethyl, methyl, ethyl, *n*-butyl, *n*-pentyl, methylphosphonium

Figure 3.2: Proposed effect of photoactivated benzoylferrocene through both Fenton and Haber Weiss reaction

3.2 Cytotoxicity Studies of 1-Benzoylferrocene Derivatives

To determine potency of the 1-benzoylferrocene derivatives, crystal violet assays were utilized to determine proliferation different concentrations of **2.1 - 2.2** and **2.4 -2.7** (Figure 3.3). The concentration to inhibited 50% of cell proliferation, (IC_{50}) was calculated on the protocols described below.

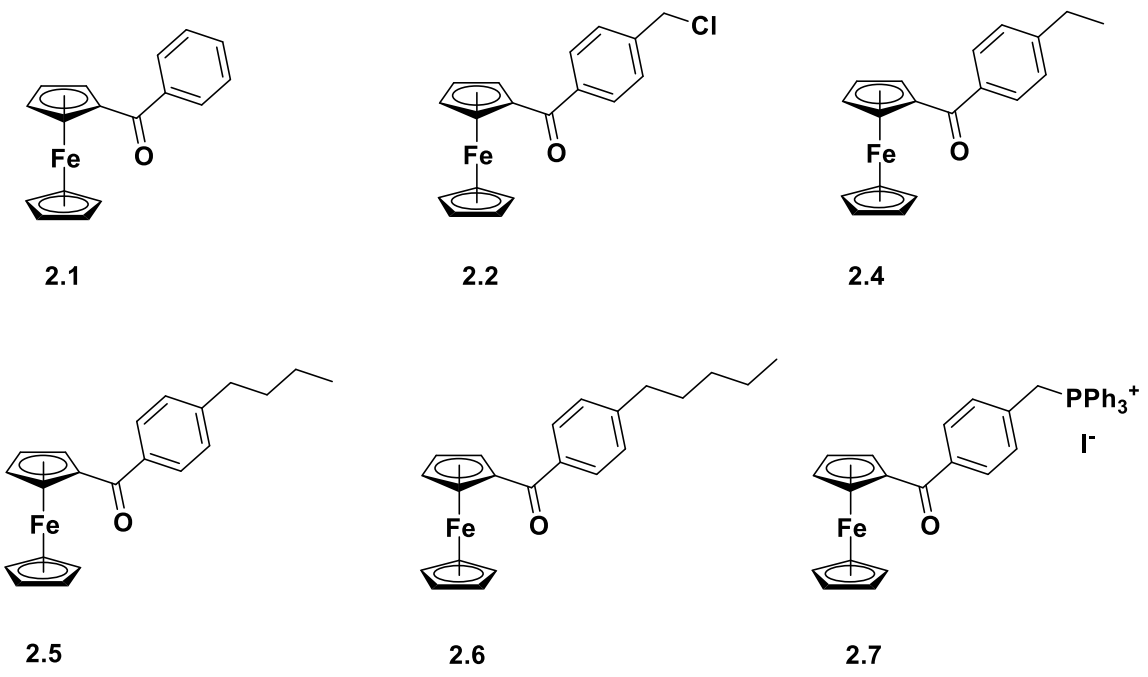

Figure 3.3: Compounds treated in the HeLa and CaOV3 cell lines to determine cytotoxicity

3.2.1 General Passaging Cell Studies Protocol

The following studies were completed using a general protocol for *in vitro* cell culture as previously reported.[67] Cells were passaged using sterile DPBS, DMEM, and trypsin kept at 37° C before passaging. Also, since the media does not contain a pH indictor, the cells were tested to ensure a pH range of 7.2-7.4. Media was removed and cells were washed with 3-5 ml of DPBS to ensure removal unadhered cells from the flask. Next, 1-2 ml of Trypsin was added to the T25 flask and incubated for 5-15 min at 37° C in an incubator. After incubation, 0.2-1.0 ml of the cells were resuspend in a new T25 flask with 5 mL of fresh DMEM media. The T25 flask was labeled with cell type, passage number (P#), date, and initials. Cells were incubated for 2-4 days to reach a minimum of 80% confluency. Every 4 days, media was changed and pH checked.

DMEM was prepared in a sterile environment and consists of: 100X antibiotic, Sodium pyruvate 100X-carbon source, Glucose, MEM NEAA 100X-amino acids, GlutaMAX 100X-dipeptide, supply of L-alanine and L-glutamine, Fetal Bovine Serum (FBS).

3.2.2 Crystal Violet Protocol

Crystal Violet is positively charged and highly conjugated compound that binds to negatively charged proteins and DNA in the cell (Figure 3.4). This dye is employed as a proliferation assay because adherent cells detach from cell culture plates upon cell death.[68, 69] The measure of cell proliferation upon stimulation with crystal violet are able to quantify the effect of benzoylferrocene derivatives at various concentrations. [70] The following protocol was adapted from published protocols and optimized for photodynamic therapy as illustrated in Figure 3.5.[68-70]

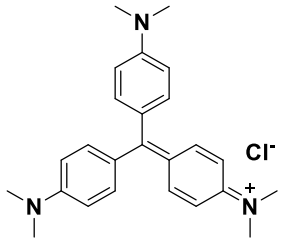

Figure 3.4: Crystal violet chemical structure

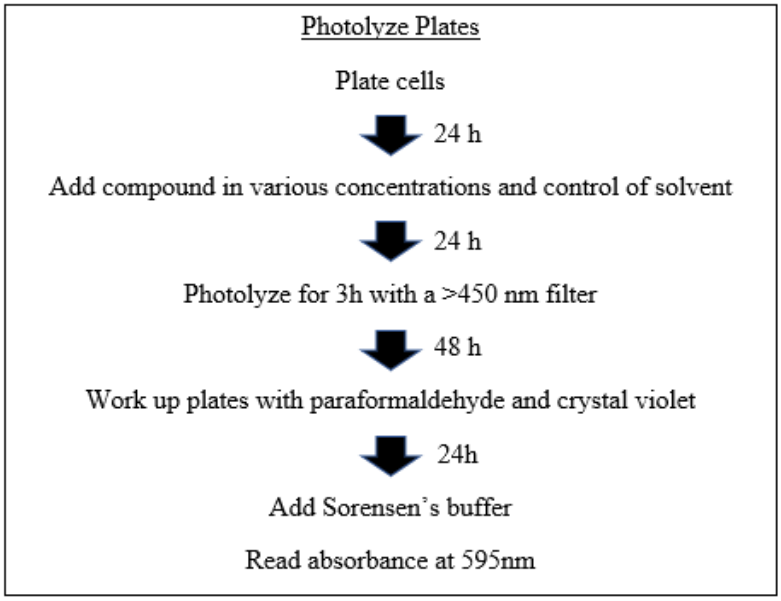

Figure 3.5: Protocol for photolyzed plates following crystal violet staining

Plating cells: Day 1

All steps were completed for cell passage up to resuspension of the cells in 5 ml of DMEM media. Next, the density of the solution was determined by counting the cells. Subsequently, 10 μL of unadhered cell solution was added to each end of the hemocytometer chip to ensure 3500 cell per well. Next, cell counts were inputed into a cell seeding spreadsheet to calculate a final density of 3,500 cells per well of 100 μl addition to a 96 well plate. Lastly, 3-4 wells were left without the addion of cells to use for control reactions.

Adding compound: Day 2

All concentrations of the benzoylferrocene derivatives were prepared so that the final concentration of all derivatives in the micromolar range. Next, 5 mL of DMEM was added for every 10 μL of benzoylferrocene derivative (or solvent control) in a sterile reservoir. Add control (solvent) first and then proceed to add the benzoylferrocene derivative from lowest to highest concentration.

Photolysis: Day 3

After 24 hours of incubation, the plates were photolyzed for 3 hours on an aluminum warming block with the yellow filter > 455 nm filter set to 37° C (Figure 3.6). The cell plate was then incubated for 48 h additional hours.

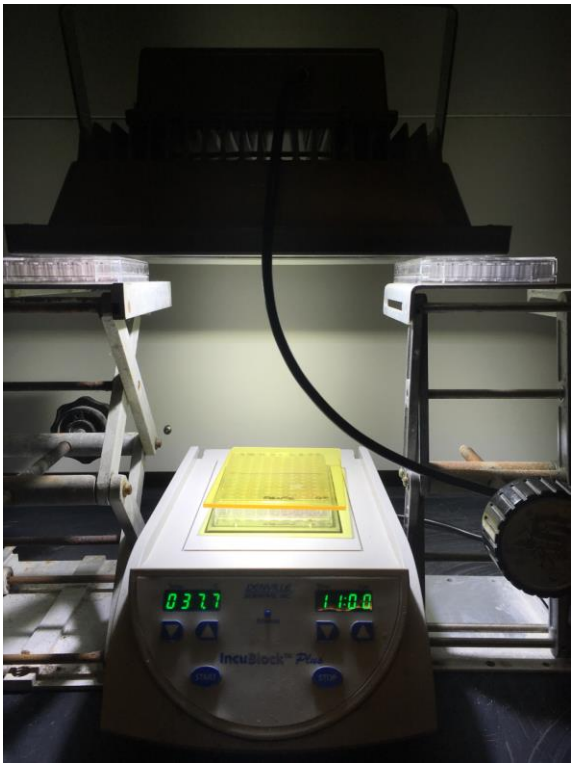

Figure 3.6: Photolysis of plate on aluminum block at 37° C

Fix cells and addition of crystal violet: Day 5

After incubating for 24 hrs, the media was removed from each well. Next, 200 μL of 4% paraformaldehyde was added to each well to fix the live cells to the plate. The paraformaldehyde was removed after 30 min and then 100 μL of Crystal Violet was added to each well. The CV was incubated for 30 min, and subsequently removed by washing the plate with di water 5x. The plates were dried by patting with paper towels and left to dry overnight.

Plate Reading: Day 6

After plate was fully dried, 180 μL of Sorensen's buffer was added to each well. The plates were then placed into a Molecular Devices SpetraMax i3x plate reader and the emission/absorbtion (IDK) wavelength was set to 595 nm. Next, the cytotoxicity was calculated by using the following equation.

3.2.3 Calculations for Cytotoxicity

The following equation was used to calculate the inhibitor concentration of 50% (IC_{50}) from a graph of percentage of cytotoxity versus concentration of compound.

$$\% \text{ cytotoxicity} = \frac{OD^{DMSO} - OD^{Sample}}{OD^{DMSO}} \times 100\%$$

Equation 3.8: Cytotoxicity equation using crystal violet absorbance

The OD^{DMSO} and OD^{Sample} is the absorbance at 595 nm after background correction with the blank well. . OriginPro8 program/software was used to generate graphs and the log[compound] (x-axis) and % cytotoxicity (y-axis) was used to illustrate the IC_{50} value

3.2.4 IC_{50} charts and analysis

The following cytotoxicity results correspond to the 1-benzoylferrocene derivatives used in the modified Crystal Violet protocol previously described (section 3.2.2) to determine a cytotoxicity graph and IC_{50}. Two cell lines were selected to complete these studies: Immortal cervical cancer cells (HeLa) (Figures 3.20-3.25) and a primary ovarian cancer with epithelial morphology cells (CaOV3) (Figures 3.26-3.30). Two cell lines were chosen to as they are different types of cancer to determine their potential as a broad chemotherapies.

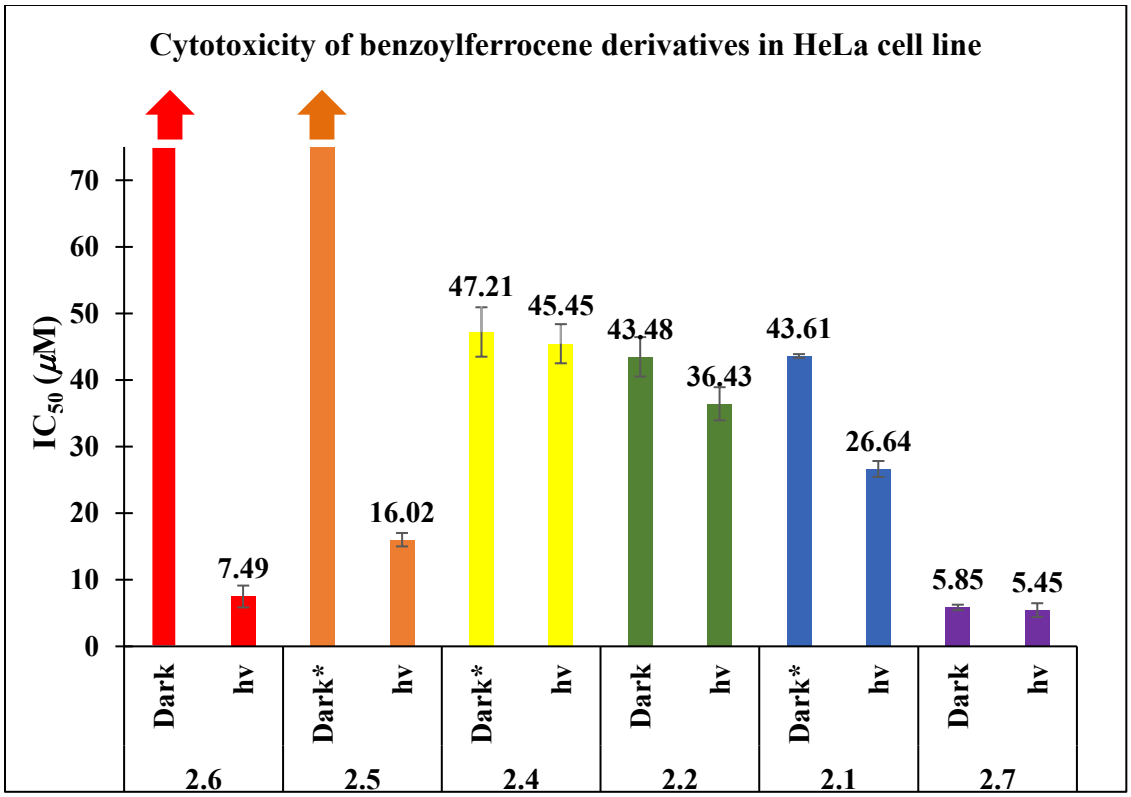

Figure 3.7: Cytotoxicity of benzoylferrocene derivatives in HeLa cell line

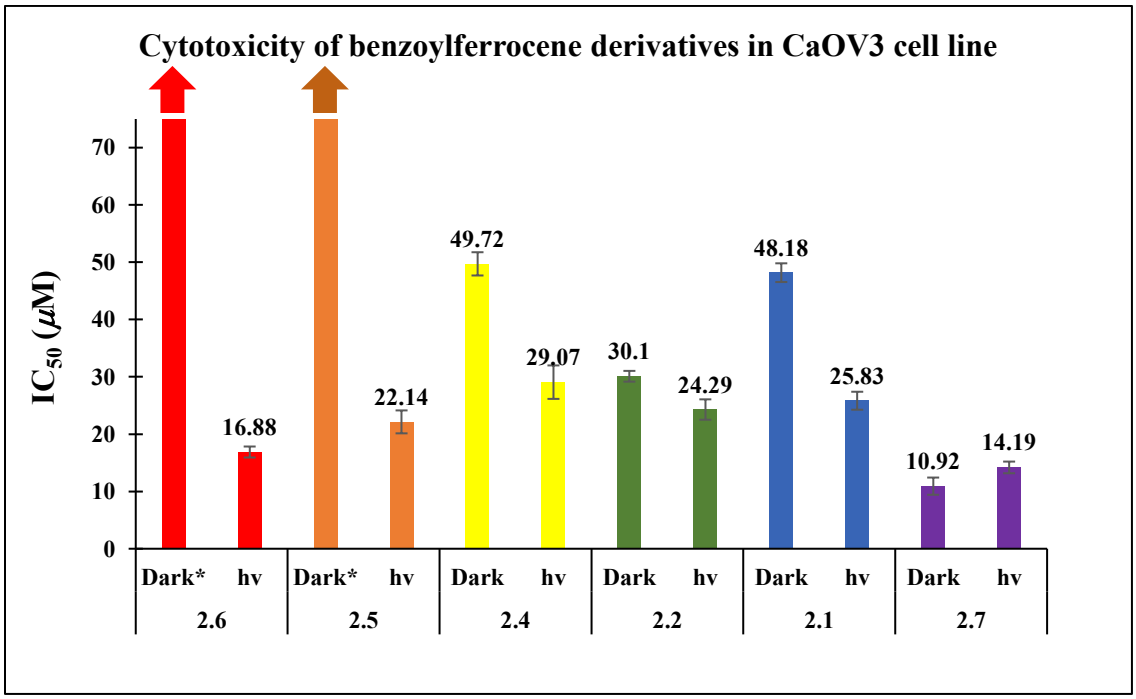

Figure 3.8: Cytotoxicity of benzoylferrocene derivatives in CaOV3 cell line

In order to calculate the PDT efficacy, the dark is divided by the light IC_{50} and the higher the value the more efficient the PDT. From the PDT values it can be concluded the functional group of the 1-benzoylferrocene derivatives is highly dependent on the compound potency and specificity as a photodynamic therapy (PDT).

Compound **2.7** was the most potent but did not have significant PDT efficacy for either HeLa and CaOV3 cell lines. Phosphonium salts have been proven to be mitochondrial targets because they are positively charged, and the inner mitochondrion has a negative charge gradient.[71-74] The mitochondrion's negative charge derives from the electrochemical gradient of protons across the inner membrane, which drive ATP synthesis for oxidative phosphorylation for the production of energy in the cell.[75] This compound proved to be a potent but not effective PDT as it likely was localized in the mitochondrial matrix.

Compound **2.4** showed a PDT efficacy in CaOV3 at 1.6 but not in the HeLa cell line. This could suggest that the ethyl group may have a better binding affinity to the CaVO3 cells. The HeLa cell line could have limited PDT efficacy due to a plethora of binding sources within or on the surface of the HeLa cell line, therefore inhibiting its light cytotoxicity. Compound **2.2** also had no significant dark and light cytotoxicity difference in both HeLa and CaOV3 cell lines.

The compound **2.1** had a cytotoxicity of 43.6 μM in the dark condition and 26.6 μM in the light condition in the HeLa cell line. Compound **2.1** had a 1.8 difference of dark and light cytotoxicity at 48.2 μM and light at 25.8 μM for a difference of 1.9, similar to that of compound **2.4** in CaOV3 cell line. The differences between dark and light cytotoxicity in the **2.1** and **2.4** suggest that there is a PDT cytotoxicity mechanism, not what would be desired for a PDT.

As a general trend, the more lipophilic the compound, the more cytotoxic and specific the PDT. This was observed for compounds **2.5** and **2.6.** Compound **2.5** has an IC_{50} in HeLa cells at 16.0 μM in the light and more significant than tested at 100.0 μM for dark versus the light difference of > 6.25. The

compound **2.6** had double the dark and light different at > 13.3 with dark and light cytotoxicity > 100 μM and 7.5 μM. HeLa cell line did not display significant dependence due to the low potency of compound **2.4**.

Compound **2.6** had higher cytotoxicity and specificity than a currently used anti-cancer PDT Photofrin® compound **1.4**. Photofrin® is photo-activated at 530 nm and 610 nm and has a different efficacy at ~3 between light and dark in human epidermoid carcinoma cells (A431) and 12.5 μM in HeLa cell line.[25, 76]

3.2.5 NCI60 screen and analysis

To assess whether benzoylferrocene derivatives were effective in various cancer cell types the compound **2.6** was sent to the US National Cancer Institute (NCI) to be tested in a 60 human tumor cell line anticancer drug screen (NCI60). The NCI60 is utilized as an *in vitro* drug-discovery tool in lieu of using animal models for anticancer drug screening. [77, 78] Compound **2.6** was shown to be ineffective in the dark condition in a one dose-response curve (Figure 3.8). These data confirm previous dark cytotoxicity data demonstrating minimal cytotoxic effect in the dark condition. Compound **2.6** was reported a decrease in cancer cell growth, meaning a more potent compound, in a variety of leukemia cancer cells. Using 10 μM of compound **2.6** resulted in a growth percentage of 49.81% in K-562 and at 55.6% and 56.8% in MOLT-4 and RPMI-8226. Limited growth percentage was observed in pancreatic cancer PC-3 at 56.8. Future studies will aim to determine the therapeutic potential of benzoylferrocene derivatives against leukemia. A leukemia photodynamic therapy could be promising as blood can be filtered from the body to induce photolysis without the need of photolyzing the body. Further mechanisms could be completed to protect the healthy cells of unwanted cytotoxicity with clinically used iron inhibitors, as will be discussed in the following section.

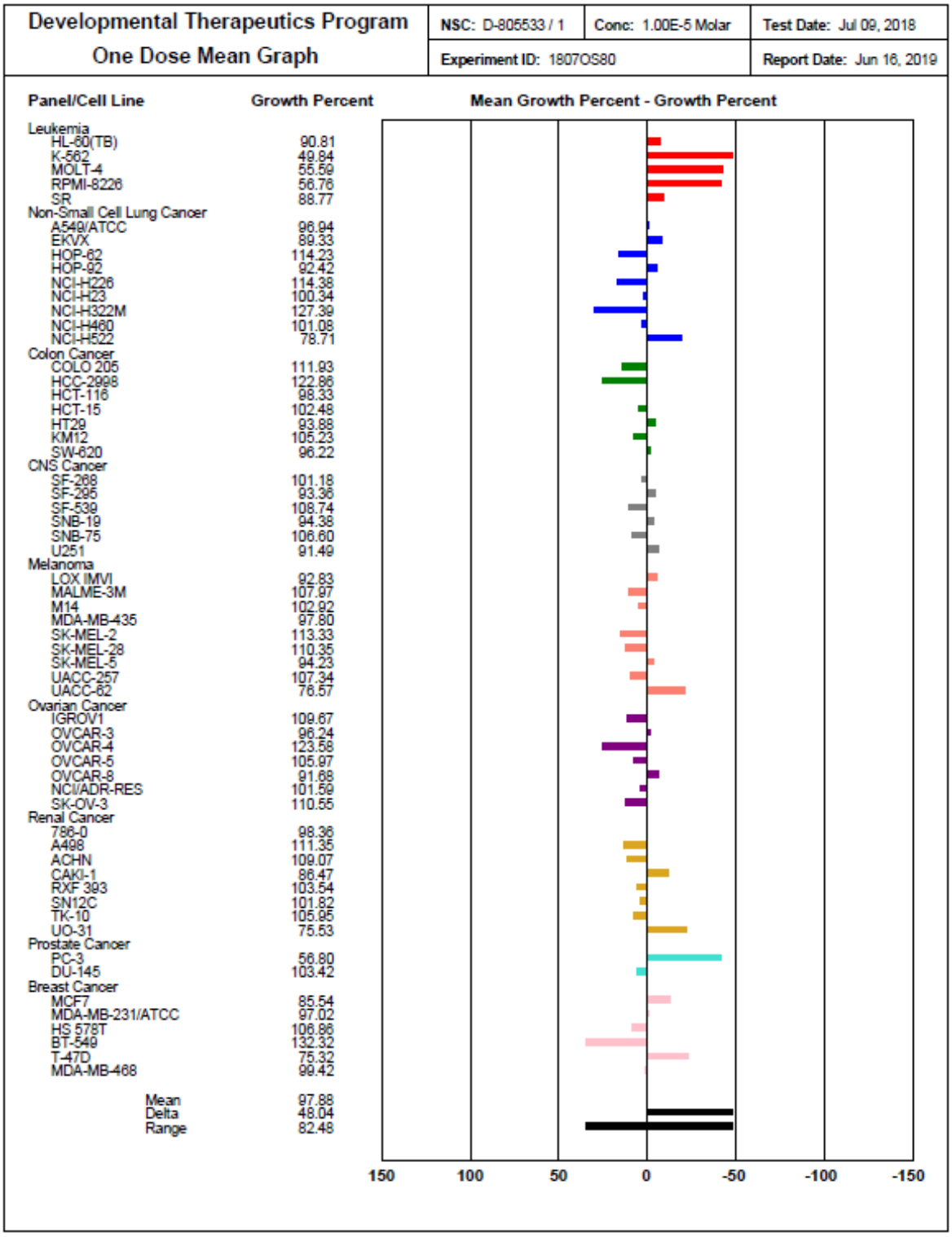

Figure 3.9: NCI60 One Dose Mean Graph

3.2.6 Iron binding studies

We next determined if the cytotoxicity of the benzoylferrocene derivatives was due to the organic cyclopentadiene or the release of iron(II) and oxidation to ferric iron through the Fenton reaction, (Figure 3.1 and Figure 3.2). A ferric specific chelator of Deferoxamine mesylate (DFO) was utilized to determine if cytotoxicity was due to the release of iron(II) (Figure 3.11).[79-83] DFO is a specific ferric chelator as it has a binding affinity of 10^{31}, 10^{17} greater than that of Cu^{2+} and even more significant than that of ferric iron. [79] Due to the oxidation state that DFO binds, it would indicate if the release of iron(II) and oxidization to ferric iron is toxic to cells.

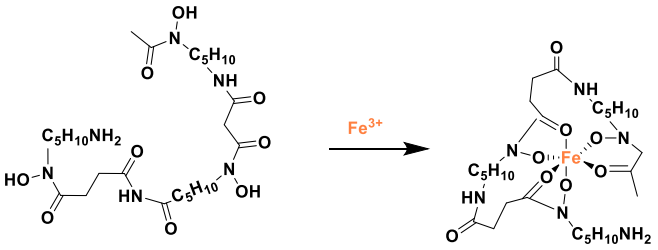

Figure 3.10. Deferoxamine mesylate binding iron(III)

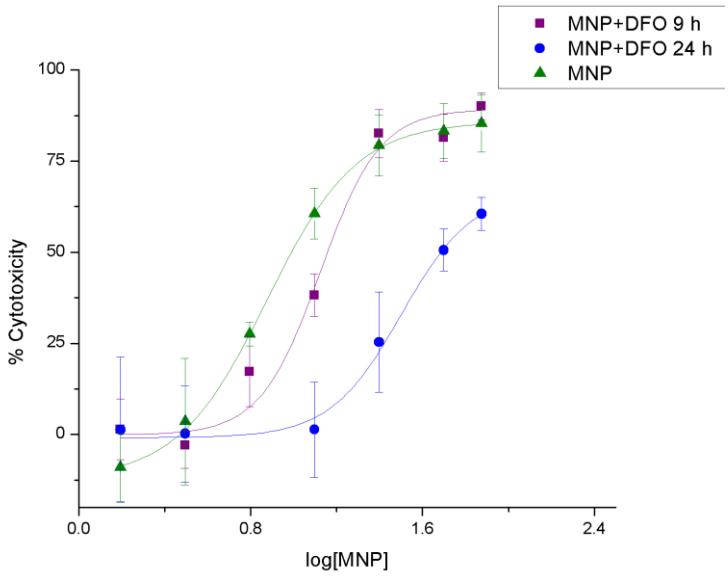

Figure 3.11: Cytotoxicity graph of 2.6 and DFO time points

Studies were done to determine DFO cytotoxicity in the HeLa cell line, and 50 μM was used for the chelation studies. Multiple time points were completed with the addition of 50 μM DFO (Figure 3.12). Original IC_{50} of **2.6** without DFO was 7.5 μM and after 9 h incubation of 50 μM DFO, the IC_{50} doubled to 13 μM. The addition of DFO at the same time as compound **2.6** altered the IC_{50} at 50 μM more than 7 times the original cytotoxicity. This study suggests the release of iron(II) induces cytotoxicity. A previous lab member, Marissa Aubrey, additionally tested this hypothesis and found no cytotoxic effect of pre-photolyzed benzoylferrocene derivatives in HeLa cells, suggesting that the cyclopentadiene is not inducing cell death.[84] It is hypothesized that the dark cytotoxicity could be due to the low oxidation potential, as discussed in chapter 2 (Figure 2.3). The oxidation potential of 0.5 μM GSH was found to be -0.16 in HeLa cell line.[85] The oxidation peak potential at 0.580 V was found for 1.0 mM or 10.0 mM GSH, which would be enough to oxidize the benzoylferrocene derivatives and induce cell death. [85]

3.2.7 Flow cytometry of ROS generation and proposed of benzoylferrocene derivatives

To better understand the cytotoxicity mechanism of the mono-substituted 1-benzoylferrocenes, flow cytometry was performed to determine localization of ROS generation within the cell. To complete these studies, two types of fluorophores were utilized, a cytosolic specific flourophore and a lipid specific phuorophore. Cytosolic ROS was studied through 2',7'-dichlorofluorescein diacetate(DCFH-DA). DCFH-DA is not active until it crosses the cell membrane. After it crosses the cell membrane it is de-esterified intracellularly, oxidized and ROS activated (Figure 3.13). [86-90].

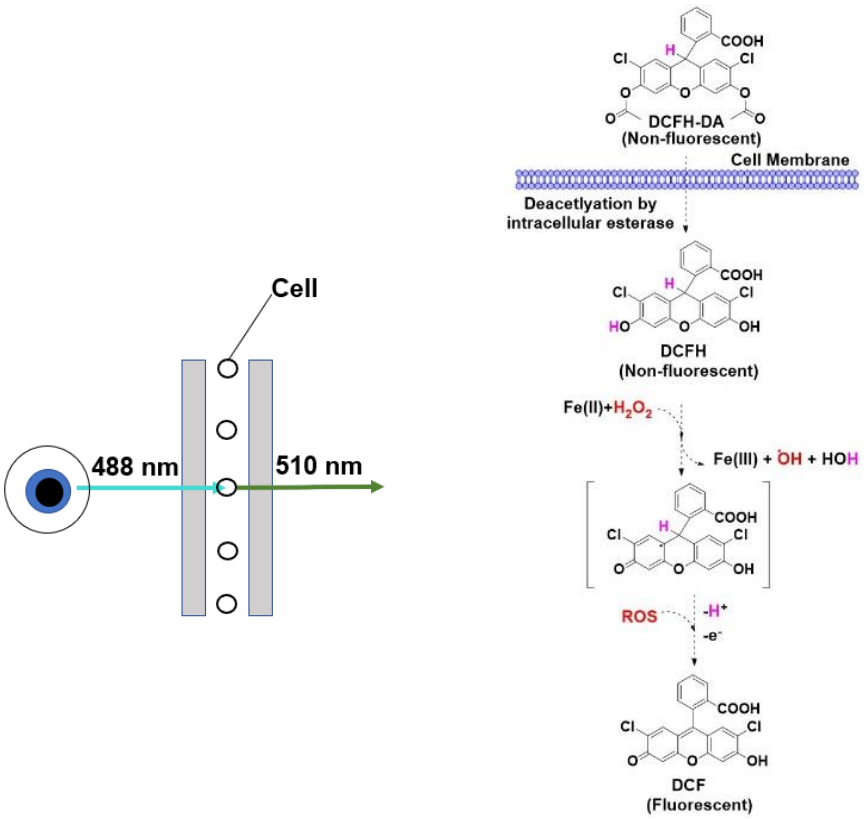

Figure 3.12: Flow cytometry with fluorophore 2',7'-dichlorofluorescein diacetate, and its reaction within the cell to initiate a fluorescent probe

Compound **2.1** displayed a dose dependence increase of cytosolic ROS in HeLa cells, as shown in Figure 3.14. Interestingly, the dose-dependence increase between light and dark are at different concentrations, which agrees with the cytotoxicity data of dark IC_{50} of 44 μM and light IC_{50} of 27 μM. As the concentration of compound **2.1** increases (37.5 μM Figure 3.14) the survival rate significantly decreases therefore an overall fluorescence decreases for the photolyed cells. This is illustrated in the cytotoxicity graphs in Figure 3.20 and Figure 3.25 as the cells are close to a 0% survival rate.

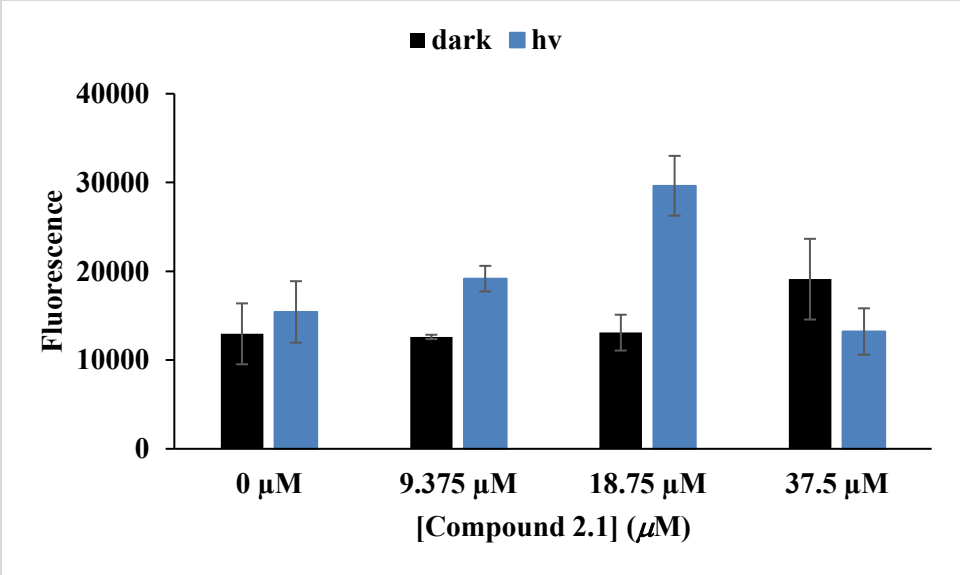

Figure 3.13: Compound 2.1 flow cytometry data with fluorophore DCHF-DA

Compound **2.6** was also studied and found to have cytosolic ROS indicated by the increase of fluorescence at the high doses (Figure 3.15). Compounds **2.6** had diminished fluorescence at high cytotoxicity due to the limited number of cells; this can also be explained from its cytotoxicity graph in Figure 3.24 and Figure 3.30, as it displayed a plateau in cytotoxicity around 80% at higher concentrations for both dark and light conditions. It was also noticed that both the dark and the light concentrations had high concentrations of cytosolic ROS.

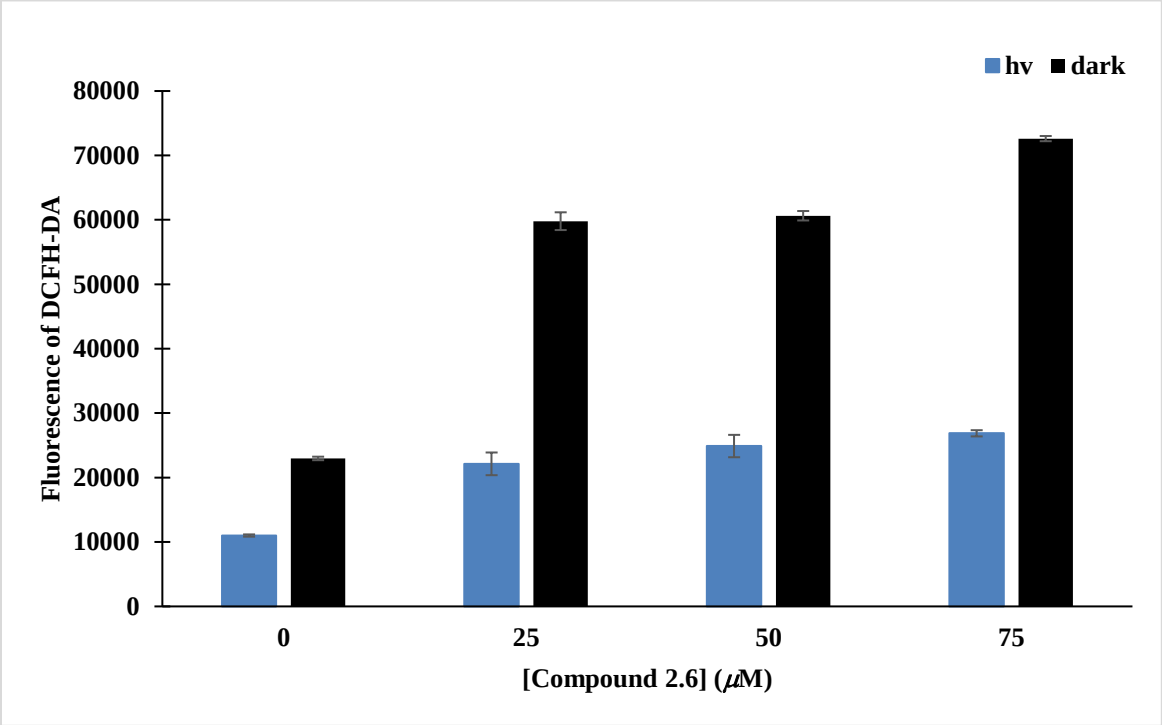

Figure 3.14: Compound 2.6 DCFH-DA fluorescence after 1 h light activation and dark

This difference suggested compound **2.6** was either less toxic than **2.1** or that it may have a different mechanism. To test this, another fluorophore was utilized, C-11 BODIPY 581/591, a lipid peroxidation indicator (Figure 3.16). This fluorophore has been used in a variety of studies to test ferroptosis as a mechanism of cytotoxicity.[91-94]

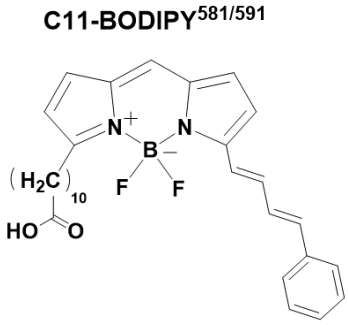

Figure 3.15: C-11 BODIPY$^{581/591}$

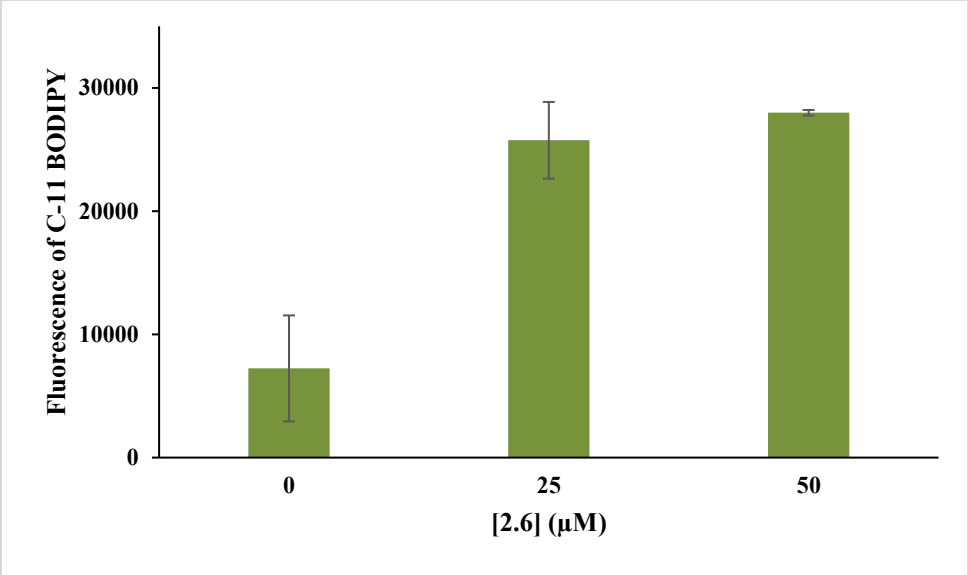

Figure 3.16: C-11 BODIPY lipid ROS fluorophore and 2.6

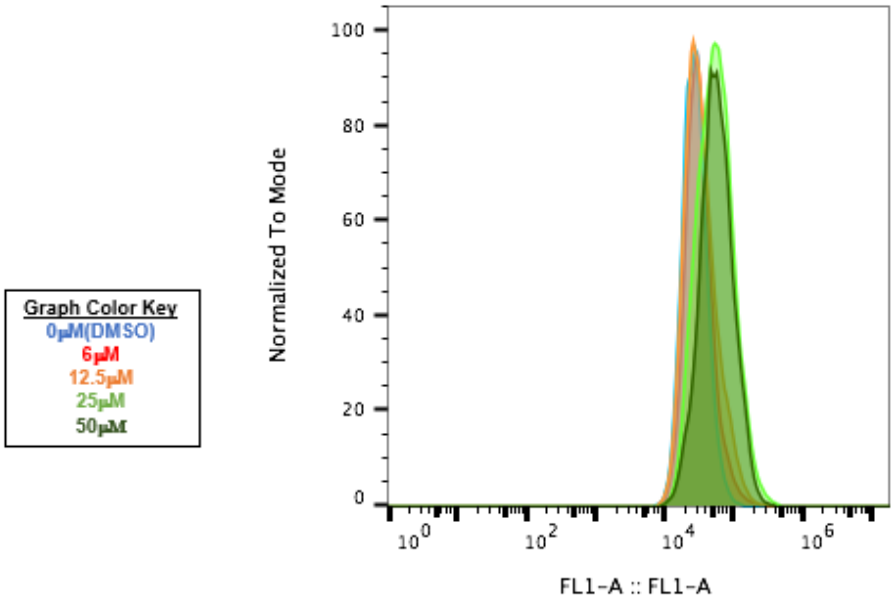

Figure 3.17: Dark BODIPY treated with compound 2.6

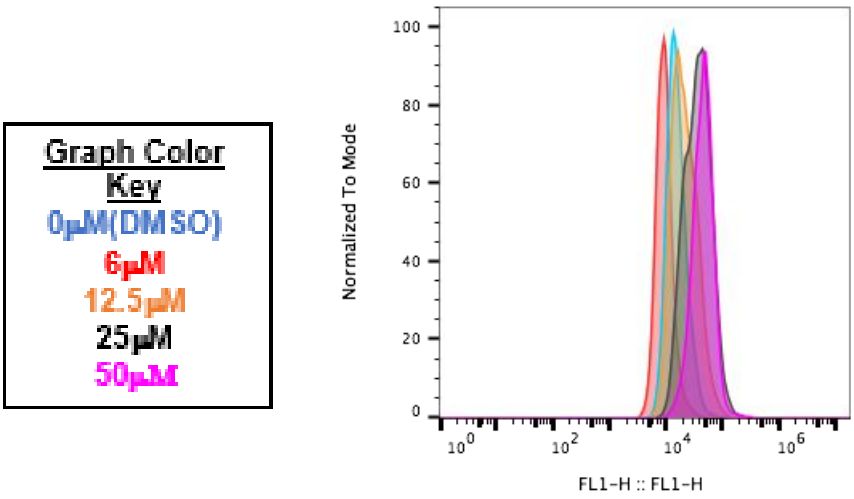

Figure 3.18: Photolyzed 1 h photolysis BODIPY treated with 2.6 at high concentrations

Flow cytometry experiments using C-11 BODIPY 581/591 demonstrated that compound **2.6** induced high concentrations of lipid peroxidation, even at lower concentrations than its IC_{50}. Additionally compound **2.6** demonstrated high concentration of cytotosolic ROS. These result suggest that ferroptosis may be induced through the photoactivation of iron(II) of benzoylferrocene.

Overall these experiments report a high ROS increase of both cytosolic and lipid ROS within induced cancer cells. This may suggest a dual cell death mechanism through apoptosis and ferroptosis. In order to conclude future studies should be completed to determine upregulation of apoptosis and or ferroptosis inducing proteins.

3.3 Supplemental Information

1. HeLa IC_{50} graphs

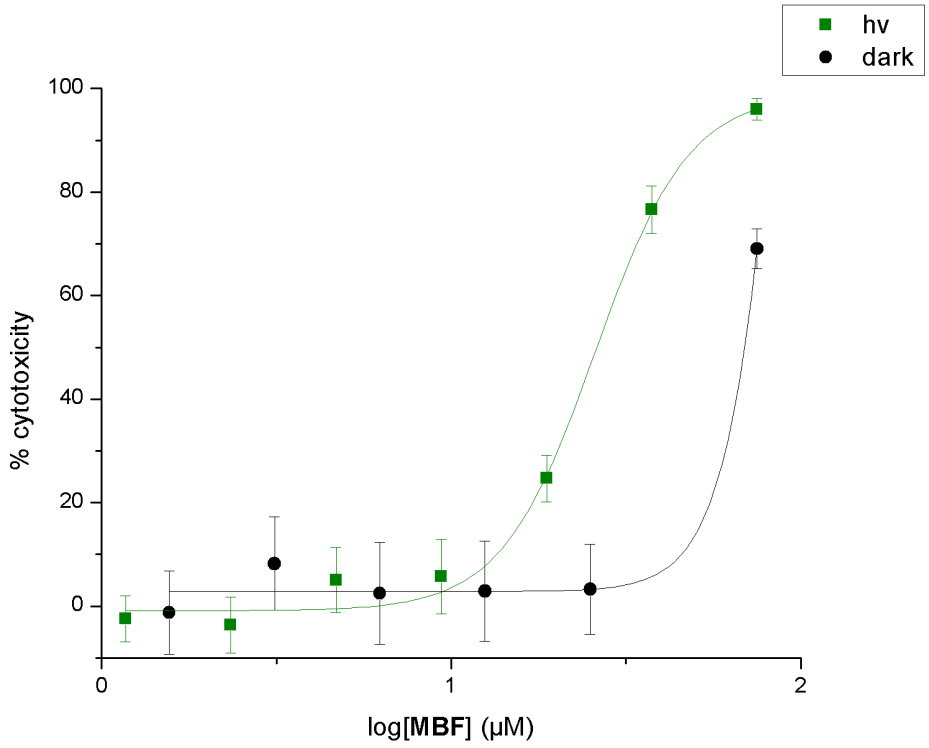

Figure 3.19: HeLa % cytotoxicity graph of 2.1 in the dark and photoactivated

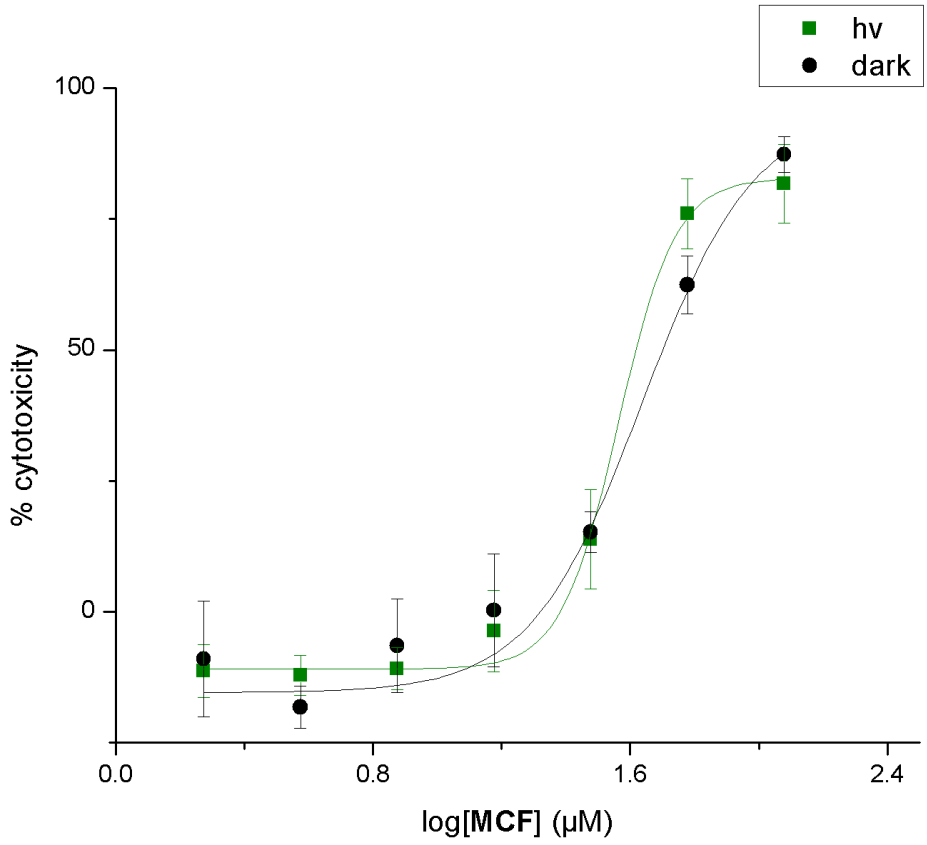

Figure 3.20: HeLa % cytotoxicity graph of 2.2 in dark and photoactivated

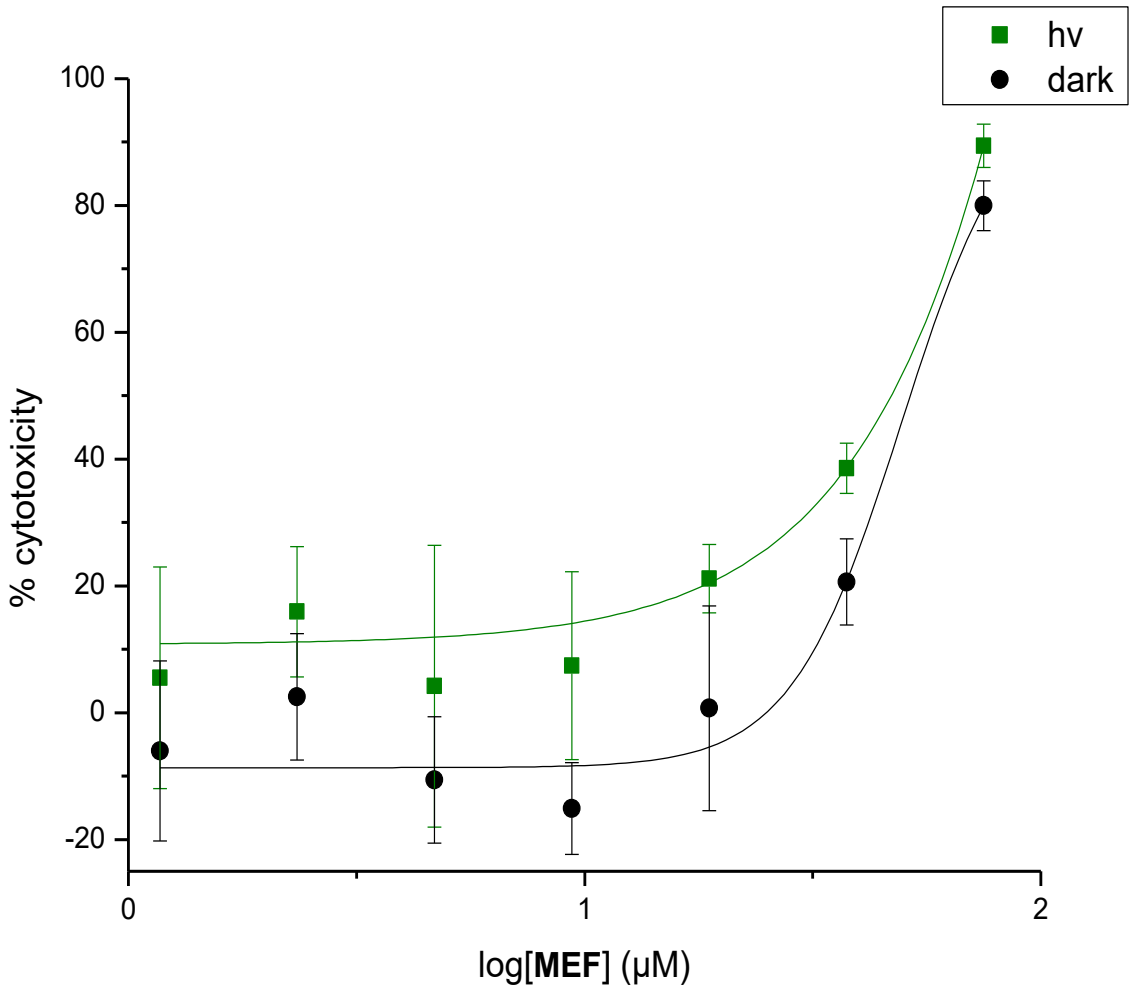

Figure 3.21: HeLa % cytotoxicity graph of 2.4 in dark and photoactivated

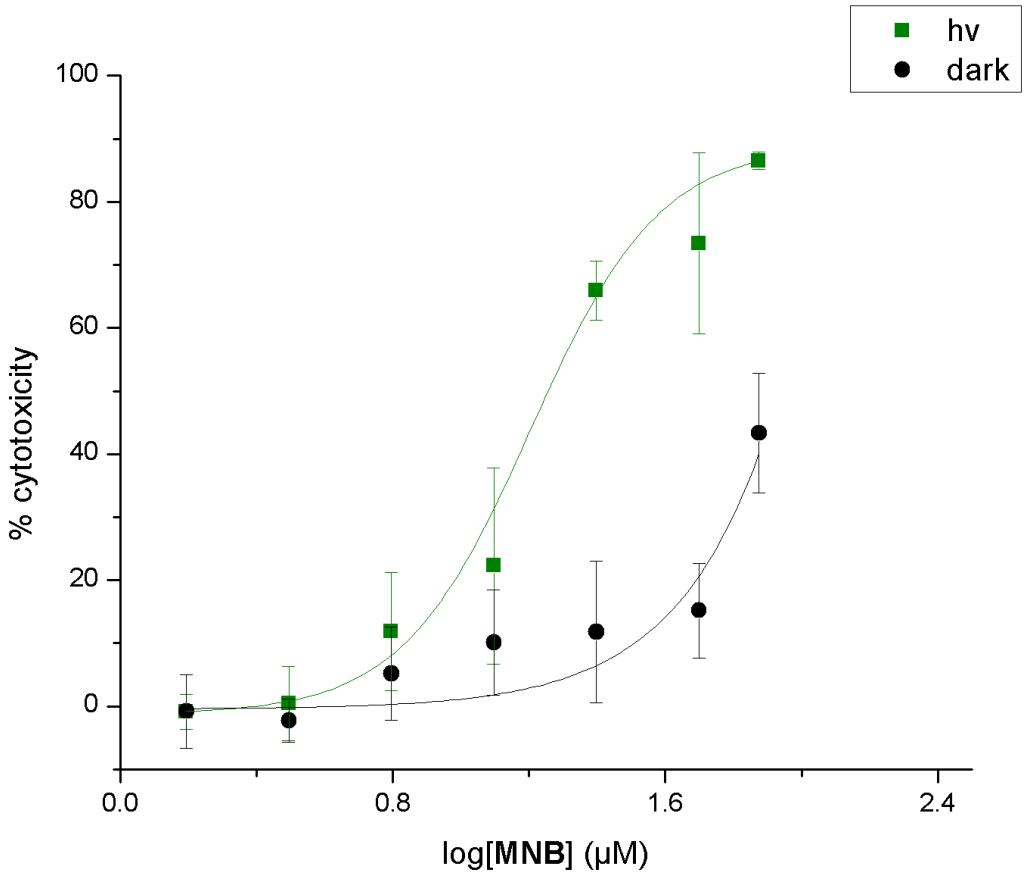

Figure 3.22: HeLa % cytotoxicity graph of 2.5 in dark and photoactivated

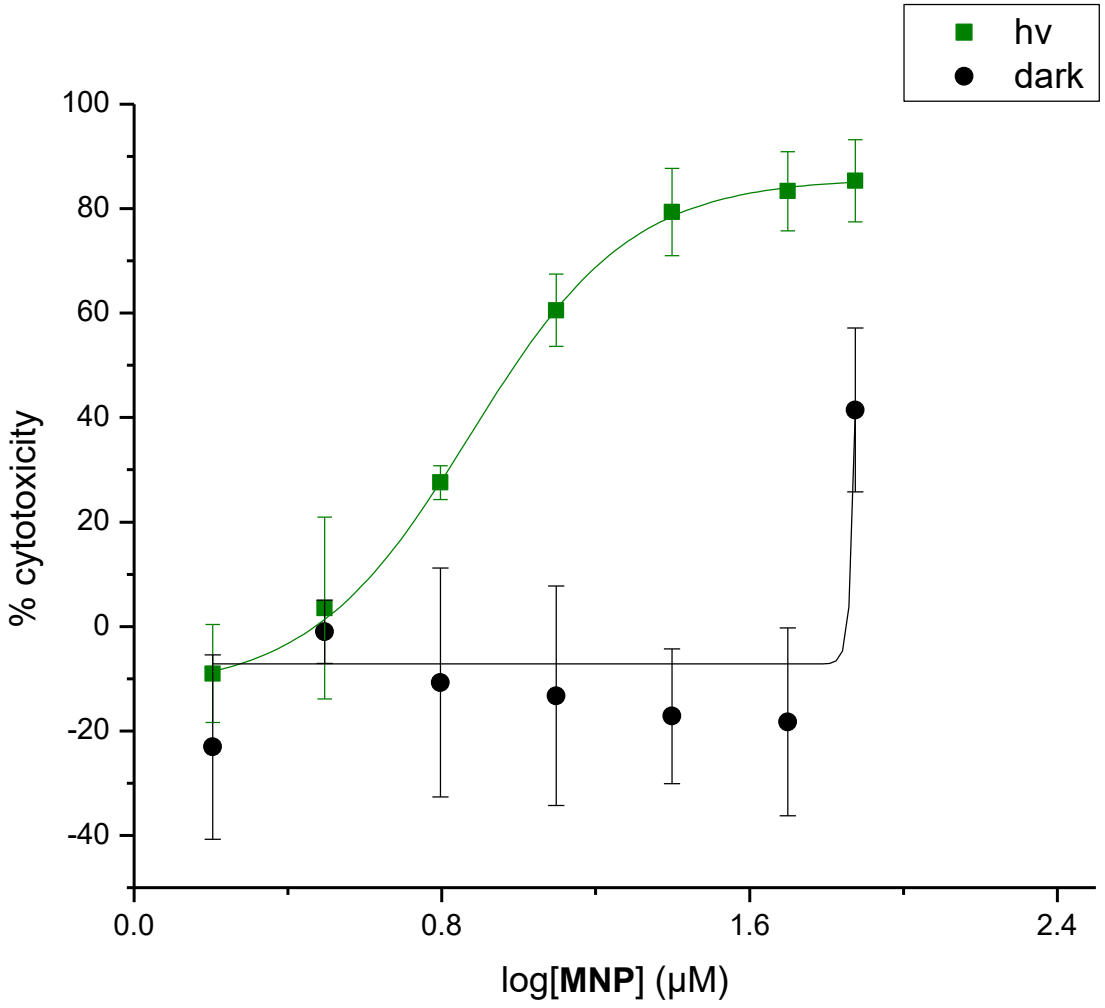

Figure 3.23: HeLa % cytotoxicity graph of 2.6 in dark and photoactivated

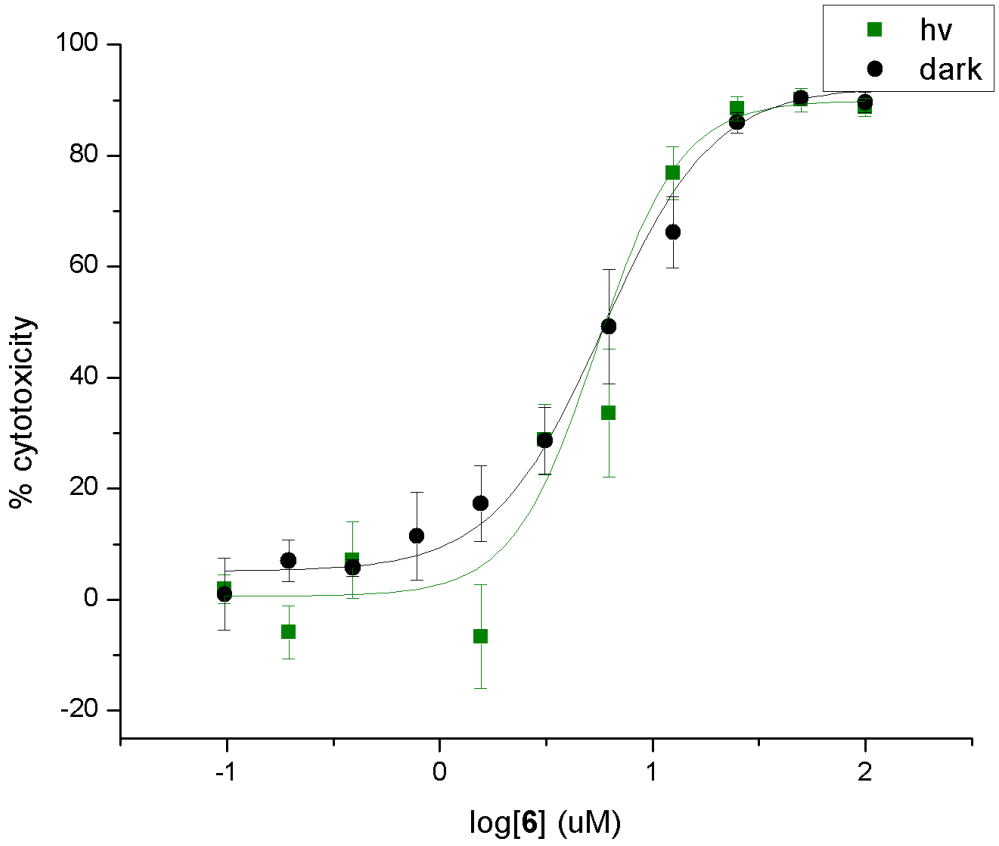

Figure 3.24: HeLa % cytotoxicity graph of 2.7 in dark and photoactivated

1. CaOV3 IC_{50} graphs

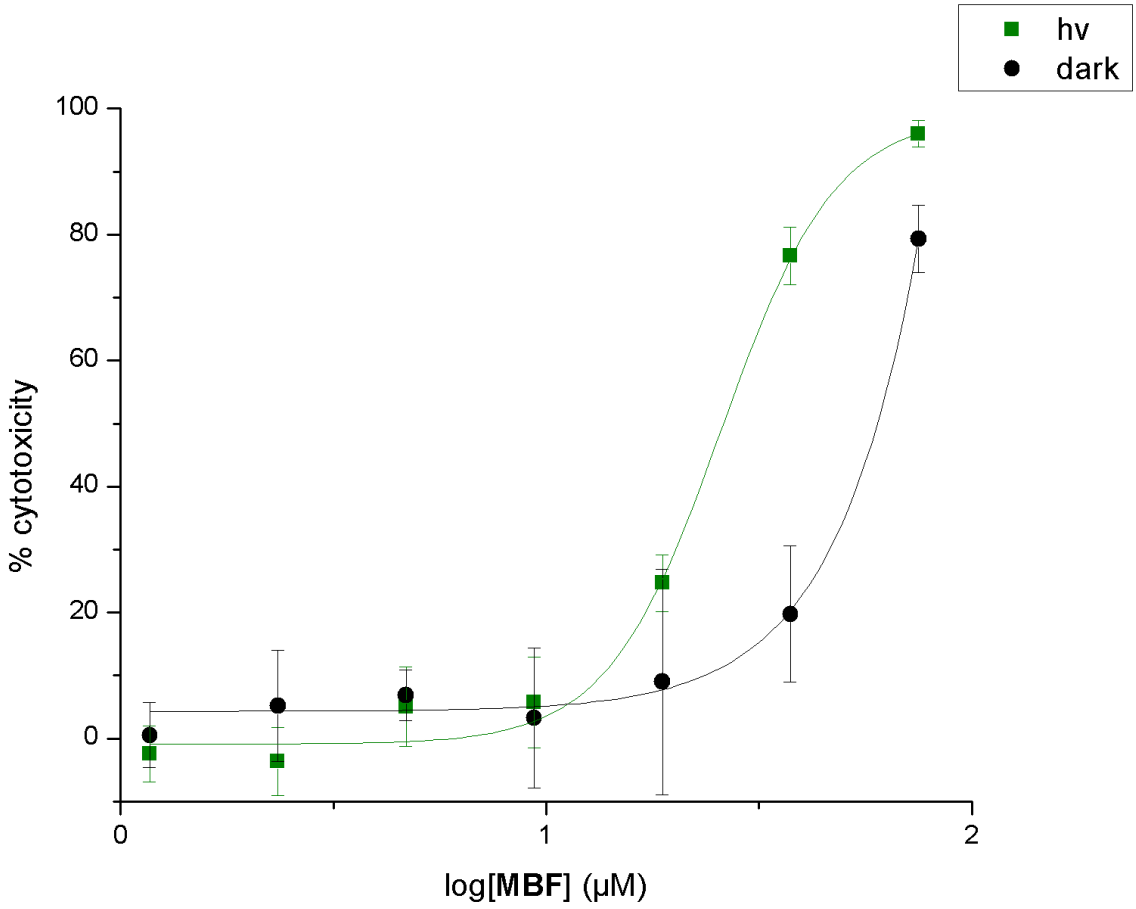

Figure 3.25: CaOV3 % cytotoxicity graph of 2.1 dark and photoactivated

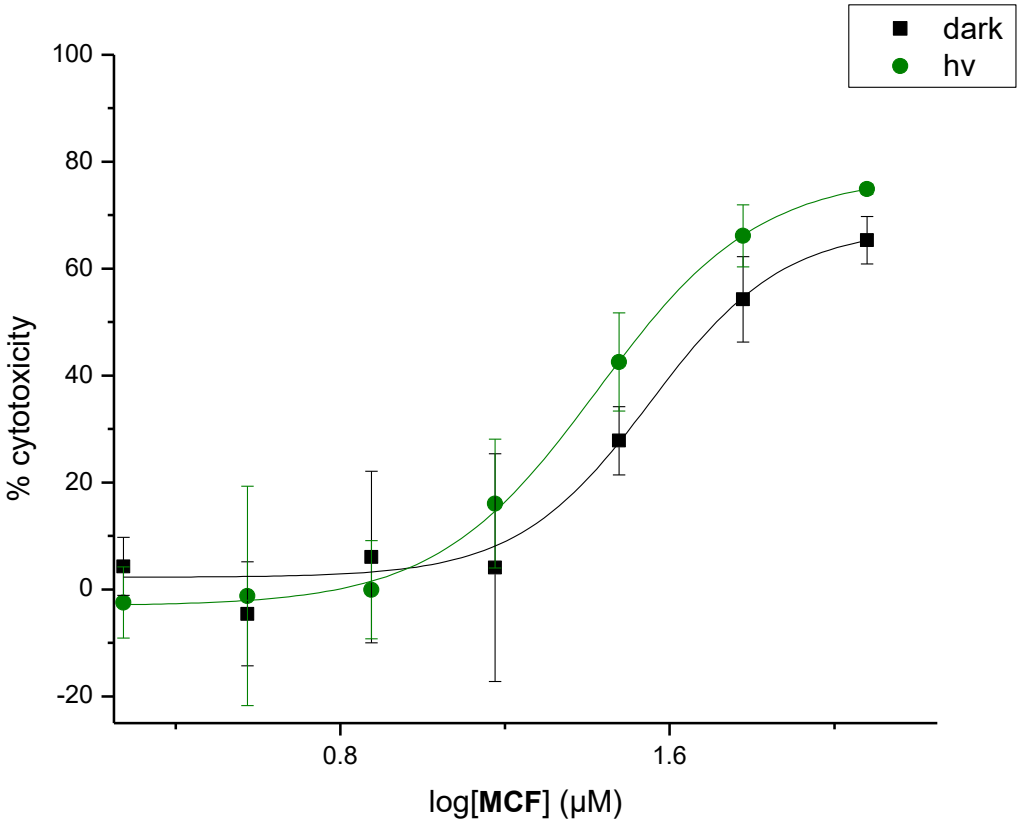

Figure 3.26: CaOV3 % cytotoxicity graph of 2.2 dark and photoactivated

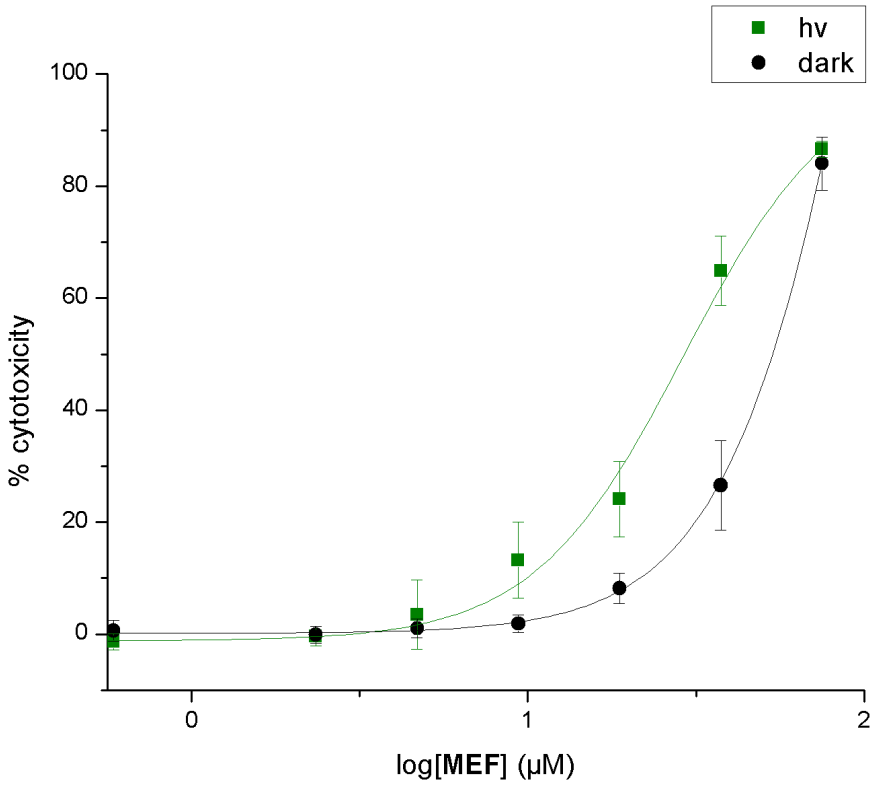

Figure 3.27: CaOV3 % cytotoxicity graph of 2.2 dark and photoactivated

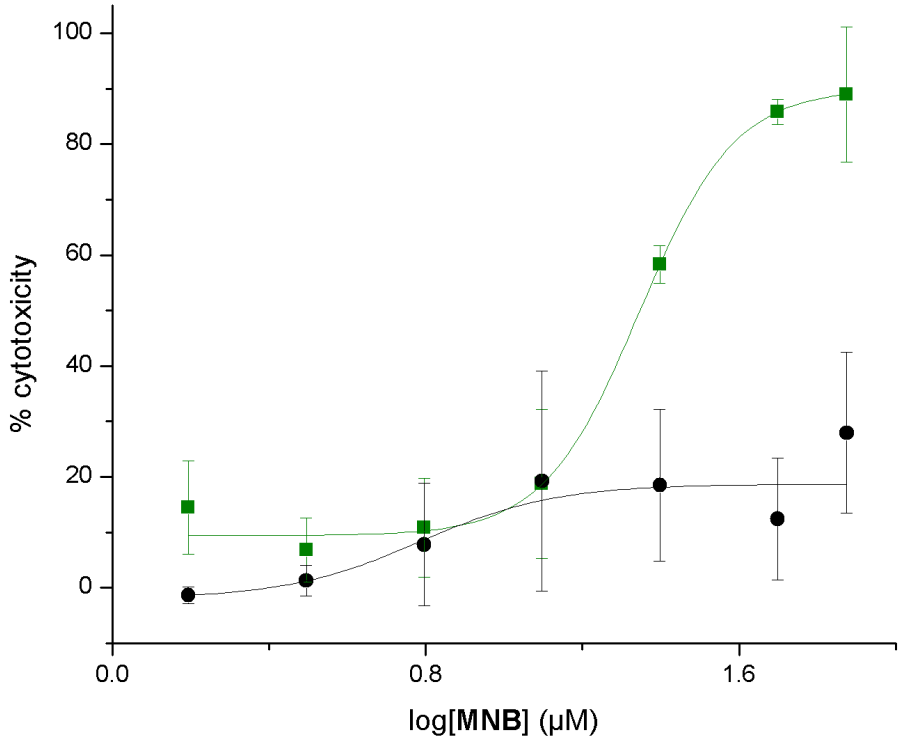

Figure 3.28: CaOV3 % cytotoxicity graph of 2.5 dark and photoactivated

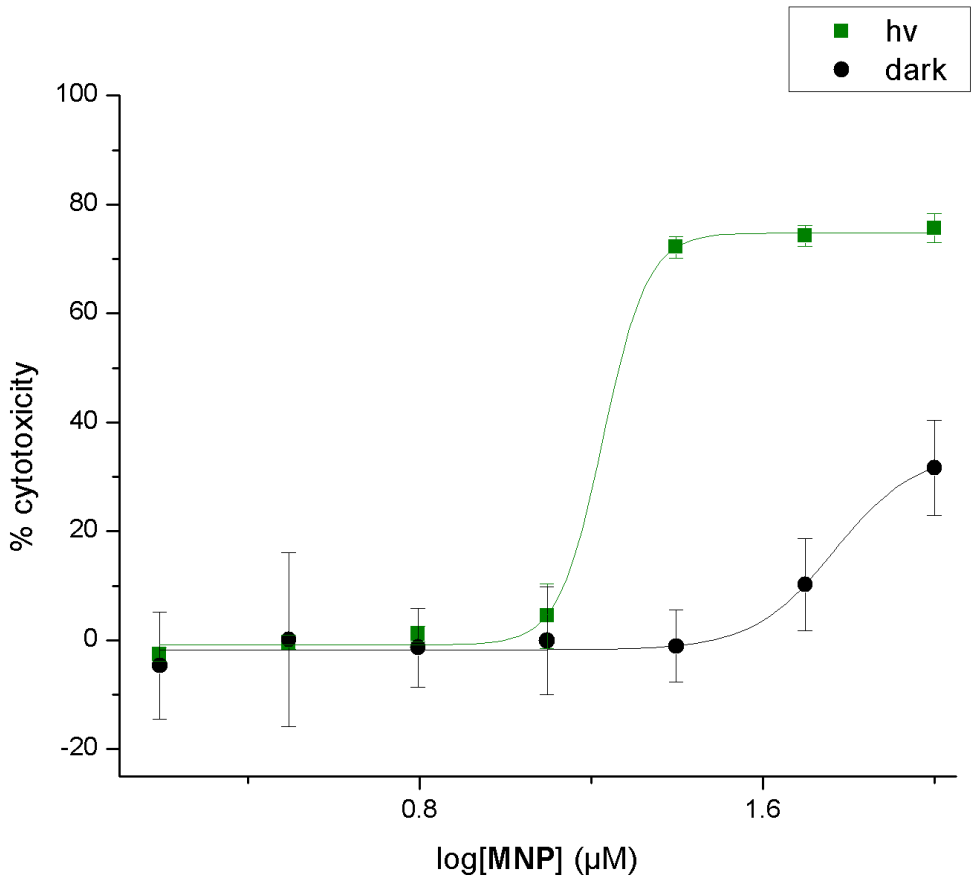

Figure 3.29: CaOV3 % cytotoxicity graph of 2.6 dark and photoactivated

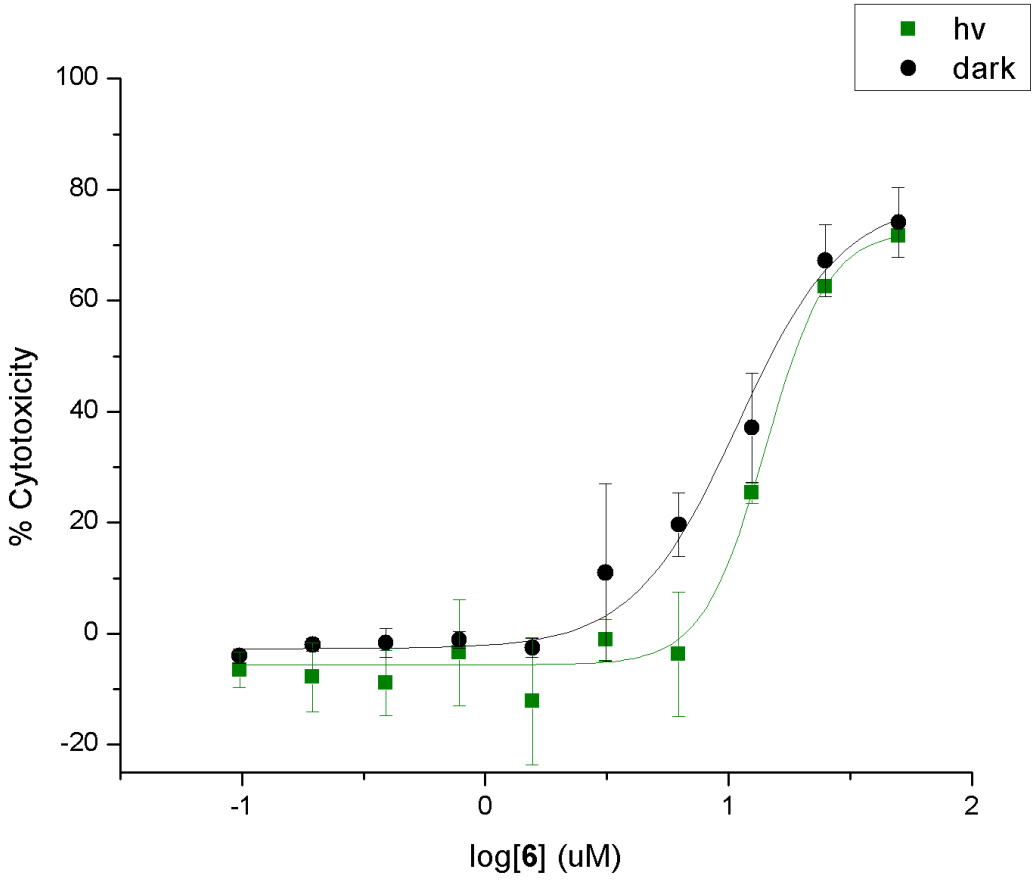

Figure 3.30: CaOV3 % cytotoxicity graph of 2.7 dark and photoactivated

3.4 Chapter 3 References

64. Viswanathan, V. S.; Ryan, M. J.; Dhruv, H. D.; Gill, S.; Eichhoff, O. M.; Seashore-Ludlow, B.; Kaffenberger, S. D.; Eaton, J. K.; Shimada, K.; Aguirre, A. J.; Viswanathan, S. R.; Chattopadhyay, S.; Tamayo, P.; Yang, W. S.; Rees, M. G.; Chen, S.; Boskovic, Z. V.; Javaid, S.; Huang, C.; Wu, X.; Tseng, Y. Y.; Roider, E. M.; Gao, D.; Cleary, J. M.; Wolpin, B. M.; Mesirov, J. P.; Haber, D. A.; Engelman, J. A.; Boehm, J. S.; Kotz, J. D.; Hon, C. S.; Chen, Y.; Hahn, W. C.; Levesque, M. P.; Doench, J. G.; Berens, M. E.; Shamji, A. F.; Clemons, P. A.; Stockwell, B. R.; Schreiber, S. L., Dependency of a therapy-resistant state of cancer cells on a lipid peroxidase pathway. *Nature* **2017,** *547* (7664), 453-457.

65. Fenton, H. J. H., LXXIII.—Oxidation of tartaric acid in presence of iron. *Journal of the Chemical Society, Transactions* **1894,** *65* (0), 899-910.

66. Kopppenol, W. H., The Centennial of the Fenton Reaction. *Free Rad Biol Med* **1993,** *15*, 6.

67. Phelan, M. C., Basic techniques in mammalian cell tissue culture. *Curr Protoc Cell Biol* **2007,** *Chapter 1* (1), Unit 1 1.

68. Incorporated, B., Crystal Violet Cell Cytotoxicity Assay Kit. In *BioVision*, BioVision, Ed. Milpitas, CA, Vol. Catalog # K329-1000.

69. Abcam, ab232855 Crystal Violet Assay Kit (Cell viability). 1 ed.; Abcam, Ed. 2018; Vol. ab232855.

70. Feoktistova, M.; Geserick, P.; Leverkus, M., Crystal Violet Assay for Determining Viability of Cultured Cells. *Cold Spring Harb Protoc* **2016,** *2016* (4), pdb prot087379.

71. Bachowska, B.; Kazmierczak-Baranska, J.; Cieslak, M.; Nawrot, B.; Szczesna, D.; Skalik, J.; Balczewski, P., High Cytotoxic Activity of Phosphonium Salts and Their Complementary Selectivity towards HeLa and K562 Cancer Cells: Identification of Tri-n-butyl-n-hexadecylphosphonium bromide as a Highly Potent Anti-HeLa Phosphonium Salt. *ChemistryOpen* **2012,** *1* (1), 33-8.

72. Battogtokh, G.; Choi, Y. S.; Kang, D. S.; Park, S. J.; Shim, M. S.; Huh, K. M.; Cho, Y.-Y.; Lee, J. Y.; Lee, H. S.; Kang, H. C., Mitochondria-targeting drug conjugates for cytotoxic, anti-oxidizing and sensing purposes: current strategies and future perspectives. *Acta Pharmaceutica Sinica B* **2018,** *8* (6), 862-880.

73. Sasmal, P. K.; Streu, C. N.; Meggers, E., Metal complex catalysis in living biological systems. *Chemical Communications* **2013,** *49* (16), 1581-1587.

74. Alta, R. Y. P.; Vitorino, H. A.; Goswami, D.; Terêsa Machini, M.; Espósito, B. P., Triphenylphosphonium-desferrioxamine as a candidate mitochondrial iron chelator. *BioMetals* **2017,** *30* (5), 709-718.

75. Mitchell, P., Chemiosmotic coupling in oxidative and photosynthetic phosphorylation. *Biol Rev Camb Philos Soc* **1966,** *41* (3), 445-502.

76. Berlanda, J.; Kiesslich, T.; Engelhardt, V.; Krammer, B.; Plaetzer, K., Comparative in vitro study on the characteristics of different photosensitizers employed in PDT. *Journal of Photochemistry and Photobiology B: Biology* **2010,** *100* (3), 173-180.

77. Shoemaker, R. H., The NCI60 human tumour cell line anticancer drug screen. *Nat Rev Cancer* **2006,** *6* (10), 813-23.

78. Selby, M.; Delosh, R.; Laudeman, J.; Ogle, C.; Reinhart, R.; Silvers, T.; Lawrence, S.; Kinders, R.; Parchment, R.; Teicher, B. A.; Evans, D. M., 3D Models of the NCI60 Cell Lines for Screening Oncology Compounds. *SLAS DISCOVERY: Advancing Life Sciences R&D* **2017,** *22* (5), 473-483.

79. Keberle, H., The Biochemistry of Desferrioxamine and Its Relation to Iron Metabolism. *Ann N Y Acad Sci* **1964,** *119* (119), 758-68.

80. Manning, T., Iron Chelators in Medicinal Applications - Chemical Equilibrium Considerations in Pharmaceutical Activity. *Curr Med Chem* **2009,** *16* (19), 2416-1429.

81. Hatcher, H. C.; Singh, R. N.; Torti, F. M.; Torti, S. V., Synthetic and natural iron chelators: therapeutic potential and clinical use. *Future Med Chem* **2009,** *1* (9), 1643-70.

82. Yu, Y.; Gutierrez, E.; Kovacevic, Z.; Saletta, F.; Obeidy, P.; Rahmanto, Y. S.; Richardson, D. R., Iron Chelators for the Treatment of Cancer. *Current Medicinal Chemistry* **2012,** *19* (17), 2689-2702.

83. Yu, Y.; Richardson, D. R., Cellular iron depletion stimulates the JNK and p38 MAPK signaling transduction pathways, dissociation of ASK1-thioredoxin, and activation of ASK1. *J Biol Chem* **2011,** *286* (17), 15413-27.

84. Aubrey, M. Organoferrous Antitumor Agents. UC San Diego, UC San Diego, 2015.

85. Zhao, L.; Zhao, L.; Miao, Y.; Zhang, C., Selective electrochemical determination of glutathione from the leakage of intracellular GSH contents in HeLa cells following doxorubicin-induced cell apoptosis. *Electrochimica Acta* **2016,** *206*, 86-98.

86. Marchesi, E. R., E.; Fann, Y. C.; Chignell, C. F.; Mason, R. P., Photoreduction of the fluorescent dye 2V-7V-dichlorofluorescein: a spin trapping and direct electron spin resonance study with implications for oxidative stress measurements. . *Free Radic. Biol. Med.* **1999,** *26*, 148– 161.

87. Rota, C. C., C. F.; Mason, R. P. , Evidence for free radical formation during the oxidation of 2V-7V-dichlorofluorescin to the fluorescent dye 2V-7V-dichlorofluorescein by horseradish peroxidase: possible implications for oxidative stress measurements. *Free Radic. Biol. Med.* **1999,** *27*, 873-881.

88. Ischiropoulos, H. G., A.; Thom, S. R.; Kooy, N. W.; Royall, J. A.; Crow, J. P. , Detection of reactive nitrogen species using 2,7-dichlorodihydrofluorescein and dihydrorhodamine 123. *Methods Enzmol.* **1999,** *301*, 367–373.

89. C. Rota, Y. C. F., R. P. Mason, Phenoxyl free radical formation during the oxidation of the fluorescent dye 2V,7V-dichlorofluorescein by horseradish peroxidase: possible consequences for oxidative stress measurements. . *J. Biol. Chem 274*, 28161–28168.

90. Winterbourn, C. C., The challenges of using fluorescent probes to detect and quantify specific reactive oxygen species in living cells. *Biochim Biophys Acta* **2014,** *1840* (2), 730-8.

91. Dixon, S. J.; Lemberg, K. M.; Lamprecht, M. R.; Skouta, R.; Zaitsev, E. M.; Gleason, C. E.; Patel, D. N.; Bauer, A. J.; Cantley, A. M.; Yang, W. S.; Morrison, B., 3rd; Stockwell, B. R., Ferroptosis: an iron-dependent form of nonapoptotic cell death. *Cell* **2012,** *149* (5), 1060-72.

92. Wu, D.; Chen, L., Ferroptosis: a novel cell death form will be a promising therapy target for diseases. *Acta Biochim Biophys Sin (Shanghai)* **2015,** *47* (10), 857-9.

93. Yang, W. S.; Stockwell, B. R., Ferroptosis: Death by Lipid Peroxidation. *Trends Cell Biol* **2016,** *26* (3), 165-176.

94. Xie, Y.; Hou, W.; Song, X.; Yu, Y.; Huang, J.; Sun, X.; Kang, R.; Tang, D., Ferroptosis: process and function. *Cell Death And Differentiation* **2016,** *23*, 369.

Chapter 4 Cytotoxicity Studies of 1-Benzoylferrocene Derivatives and Proposed Cytotoxicity Mechanism

4.1 Anti-cancer Cytotoxicity of 1,1′-Dibenzoylferrocene Derivatives

As 1-benzoylferrocene derivatives displayed potential as photodynamic compounds against cancer, the 1,1′-dibenzoylferrocene derivatives were subsequently studied to determine their potential as a therapy. It is hypothesized that the photo-release of free iron(II) from benzoylferrocene derivatives would be more efficient due to high oxidative potential. These compounds are postulated to elevate ROS levels from the generation from iron-catalyzed cycling of the Fenton and Haber Weiss reactions. [64-66]

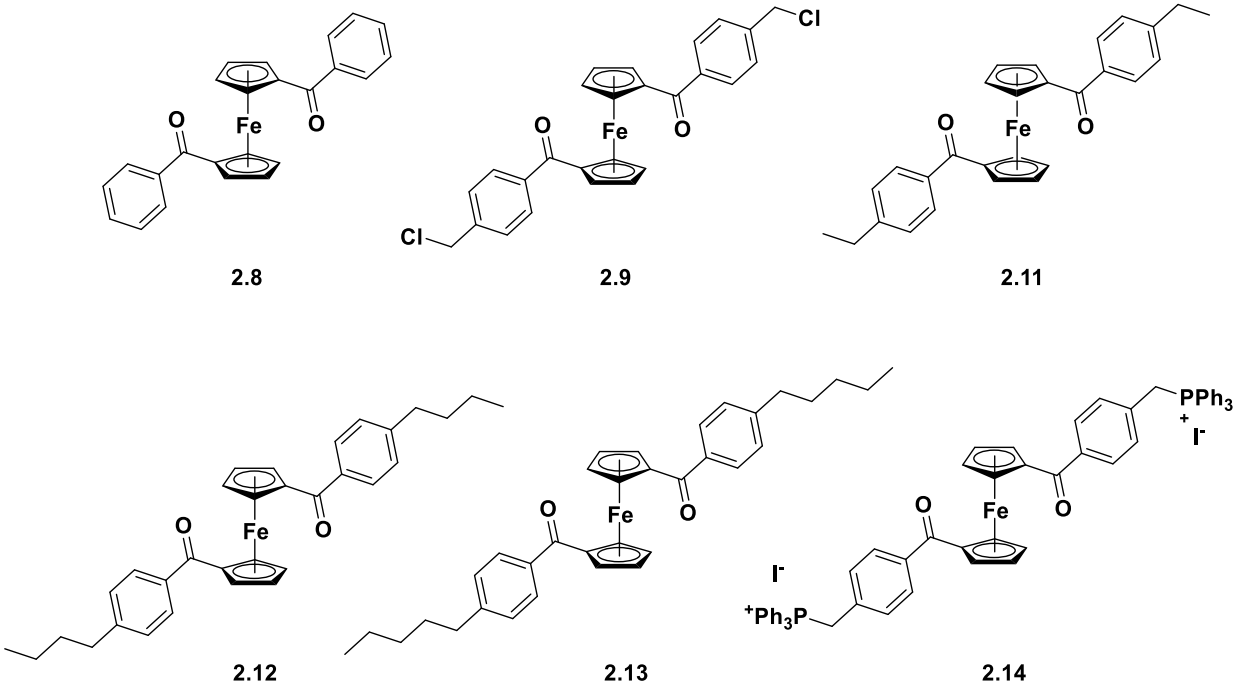

Figure 4.1: Chemical structures of the 1,1′-Dibenzoylferrocene derivatives tested *in vitro*

Similarly, to the 1-benzoylferrocene derivatives in chapter 3, 1,1'-dibenzoyl ferrocenes cytotoxicity was studied *in vitro* in both HeLa and CaOV3 cell lines. Crystal violet dye was used as a histological stain to determine cytotoxicity through the proliferation of treated cell wells at various concentrations. Technical duplicate of a biological triplicate was studied to create all cytotoxicity graphs of

HeLa cell line (Figure 4.25-4.30**),** and CaOV3 (Figures 4.31-4.36). Bar graphs of all dark and light cytotoxicity were generated for HeLa, (Figure 4.2), and CaOV3 (Figure 4.4).

4.1.1 HeLa cytotoxicity

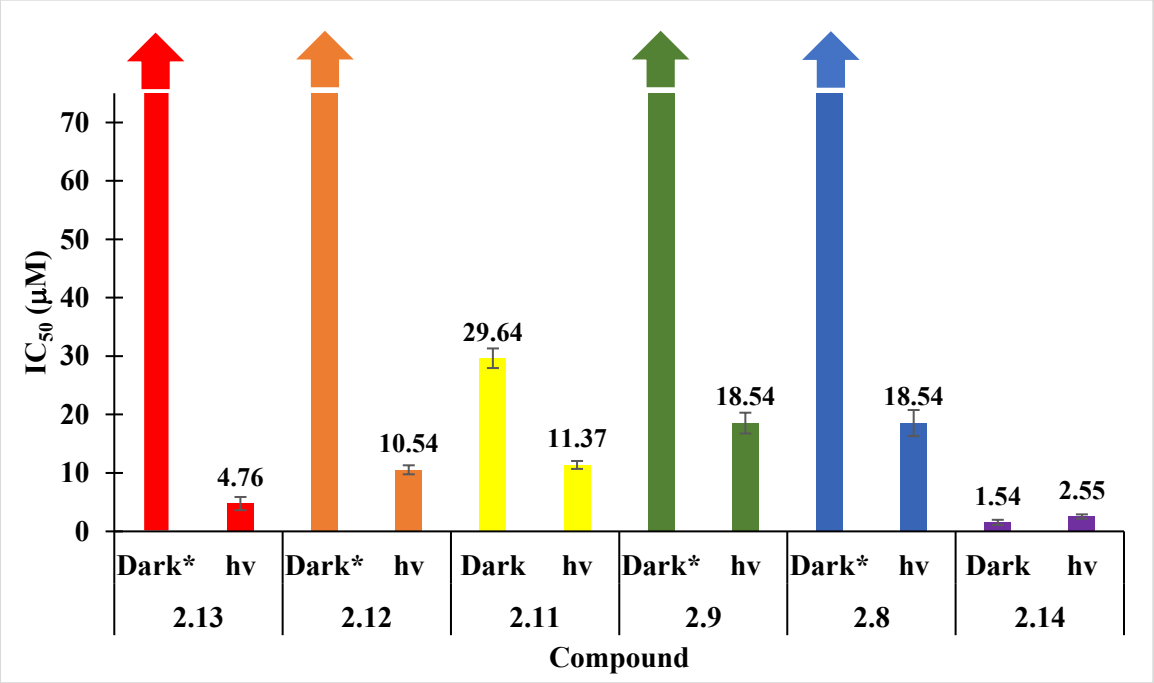

Figure 4.2: HeLa IC_{50} graph of 1,1′-dibenzoylferrocene derivatives in both dark and 3h photolyzed conditions

All derivatives displayed high cytotoxicity in the HeLa cell line after photolysis and displayed no significant cytotoxicity in the dark up to solubility, except **2.11**. The data reported that **2.11** has dark cytotoxicity at 29.64 μM, and the light was 11.37 μM cytotoxicity, which affects it's photodynamic (PDT) efficacy to be the weakest of the bis-substituted derivatives, which is calculated to be **2.6**. Other PDT efficacies (the difference between dark and light cytotoxicity) were more significant than 4.04-15.75 because all dark cytotoxicity was higher than tested. The highest difference in PDT efficacy, was **2.13** as it was more significant than 15.75, which is the most specific and one of the most potent PDT of the benzoylferrocene derivatives. Also, as a similar trend to its mono-substituted derivates, the higher the lipophilicity, the more potent the compound. **2.8** and **2.9** displayed light cytotoxicity of 18.54 μM, which suggests that they contain similar cytotoxicity mechanism and likely due to it is limited compared to other

bis-substituted derivatives. As the compounds contain a higher carbon content, the more potent the complex is due to its increased lipophilicity. Also, the phosphonium derivative similarly to the mono-substituted, **2.13** was twice as potent as **2.12**. **2.14** displayed a similar trend as previously described in the monosubstituted derivative as it displayed no PDT efficacy, even more surprisingly the dark was slightly more potent than the light.

4.1.2 CaOV3 Cytotoxicity

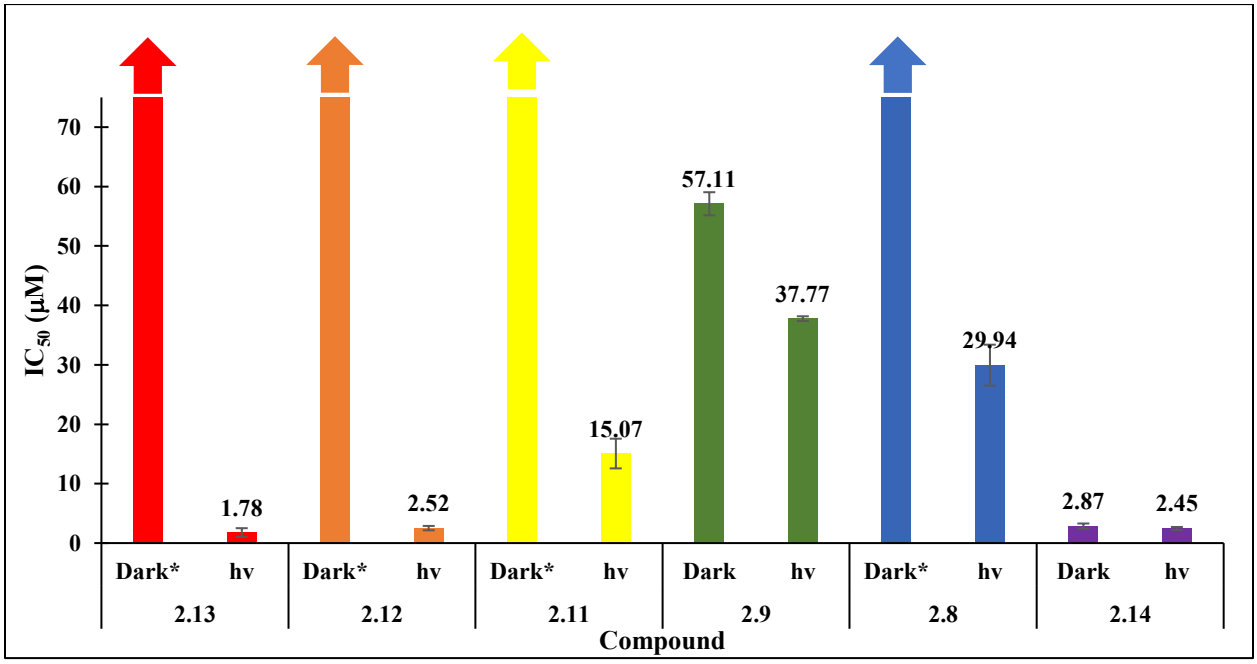

Figure 4.3: IC_{50} graph of 1,1′-dibenzoylferrocene derivatives in CaOV3 with dark and 3h photolyzed conditions

To determine if the trends of cytotoxicity would be consistent with two cell lines, CaOV3 was tested. CaOV3 displayed very similar trends as HeLa: more lipophilicity the more potent. Differing from the HeLa cytotoxicity studies, **2.9** proved to have low efficacy as a PDT with a difference of dark and light at 1.5 with dark and light IC_{50} at 57.11 μM and 37.11 μM. Also, **2.9** displayed less light cytotoxicity than the **2.8** at 29.94 μM. Phosphonium salt derivative **2.14** proved to keep with the previous trending of high potency but no PDT efficacy on either cell line. This trend further indicates that the mitochondrial target

was successful as a target but lost all specificity as a PDT. This trend was seen throughout all cell lines, spanning both the mono and bis-substituted derivative **2.14** and **2.7**.

Similarly, to the HeLa the cell line there were similar trends of lipophilicity correlated to cytotoxicity as **2.13** was the most cytotoxic at 1.78 μM. Compound **2.12** derivative that was seen in both the cell lines to have half the cytotoxicity of **2.13**. Throughout the studies of the 1,1′-dibenzoylferrocene derivatives, **2.13** proved to be the most potent PDT of the small group of molecules and went on to further testing.

4.2 NIH 60 Cancer One Dose Mean Graph

To assess the variability and versatility of the potent 1,1′-dibenzoylferrocene derivatives, Compound **2.13**, investigation of cytotoxicity in various cancer types were considered, similar to experiment carried out on compound 2.6 in chapter 3. Compound **2.13** was sent to the US National Cancer Institute (NCI) for the 60 human tumor cell line anticancer drug screen (NCI60). [77, 78] Similarly to **2.6,** Compound **2.13** was determined not cytotoxic enough to perform further studies past the one dose-response curve, (Figure 4.6). The NCI60 assay results for compound **2.13** in the dark was found to be 10 μM. This supports previous dark cytotoxicity data that it would have little to no cytotoxic effect, but **2.13** is less toxic in the dark than **2.6** as most cell lines had a growth percentage above the control. Unfortunately, no accommodations could be made to induce light to determine cytotoxicity in the light with the 60 cancer cell lines.

Despite this, leukemia cancer cell lines proved to be the only cell lines showing cytotoixic effect of **2.13**. From the introduction of 10 μM of **2.13,** there was a significant inhibition of growth percentage cell lines K-562 at 38.23%, MOLT-4 at 47.30% and the most inhibited growth in CCRF-CEM at 5.52%. Some leukemia cell lines had no significant inhibition of cell growth in HL-60(TB) at 98.35%, ROPMI-8226 at 81.81% and SR at 90.11%.

Based upon the above results, it can be concluded that the dark cytotoxicity is limited in **2.13,** and furthermore could contain more potency in the light as a specific and potent PDT therapy. This shows promise for future studies to determine its potential as a leukemia anti-cancer agent. A leukemia photodynamic therapy could be useful as blood can be filtered from the body to induce photolysis. Further mechanisms could be completed to protect the healthy cells of unwanted cytotoxicity with clinically used iron inhibitors, as shown in the next section.

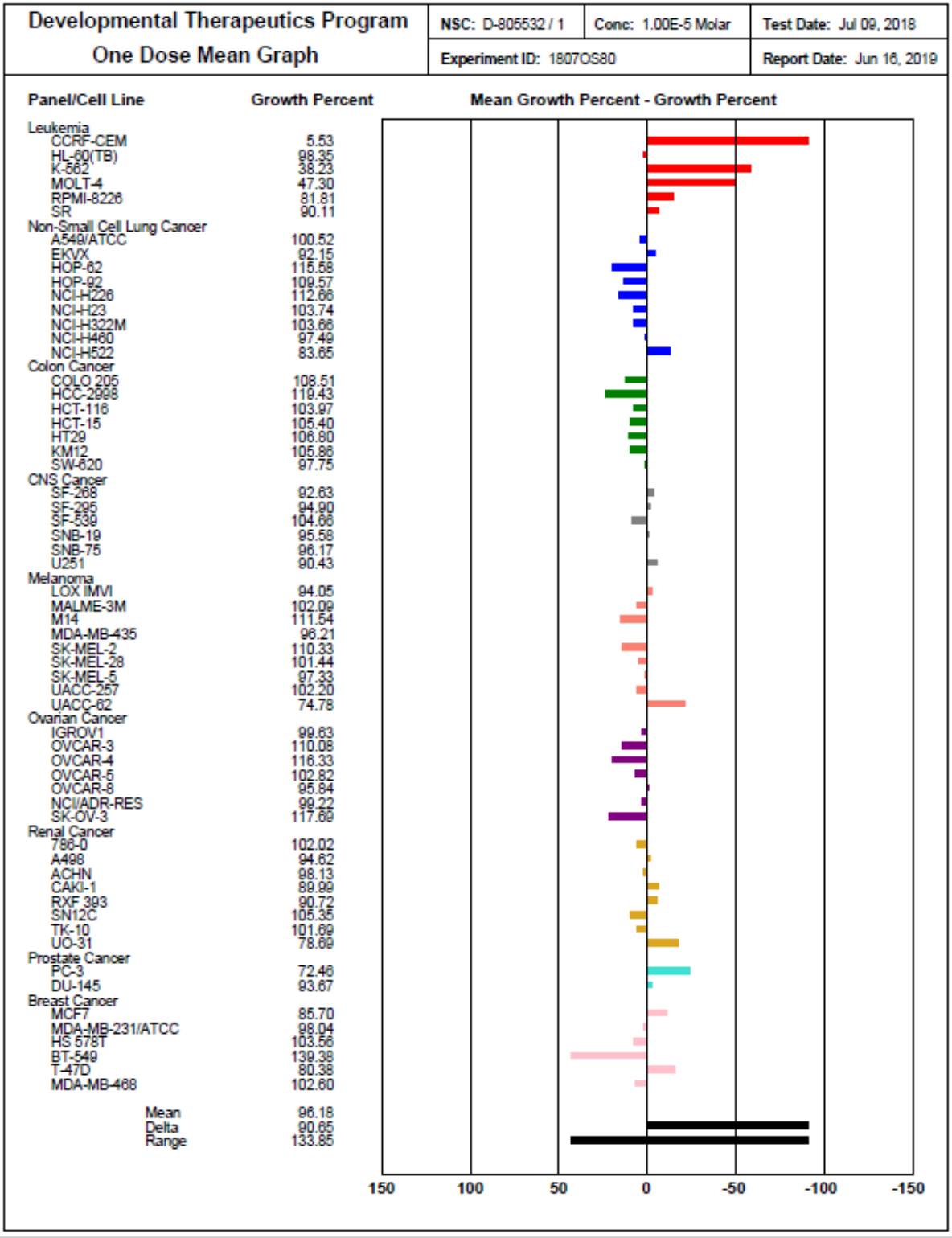

Figure 4.4: NCI60 dark cytotoxicity test

4.3 Ferric Iron Chelation Experiments

To determine the cytotoxicity of the compounds, chelation experiments were carried out with deferoxamine (DFO) in the HeLa cell line similarly to chapter 3 for compound **2.13**. The cytotoxicity was inhibited by dosing the 96 well plates with various concentrations of compound **2.13** with 50 uM of DFO before photolysis. After dosing with DFO, there was less than 10% cell death (Figure 4.4), which is similar to the dark cytotoxicity. Additionally, the CaOV3 cell line displayed no cytotoxicity with the addition of DFO 4 hours before photolysis, as shown in Figure 4.7. These studies suggest the iron release is highly dependent on the potency of cytotoxicity. Both cell lines displayed better-decreased cytotoxicity than its **2.6** derivatives. This suggests that the 1,1`-dibenzoylferrocene derivative has cytotoxicity dependent on iron release. After iron release, the iron oxidize to ferric iron, likely through the Fenton (Figure 3.1). Further studies should determine the iron cytotoxic mechanism of the most potent and specific PDT **2.13**. Therefore flow cytometry studies were carried out to determine the mechanism of action. (section 4.4)

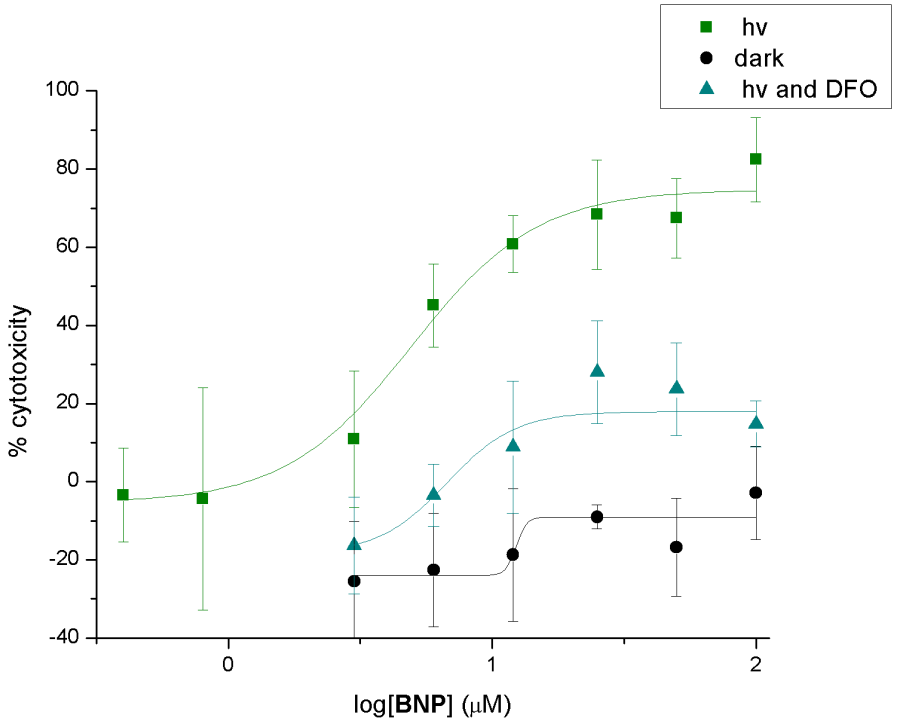

Figure 4.5: HeLa cytotoxicity of DFO with 2.13

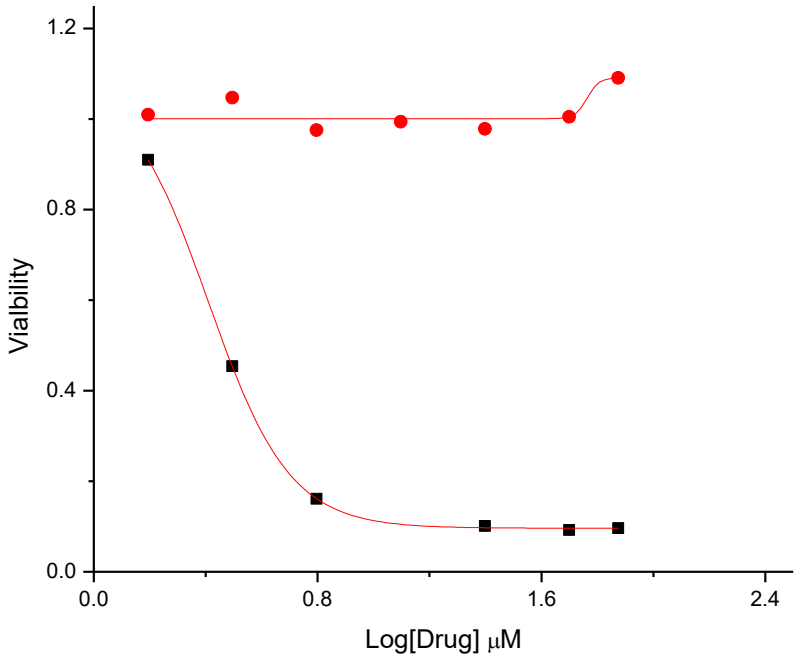

Figure 4.6: CaOV3 cytotoxicity with 2.13 and a DFO chelator added 7h before photolysis

4.4 Flow cytometry of ROS generation

Flow cytometry is a powerful analysis tool in which individual live cells are analyzed through size and granularity with a fluorescence through a capillary, (Figure 4.9). To determine if the Fenton reaction is generating reactive oxygen species(ROS) upon photolysis, cytosolic ROS fluorophore dichlorofluorescein diacetate, and lipid peroxidation C-11 BoDIPY were studied in live-cell flow cytometry.

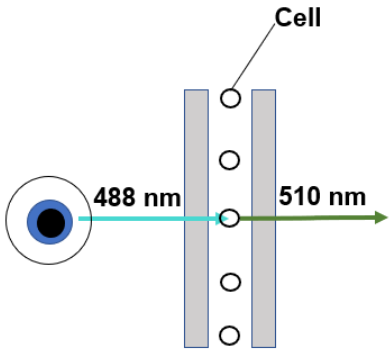

Figure 4.7: Flow cytometry diagram

4.4.1 Flow cytometry with lipid peroxidation C-11 BODIPY 581/591

Compound **2.13** was selected for the ROS study as it was the most specific and potent compound of the bis-substituted derivatives (Figure 4.10). The blue shift of the fluorescence emission peak from 590 nm to 515 nm indicated the oxidation of the polyunsaturated butadienyl. There was no significant blue shift in **2.13** after 12 h incubation. This suggests no lipid peroxides are affecting the cell at these concentrations. After 1 h photolysis followed by 1 h incubation of fluorophore the cells were analyzed by flow cytometry and a dose-dependent increase of lipid ROS within the cell for **2.13**. These results are consistent with cytotoxicity of **2.13** as previously described. From these studies, **2.13** is suggested to induce lipid peroxidation. After high concentrations of **2.13** high amount of lipid peroxidation was induced and the fluorophore was quenched, and cell had a highly reduced survival rate as shown in the 25 μM. This suggests that the cell has high concentrations of lipid ROS around and above the IC_{50} 4.76 μM of **2.13**.

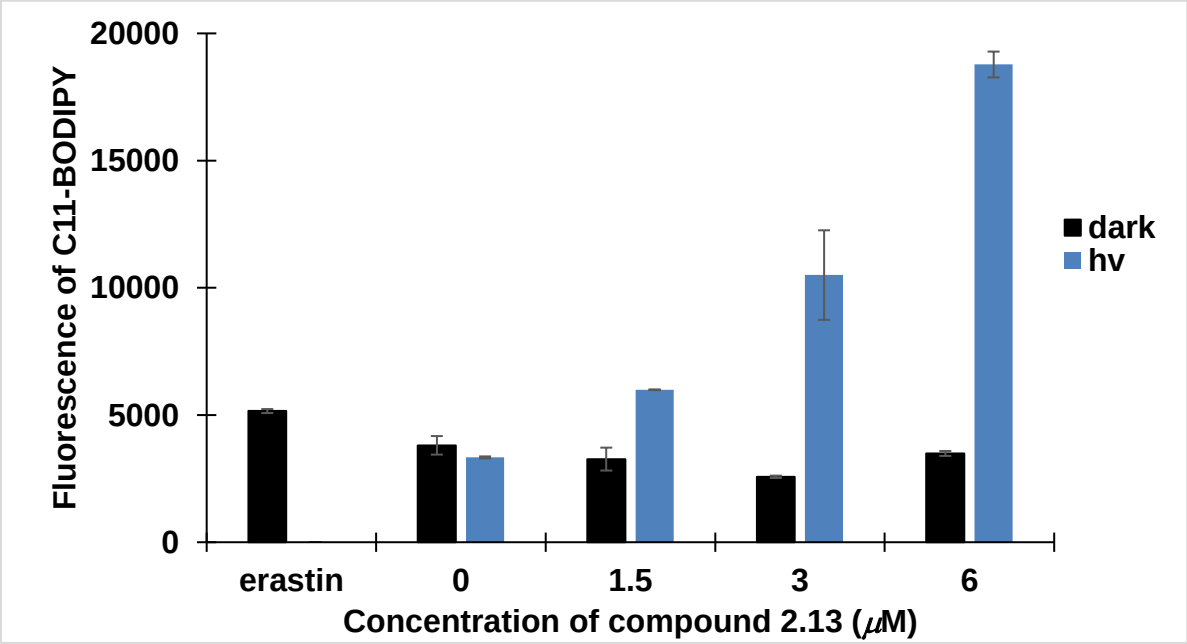

Figure 4.8: Flow cytometry data of lipid ROS of HeLa cell incubation of 2.13 with 1 h photolysis and dark control

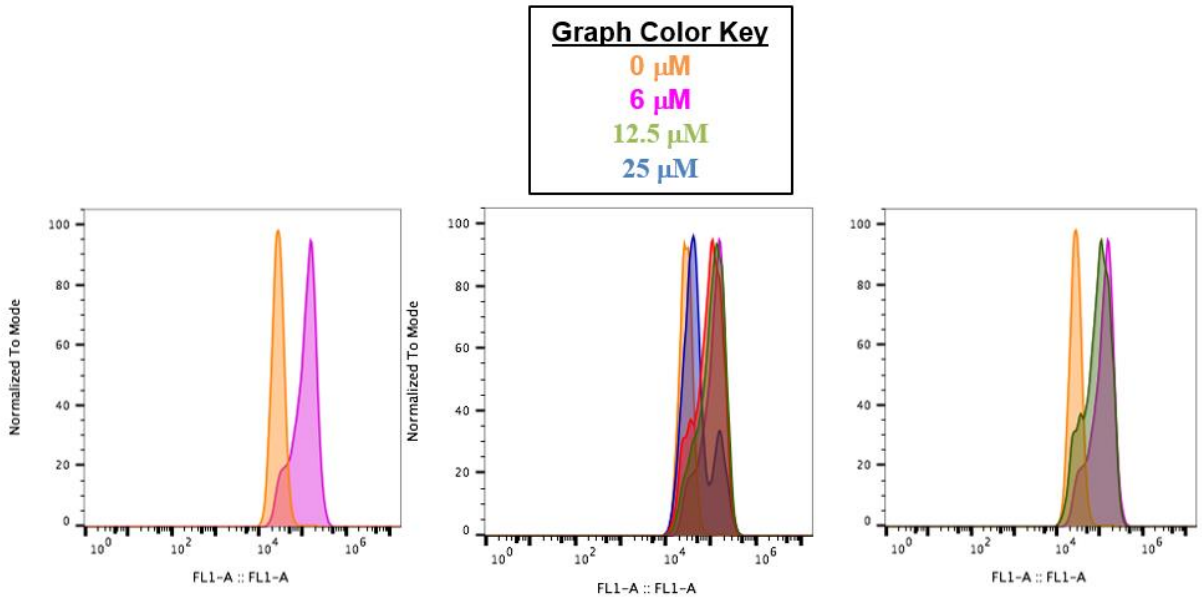

Figure 4.9: Flow cytometry data of HeLa cells incubation with 2.13 with lipid peroxidation fluorophore BoDIPY

4.4.2 Flow cytometry with dichlorofluorescein diacetate

Compound **2.13** was studied with cytosolic ROS fluorophore dichlorofluorescein diacetate, (Figure 4.12). Cytosolic ROS was studied to gain insight in wherein the cell ROS is being generated and if it is. The fluorescence increase demonstrates the increased cytosolic ROS concentration in the cell. From no significant shift of increasing concentration of **2.13** demonstrated no cytosolic ROS generation within the cell at the same concentrations as its lipid peroxidation fluorophore. It was shown that there was no significant cytosolic ROS generation below and above the IC_{50} of **2.13**. This is different from that of the mono-substituted derivative, **2.6** as cytosolic ROS was increased. From the limited cytosolic ROS and increase in lipid ROS, ferroptosis was suggested as a mechanism of cytotoxicity.[91, 93, 95]

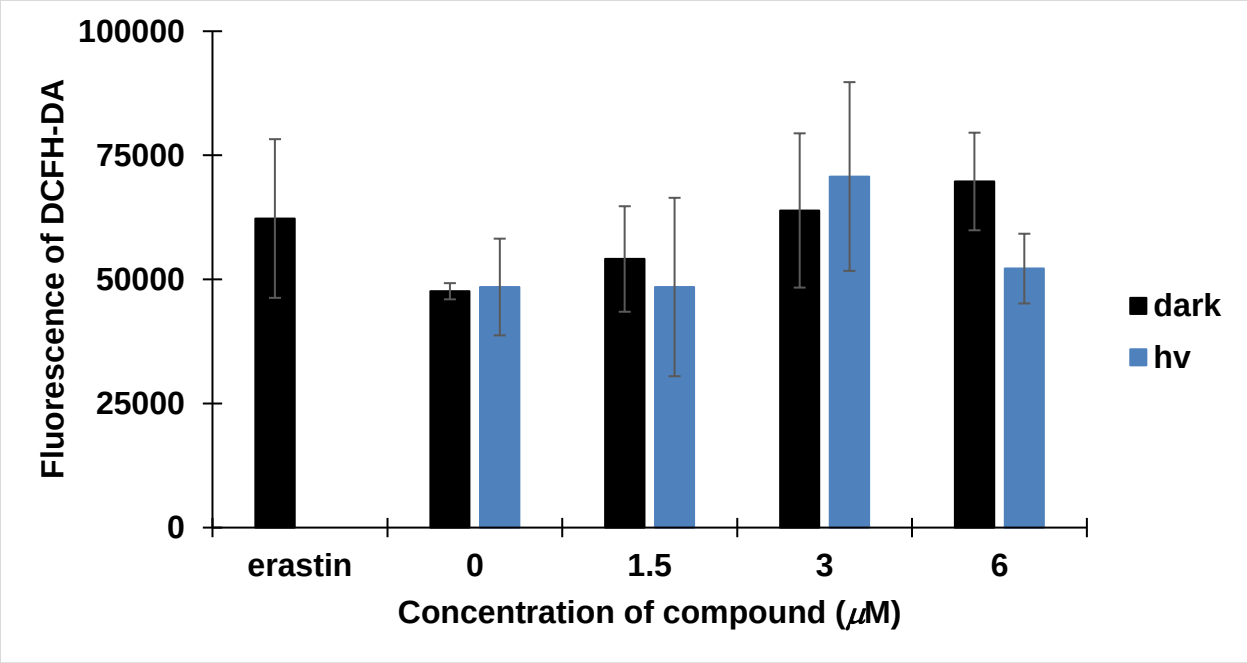

Figure 4.10: Cytosolic fluorophore flow cytometry data of HeLa cells incubation with 2.13 in the dark and after 1 h photolysis

4.4.3 Flow cytometry of intracellular labile iron pool, Calcein-AM studies

To determine the release of intracellular labile iron pool fluorophore Calcein-AM was studied. Calcein-AM fluorescence is quenched from the interaction with intracellular ferric iron. This study would complement the previously described DFO experiment of the release of iron(II) from benzoylferrocene and oxidation of iron(III) through the suggested Fenton reaction. This study demonstrated a dose-dependent increase of ferric iron within the cell after 1 h photolysis while in the dark does not affect the ferric iron concentrations showing in live cells that ferric iron was released after photolysis suggesting that ferric iron is only released after photolysis. Further indication that **2.13** is biologically stable in the cell without photolysis and is oxidized to iron(III).

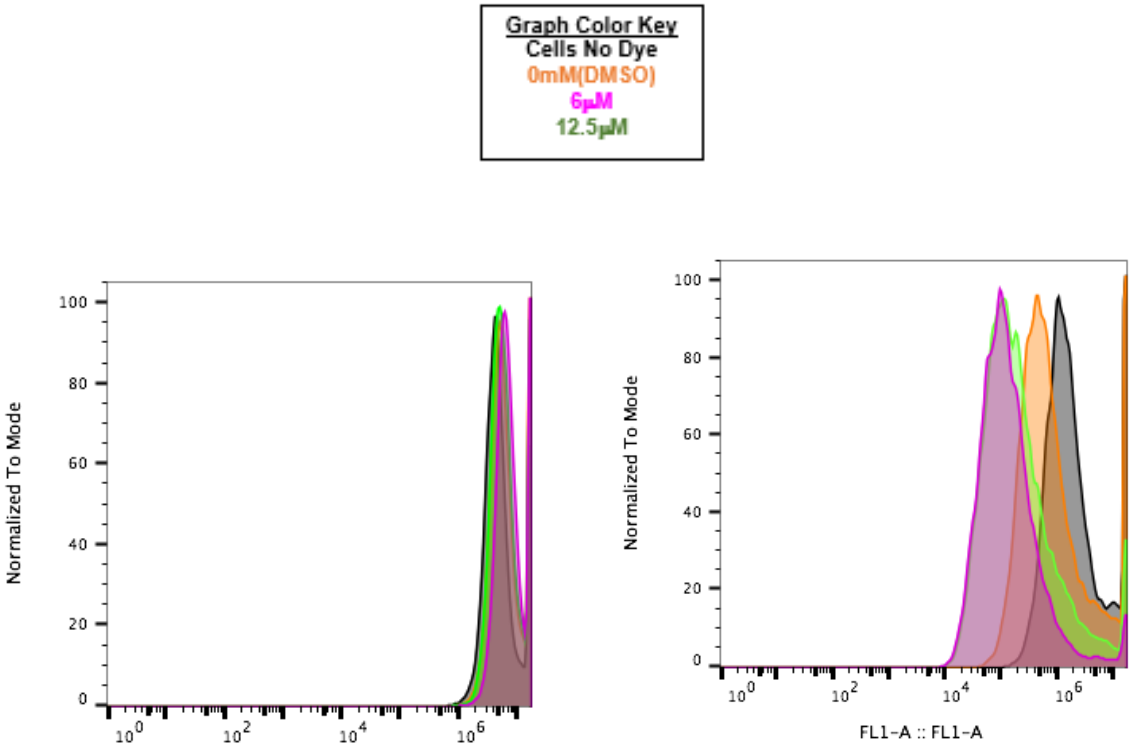

Figure 4.11: Calcein-AM treated cells treated with 2.13. (left) Dark treated HeLa cells, (right) 1h h photolyzed treated HeLa cells

4.4.4 Iron Uptake ICP-MS Studies

Previous ICP-OES studies were completed by Marissa and Christina to determine iron concentrations within the cell of previously synthesized compounds. From these studies it was reported that compound 2.13 and 2.6 had a 51 and 18.9 after 2 h incubation while 2.1 reported a less than that of the control.[84, 96] As a control, HeLa cells were not treated with any compound. We utilized inductively coupled plasma optical mass spectrometry (ICP-MS) to detect iron concentration due to the instrument's sensitivity and lower detection limit. HeLa cells were grown in a 150 cm^2 flask confluent, and then treated with 12 μM solution of each compound in FBS-free media for either 2 h while the control flask was prepared with an identical concentration of DMSO. The cells were then harvested for iron and protein analysis. Protein content was determined by the Pierce BCA Protein Kit. Following lyophilization and treatment with concentrated HNO_3, iron concentration was quantified by ICP-MS, at the UCSD CAICE facility ran by Neal K Arakawa. Experiments were performed in triplicate.

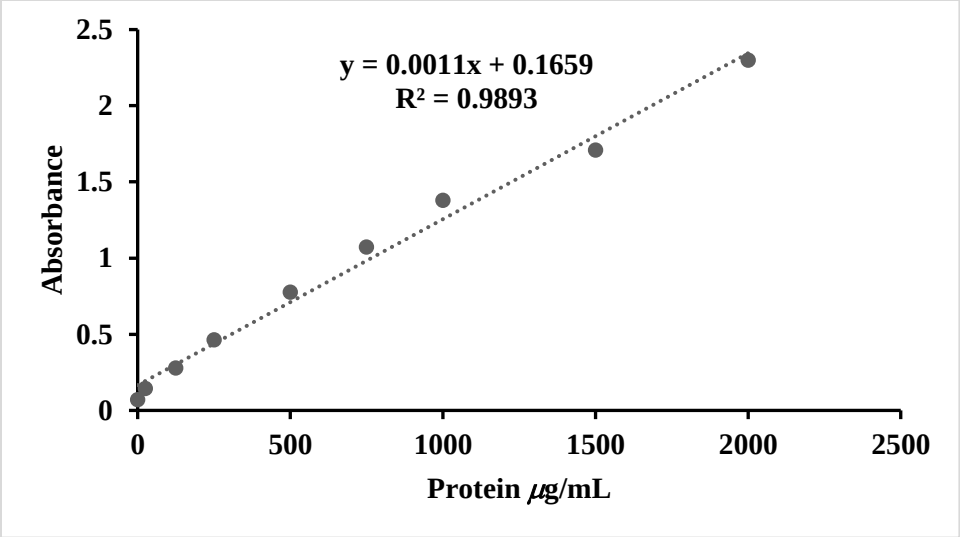

Figure 4.12: Standard calibration curve of BCA Protein Assay

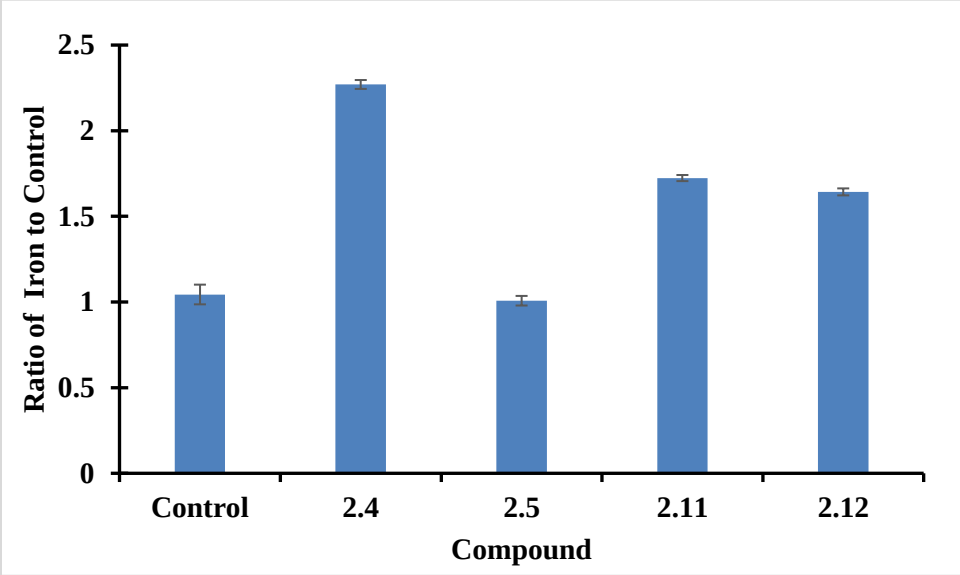

Figure 4.13: Ratio of iron compared to controlled from ICP-MS

The experiment displayed a limited increase of iron in cells incubated with 2.4, 2.11 and 2.12 compared to the control. Unfortunately 2.5 was similar to that of the control which is what 2.1 reported.[84]

4.5 Ferroptosis Mechanism

From previously described flow cytometry and DFO studies, iron overload was initiated after photoactivation. More specifically, ferroptosis is proposed as **2.13** cytotoxic mechanism as described in Figure 4.14. The 1-benzoylferrocene and 1,1′-dibenzoylferrocene derivatives have proven to induce cytotoxicity. The compound **2.13** additionally reported the released iron(II) into the cell after photolysis, which likely oxidizes to iron(III) within the cell as suggested from the DFO and Calcein-AM experiments.

To further determine cytotoxic mechanism protein and RNA expressions of induced live, HeLa cells were studied in multiple time points by western and RT-qPCR. To study the mechanism of **2.13**, the expression of VDAC, GPX4, and SOD1 were studied.

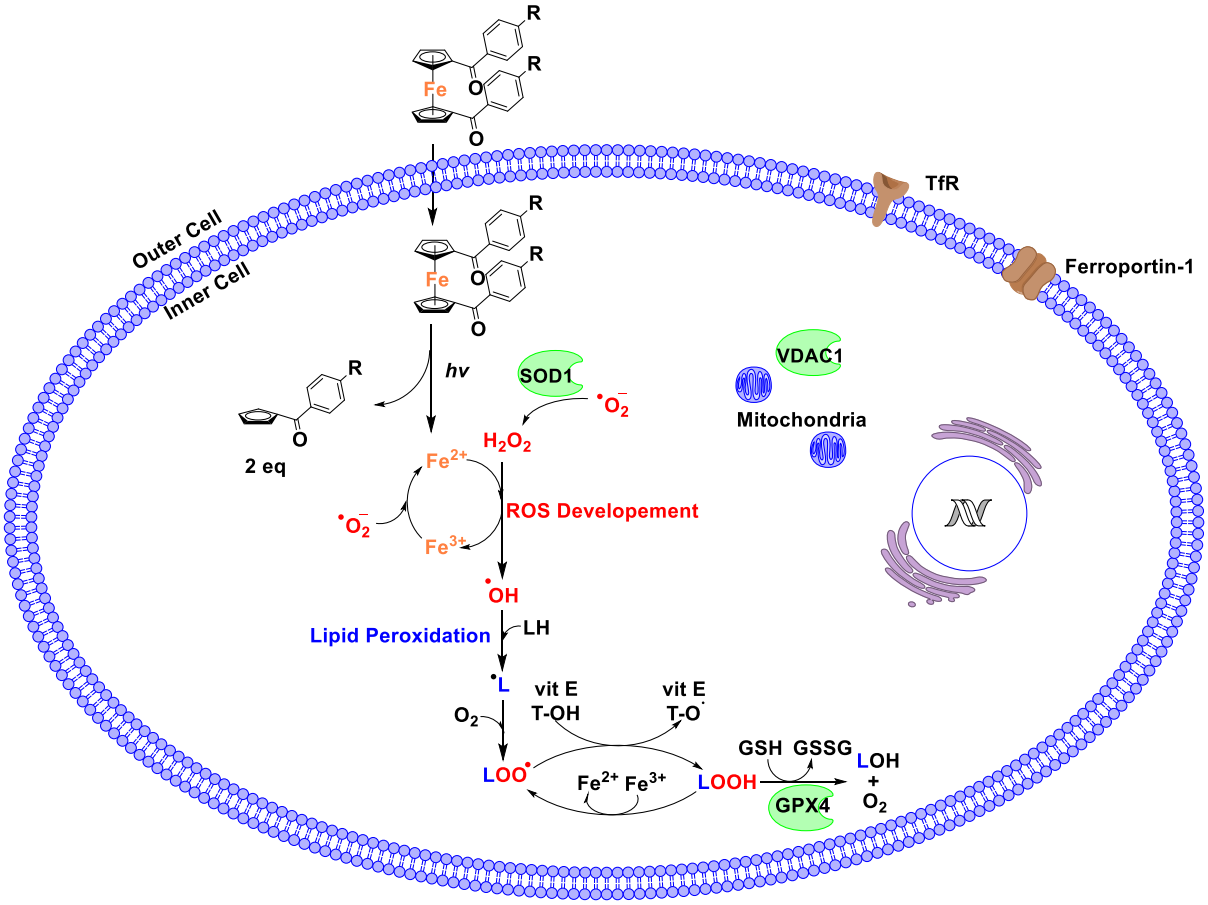

Figure 4.14: Proposed cytotoxicity mechanism of 1,1′-dibenzoylferrocene

4.5.1 SOD1 RT-qPCR and western blot

Superoxide dismutase (SOD1, SOD2, SOD3) is an enzyme that limits the detrimental effects of ROS.[97] SOD1 contains a copper-zinc active site responsible for catalyzing the oxidation of superoxide to hydrogen peroxide and dioxygen.[97-99] SOD1 has been reported to be activated during ferroptosis cell death mechanism.[100, 101] Therefore to tease out the mechanism of actions I decided to do western blots of both dark and photolysis with a one hour and four-hour incubation, there was an apparent dose-dependent increase of expression only after photolysis with a 4 h incubation of **2.13**. This trend is also seen on RT-qPCR. Hydrogen peroxide at 125 μM incubated for three hours before lysing the cell and purification of protein as apoptosis and sod1 control.[102] It was seen to have an increase in SOD1 production, which was expected additionally.

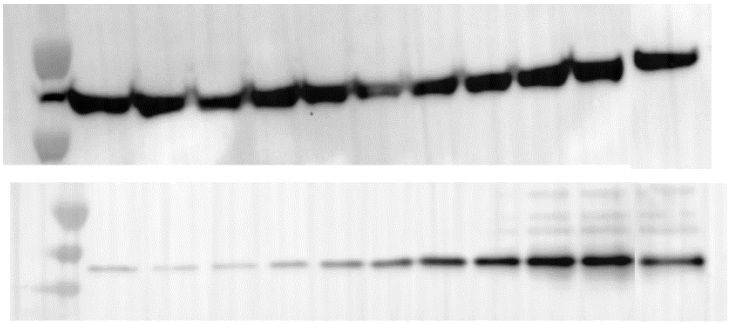

Figure 4.15: Western blot raw data image of b-actin and sod1 after 1h photolysis

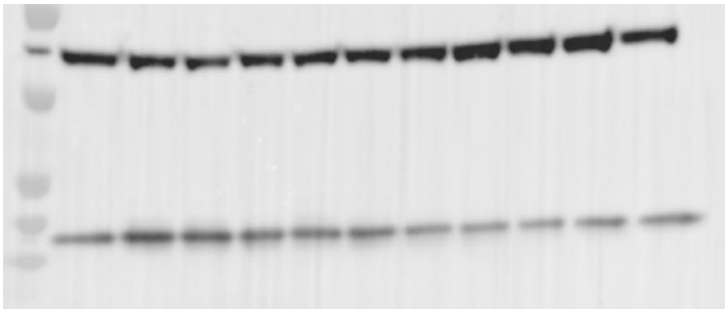

Figure 4.16: Western blot raw data image of b-actin and sod1 dark control

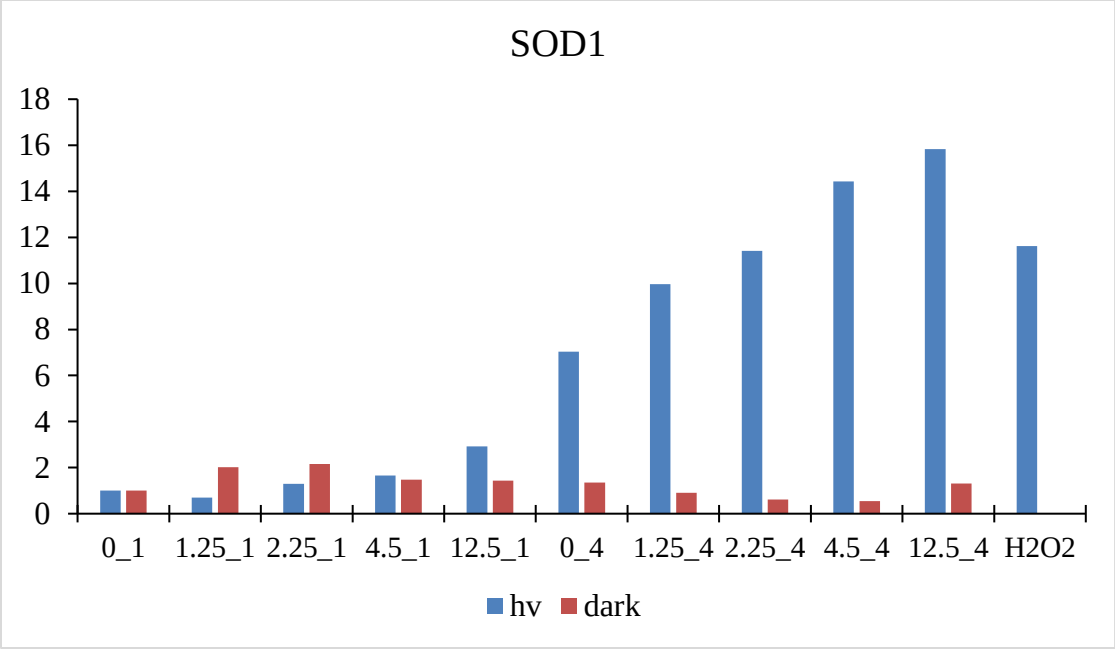

Figure 4.17: Western blot quantization of SOD1 from incubation HeLa cells with 2.13

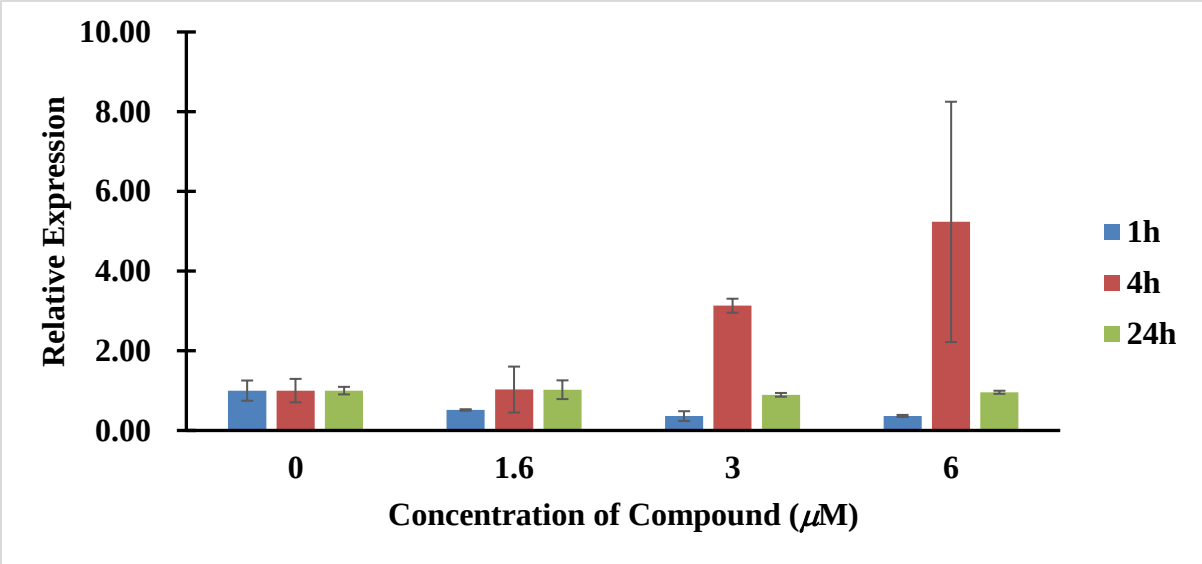

Figure 4.18: SOD1 PCR data of HeLa cells incubated with 2.13 with and without 1 h photolysis

Both the western and PCR data report an increase in SOD1 after photoactivation and 4 h incubation of compound **2.13**.

4.5.2 VDAC1 RT-qPCR and VDAC2 western blot

Voltage-dependent anion-selective channel (VDAC1, VDAC2) are human beta-barrel proteins that form ion channels in the outer mitochondrial membranes and the outer cell membrane. [103-105] The mitochondria are responsible for the synthesis of ATP for cell survival. VDAC1 and VDAC2 regulate the volume of ATP, ADP, and NADH diffusion out of the mitochondria into the cytoplasm.[106] VDAC1 allows for communication between the mitochondrion and the cell; this regulates cell metabolism and signaling for cell death initiation.[107, 108] VDAC isoforms are essential for the regulation of cell metabolism, mitochondrial apoptosis, and spermatogenesis and overexpression of this pore could lead to apoptosis in the cell. Erastin, a ferroptosis inducer, has been reported be VDAC modulator and upregulated. [109]

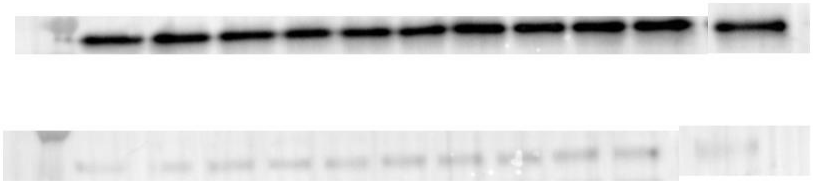

Figure 4.19: Raw data of 2.13 incubation HeLa cells with b-actin and vdac1 after 1 h photolysis

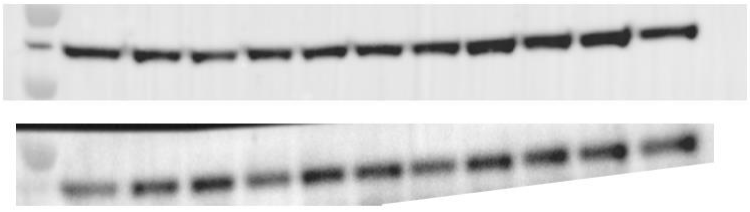

Figure 4.20: Raw data of 2.13 incubation HeLa cells with b-actin and vdac1 dark

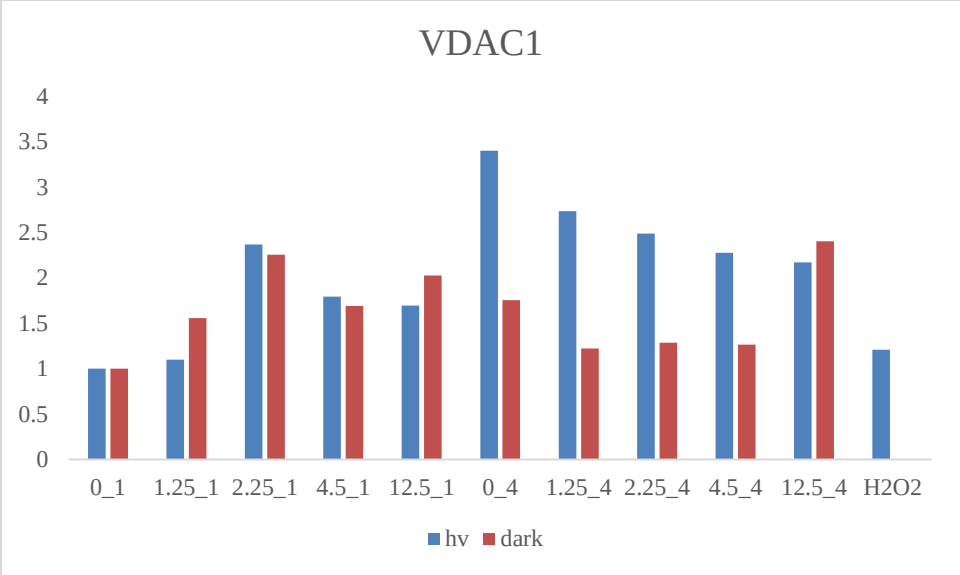

Figure 4.21: VDAC1 western blot data with incubation of compound 2.13 with and without photolysis

RT-qPCR displayed a dose-dependent gene increase after 1 hour and overall increase of gene expression 4 h but was back to homeostasis with consistent regulation after 24 hours.

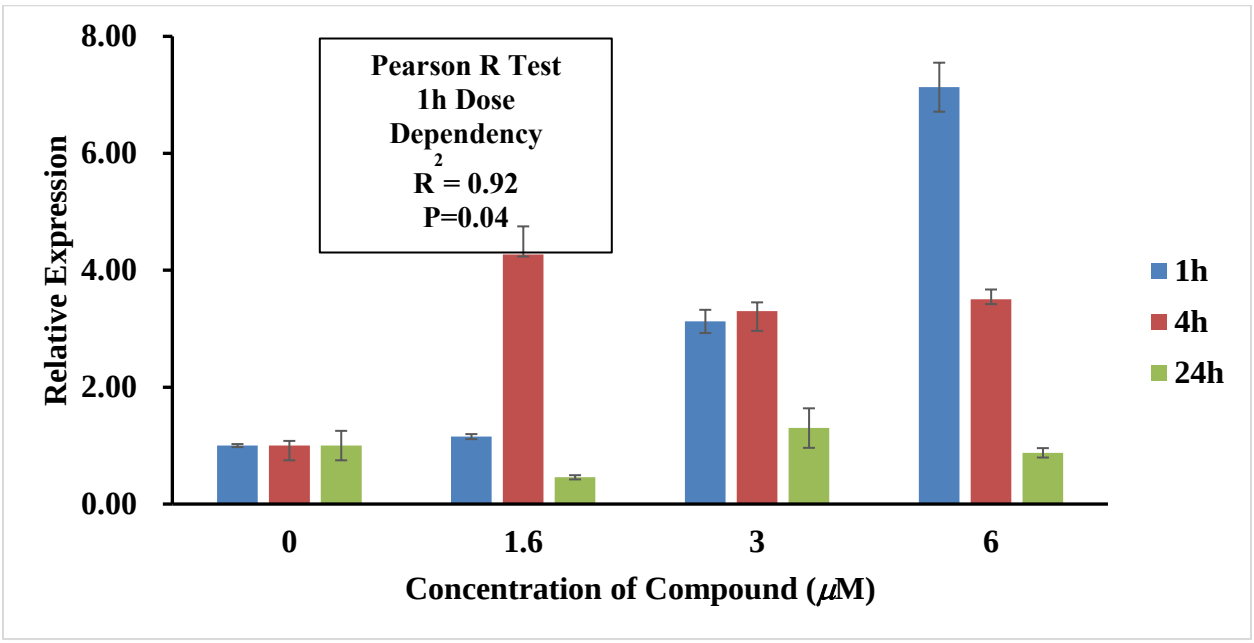

Figure 4.22: VDAC1 PCR data with incubation of compound 2.13 with and without photolysis

4.5.3 GPx4 RT-qPCR and western blot

Glutathione peroxidase 4 (GPx4), is one of eight mammalian isoenzymes(GPx1-8).[101, 110-114] GPx4 is a phospholipid hydroperoxide that inhibits lipid peroxidation by catalyzing the reduction of hydrogen peroxide, organic hydroperoxides, and lipid peroxides from the reduction of glutathione to glutathione disulfide, (Figure 4.23). This reaction occurs from activation of selenol (-SeH) is oxidized by peroxides to selenenic acid (-SeOH), which is then reduced with glutathione (GSH) to an intermediate selenodisulfide (-Se-SG). GPx4 is reactivated by a second glutathione molecule, releasing glutathione disulfide (GS-SG). Inactivation of GPx4 leads to an accumulation of lipid peroxides, resulting in ferroptosis cell death.[112, 115, 116]

2 glutathione + lipid–hydroperoxide → glutathione disulfide + lipid–alcohol + H_2O

Figure 4.23: GPx4 Cell saving mechanism

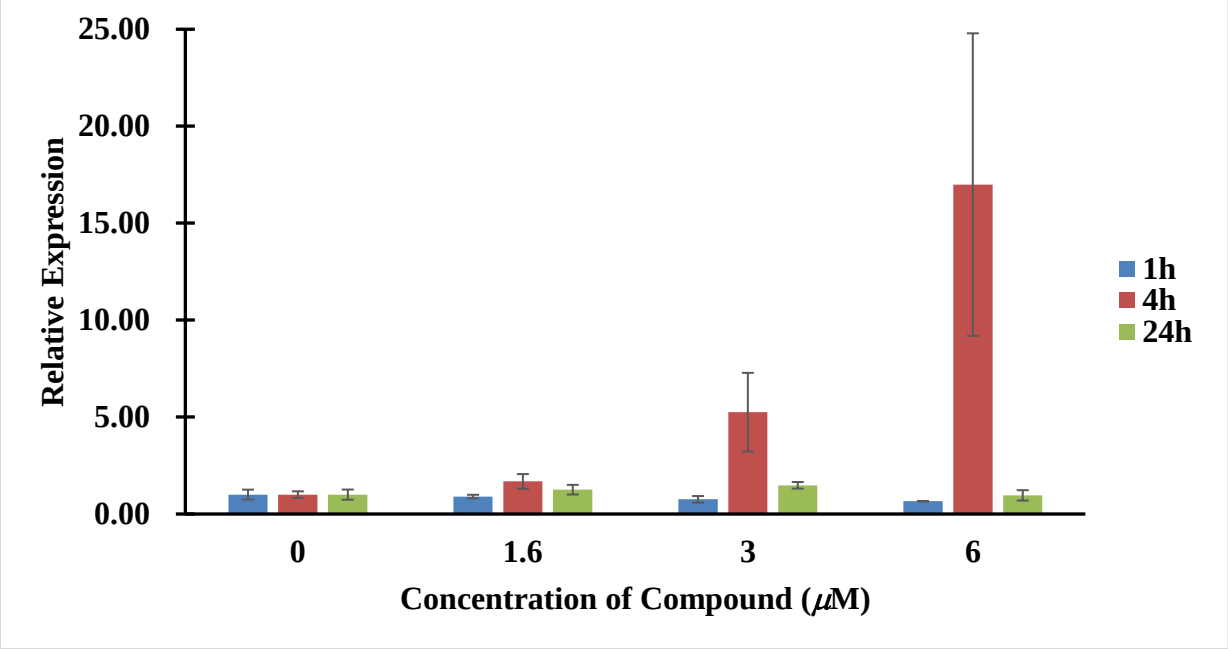

Figure 4.24: GPx4 RT-qPCR

Through studies of VDAC, GPx4 and SOD1 were all upregulated. After 1 h irradiation VDAC1 was increased in a dose-dependence, while either GPx4 and SOD1 was not significantly affected. After 4 h irradiation, GPx4 and SOD1 were also upregulated in both the protein and RNA levels. These studies suggest that **2.13** is indeed going through a ferroptosis mechanism. While this does not eliminate other cell death mechanisms, other studies should be completed to determine if apoptosis is also induced as ROS levels displayed increased.

4.6 Supplemental Information

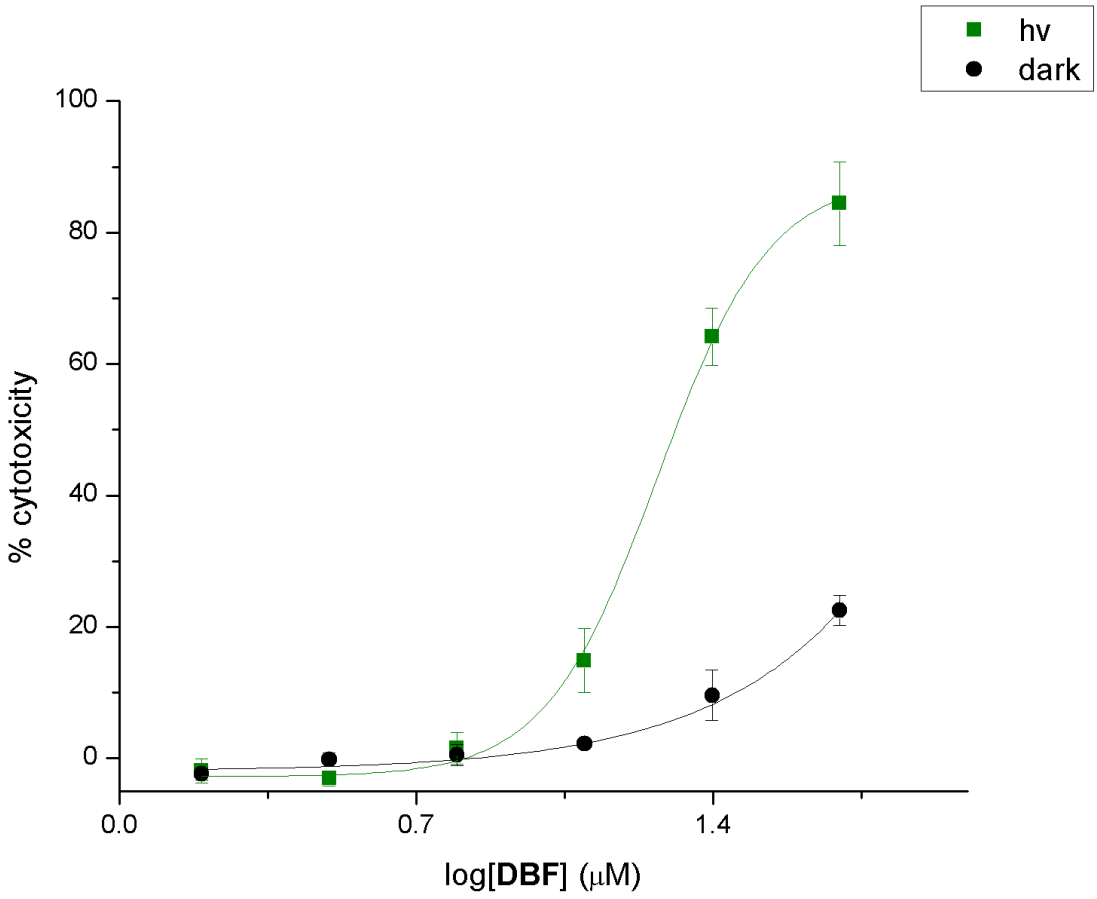

Figure 4.25: IC_{50} graph of 2.8 in Hela with dark and 3h photolyzed conditions

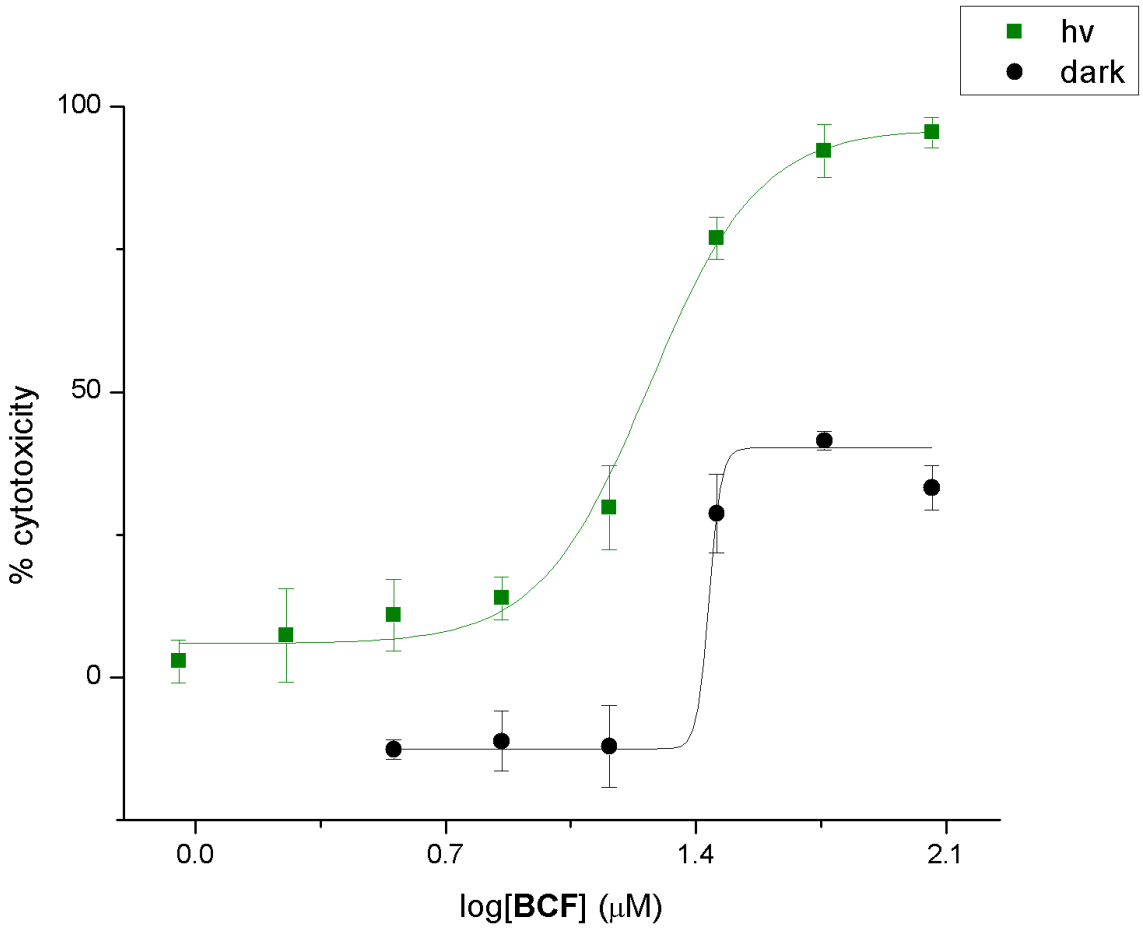

Figure 4.26: IC_{50} graph of 2.9 in Hela with dark and 3h photolyzed conditions

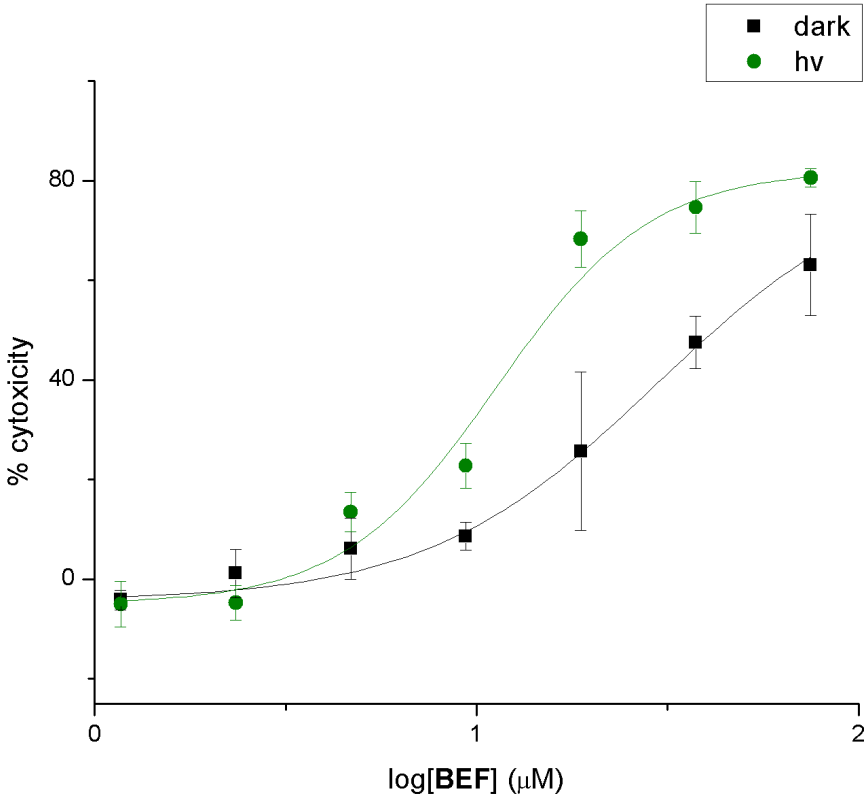

Figure 4.27: IC_{50} graph of 2.11 in Hela with dark and 3h photolyzed conditions

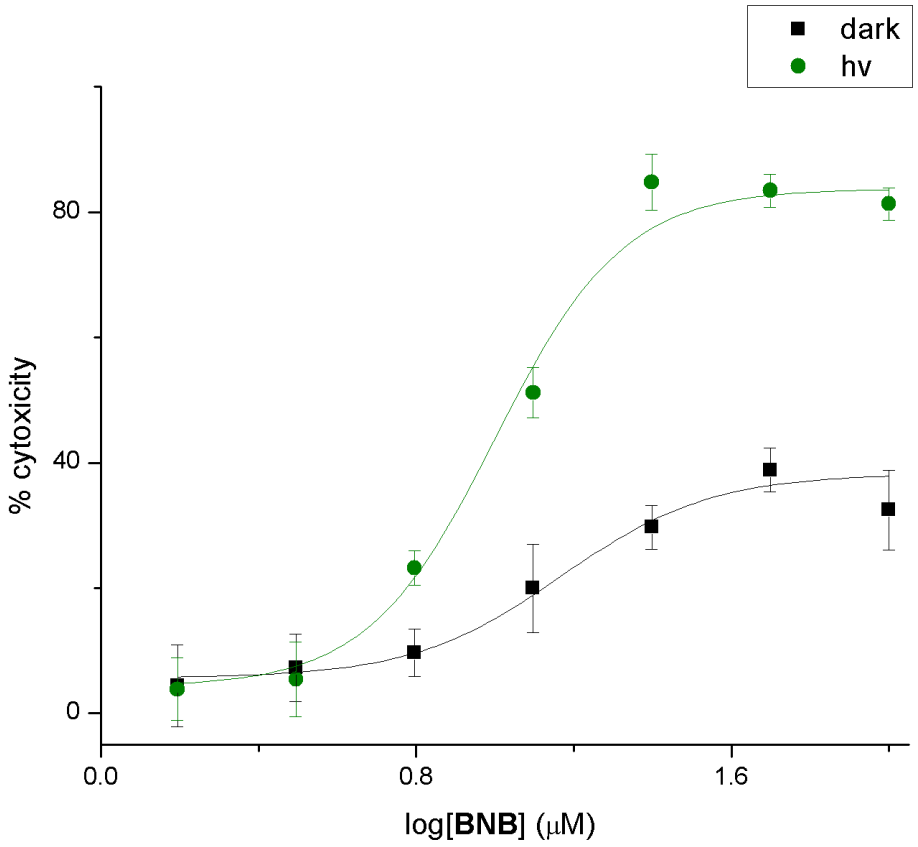

Figure 4.28: IC_{50} graph of 2.12 in Hela with dark and 3h photolyzed conditions

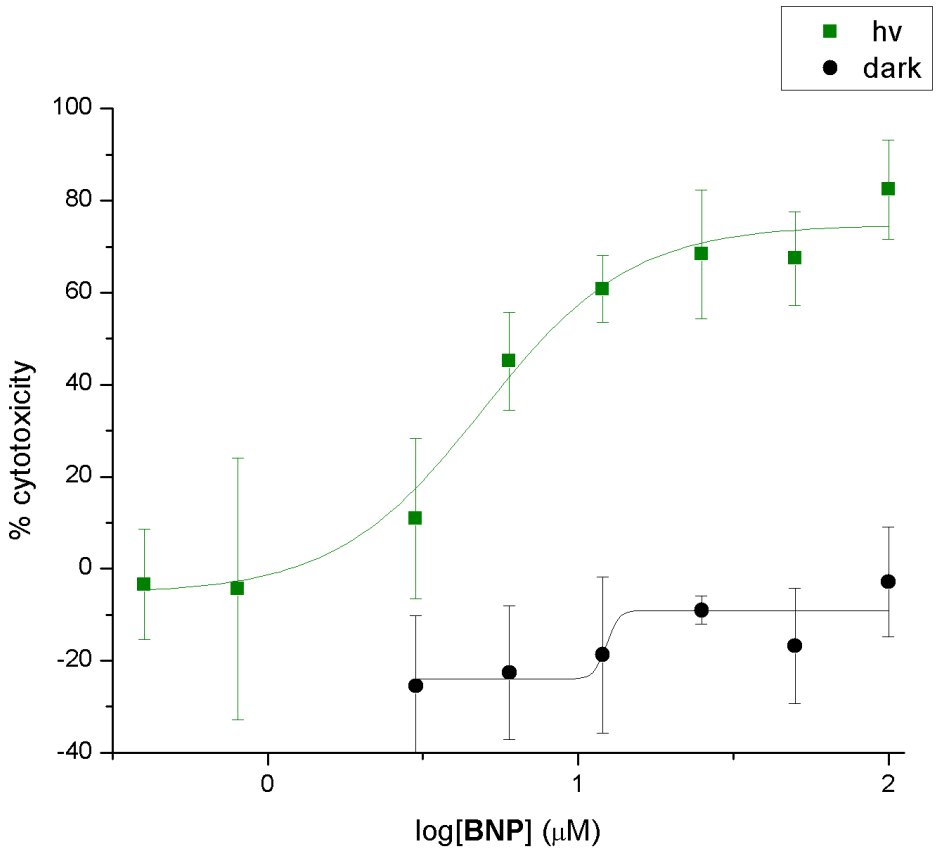

Figure 4.29: IC_{50} graph of 2.13 in Hela with dark and 3h photolyzed conditions

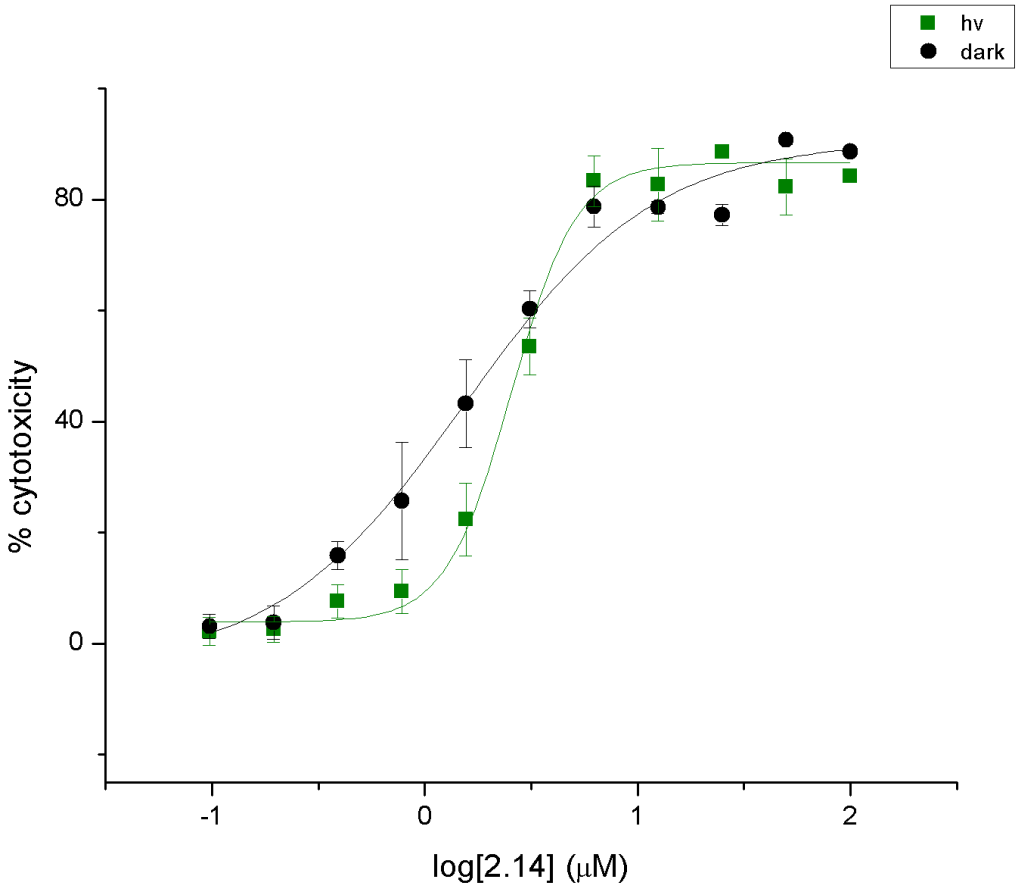

Figure 4.30: IC_{50} graph of 2.14 in Hela with dark and 3h photolyzed conditions

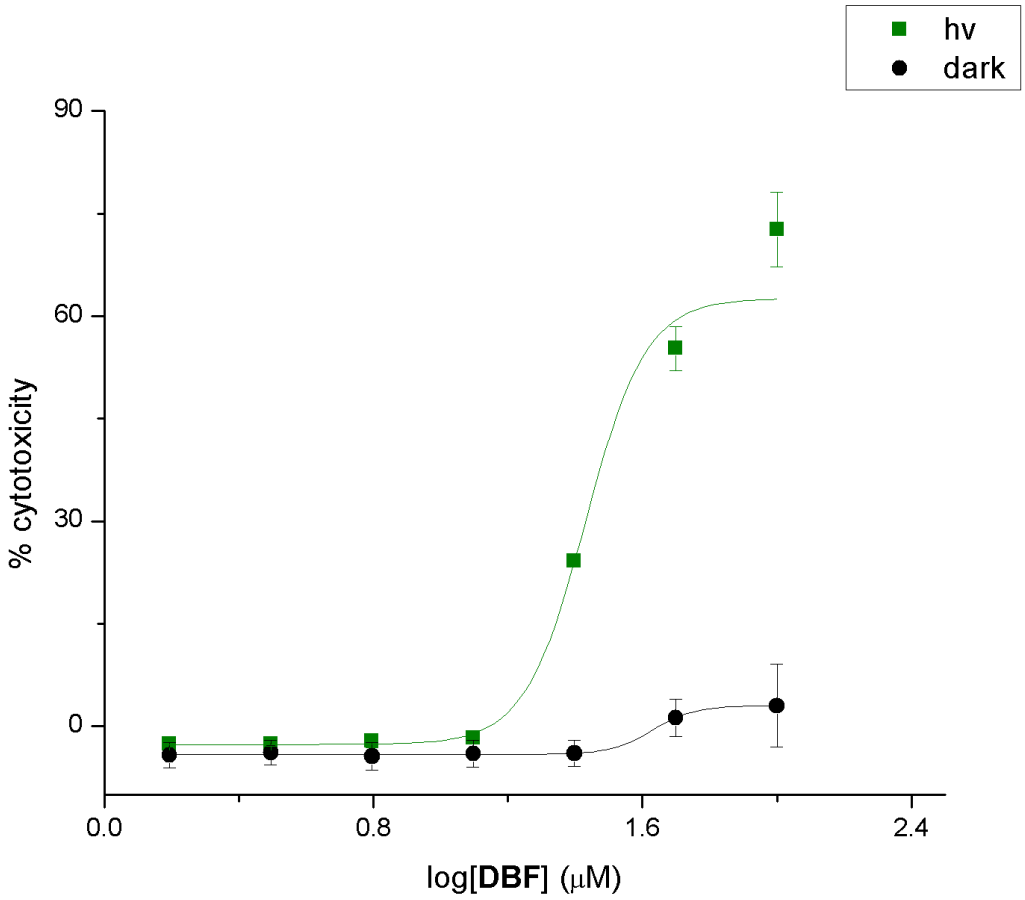

Figure 4.31: IC_{50} graph of 2.8 in CaOV3 with dark and 3h photolyzed conditions

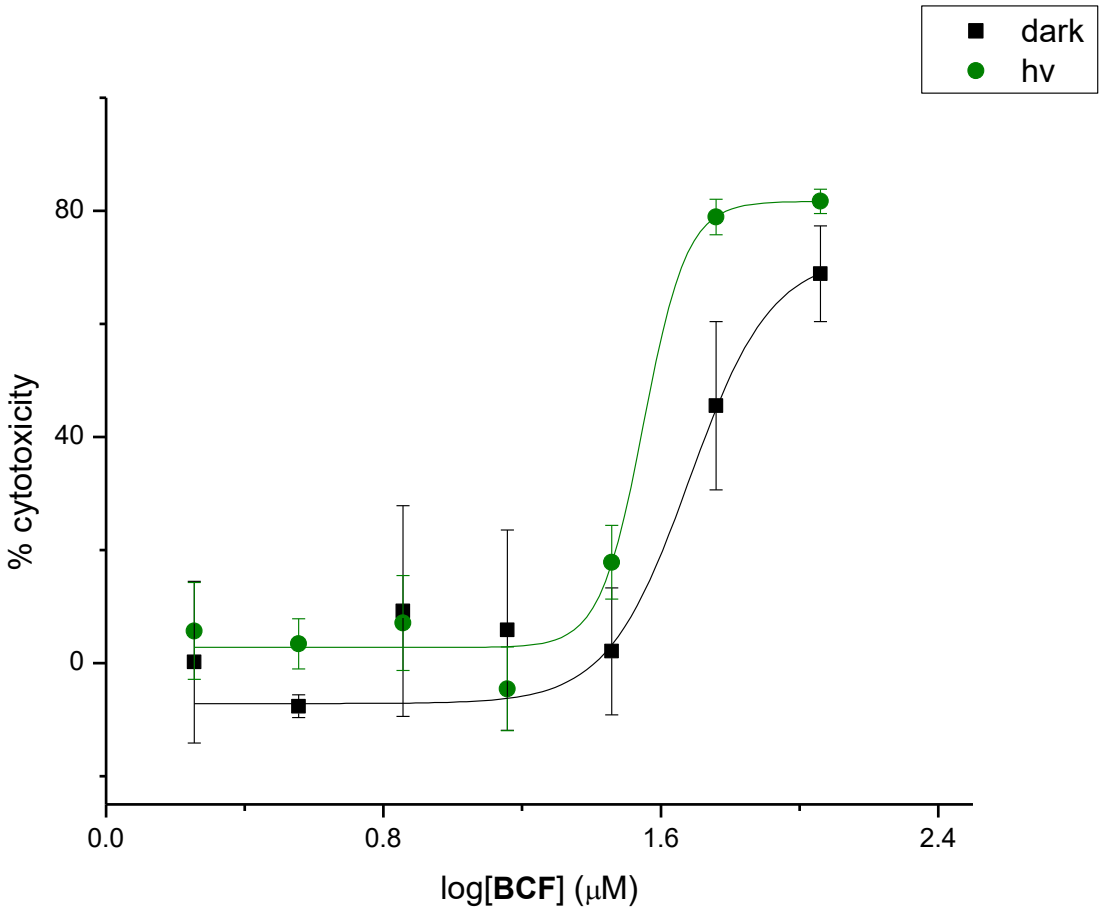

Figure 4.32: IC_{50} graph of 2.9 in CaOV3 with dark and 3h photolyzed conditions

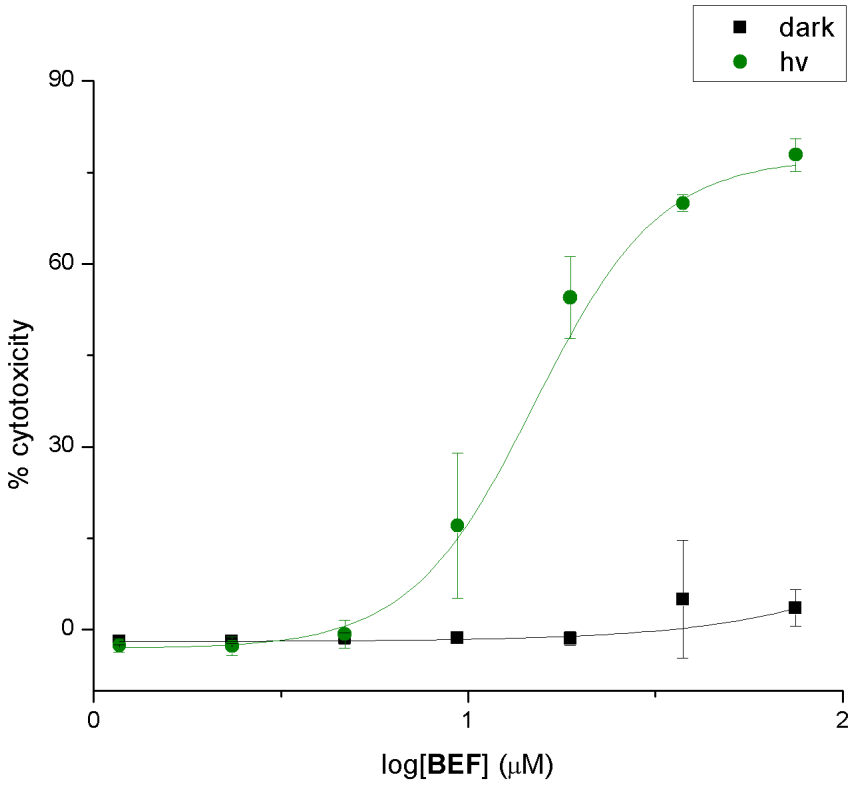

Figure 4.33: IC_{50} graph of 2.11 in CaOV3 with dark and 3h photolyzed conditions

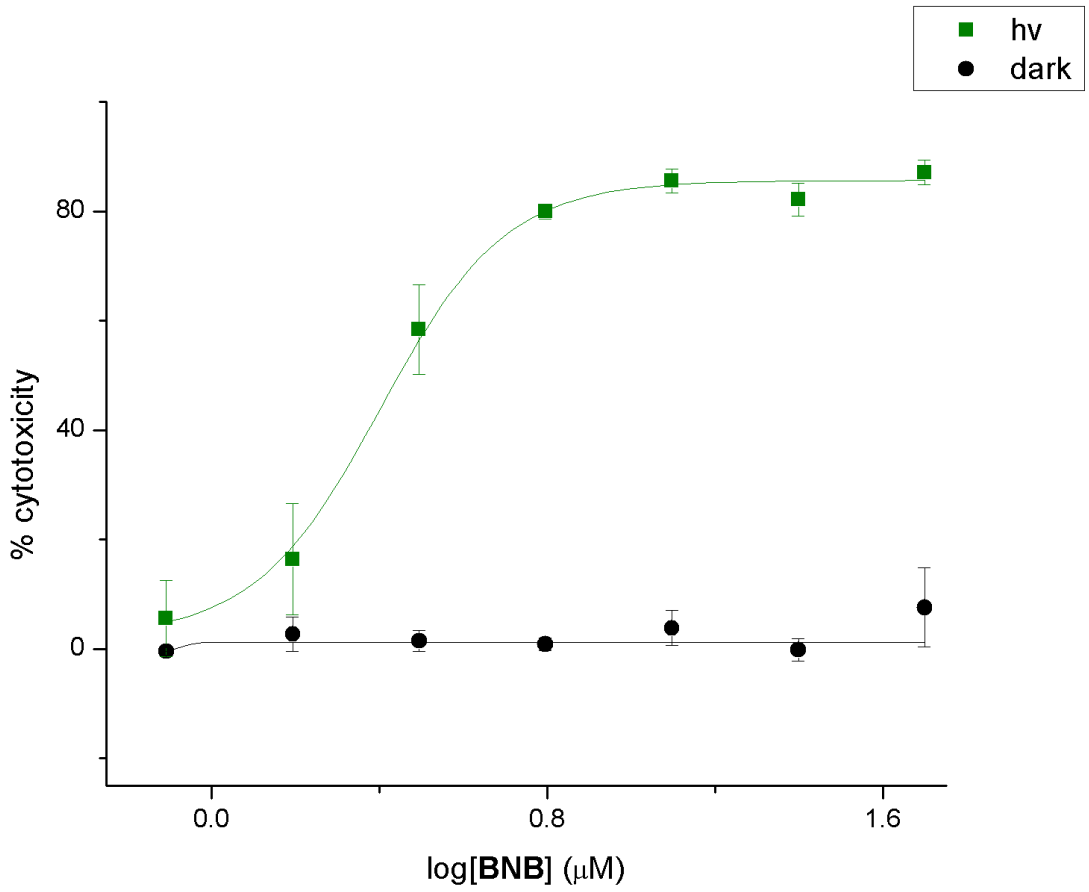

Figure 4.34: IC_{50} graph of 2.12 in CaOV3 with dark and 3h photolyzed conditions

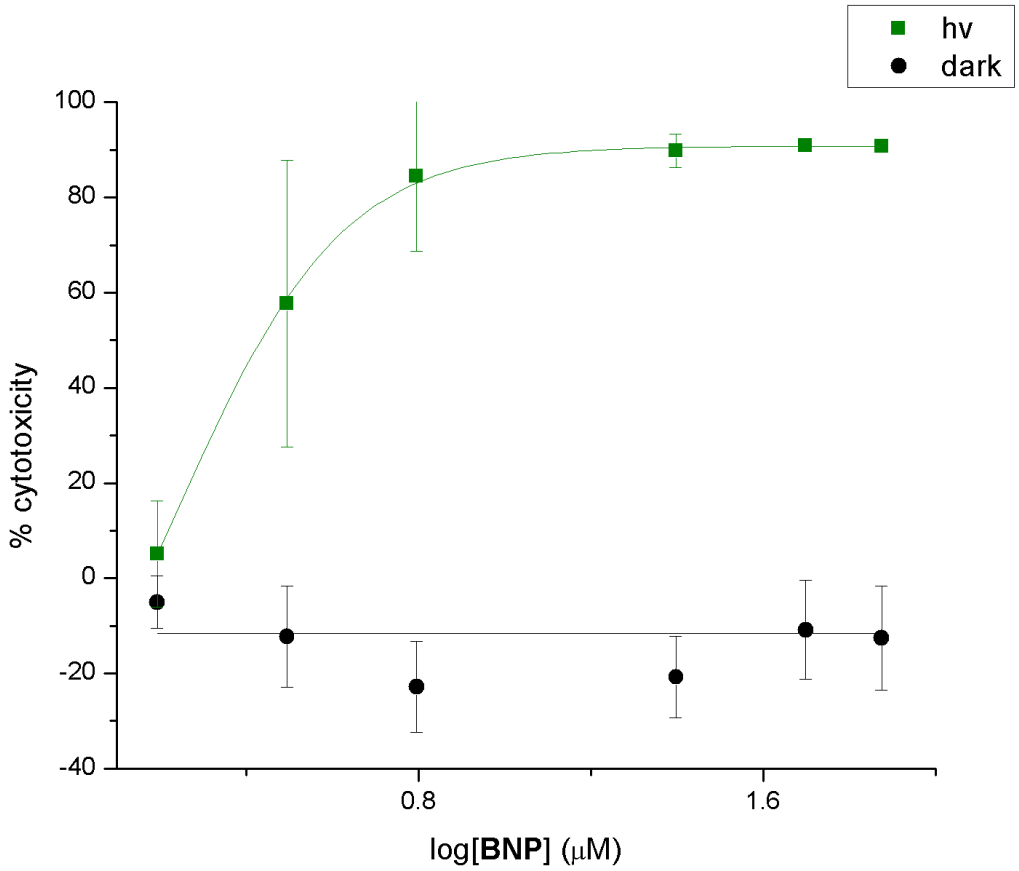

Figure 4.35: IC_{50} graph of 2.13 in CaOV3 with dark and 3 h photolyzed conditions

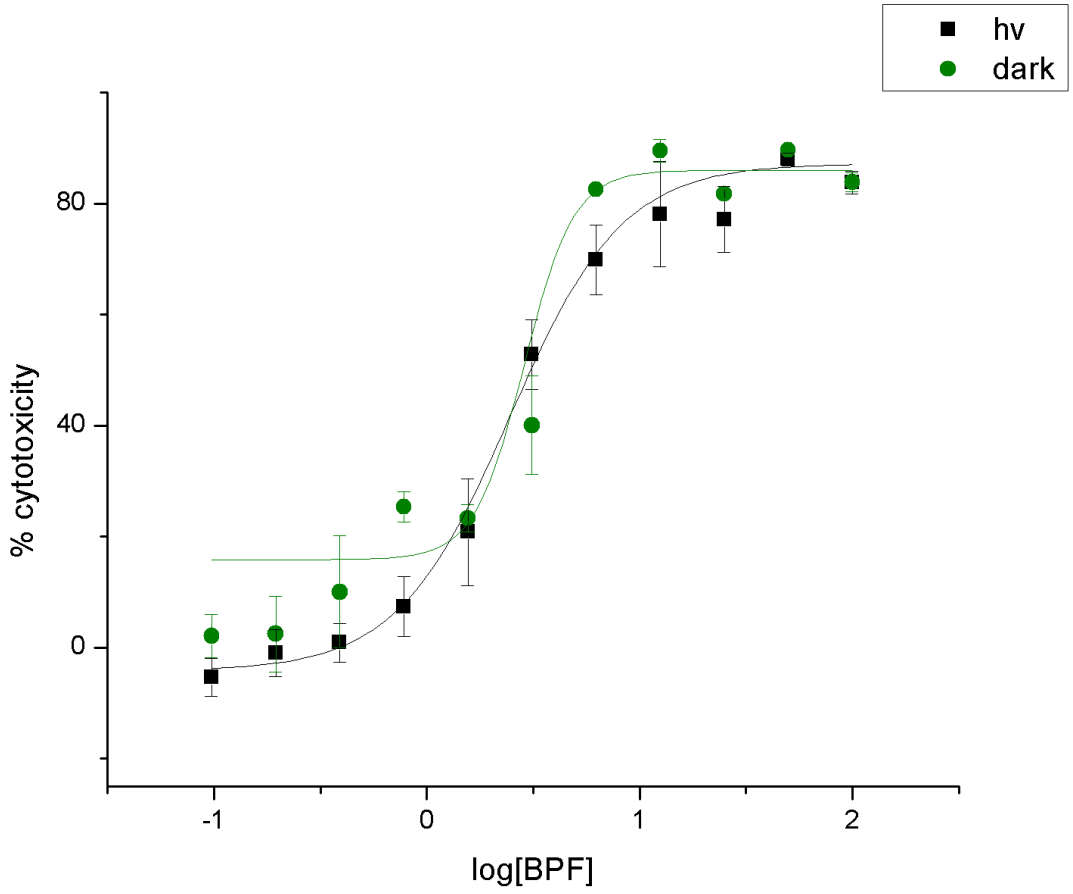

Figure 4.36: IC_{50} graph of 2.14 in CaOV3 with dark and 3h photolyzed conditions

Experimental of Lipid Peroxidation C-11 BODIPY 581/591

Lipid ROS was measured on a flow cytometer with treated HeLa cells with fluorophore C11-BODIPY 581/591. Cells were plated on a 6-well plate and treated with various concentrations of either **2.13** then incubated for 12 hours. Cells were then kept dark as control or photolyzed for one h with a >450nm filter. The cells were then treated with 50 μM C11-BODIPY for 1h. Cells were then washed three times with DPBS, trypsinized, and resuspended in a 5% FBS DPBS solution. A minimum of 10,000 cells was analyzed per condition.

Experimental of DCFH-DA indicator dichlorofluorescein diacetate

Cytosolic ROS was measured on a flow cytometer with HeLa cells treated with DCFH-DA. Cells were plated on a 6-well plate and treated with **2.13** and incubated for 12 hours. Cells were kept dark control or photolyzed for 1 hour with a >450nm filter. Cells were treated with 10 μM DCFH-DA for one h then excess fluorophore was washed with DPBS, trypsinized and resuspended with DPBS with 5% FBS. Oxidation of DCFH-DA is proportional to cytosolic ROS generation and was analyzed using a flow cytometer. A minimum of 10,000 cells was analyzed per condition.

Experimental of Calcein-AM

Intracellular labile iron pool(LIP) was measured on a flow cytometry with a *LIVE/DEAD ® Viability/Cytotoxicity Kit *for mammalian cells**. Cells were plated on a 6-well plate and treated with di-n-pentyl-benzoylferrocene then were incubated for 24 hours. Cells were then kept either as a dark control or photolyzed for 1 h with a >450 nm filter. Next, the cells were then washed with DPBS, trypsinized, and resuspended in 1mL DPBS with 5% FBS. The cell suspension was treated with 2 μL of 50 μM Calcein-AM and 4 μL of 2 mM ethidium homodimer-1 then allowed to incubate for 20 min in the dark. The cells were then analyzed the flow cytometer. A minimum of 10,000 cells was analyzed per condition.

Iron Uptake Studies

Cell Cultivation, Addition of Complexes, and Cell Harvesting

In a 75 cm^2 flasks HeLa cells were cultivated as a monolayer in dMEM. The substances were diluted in DMSO (2.4, 2.5, 2.11, 2.12, 5.6, 5.7) or water ($FeSO_4$) then added to FBS-free cell growth medium. The HeLa cells were exposed to the drug and controls containing media for a period of 2h. The media was removed and the cell monolayer was washed gently three times with 15 mL of warm dPBS. The cells were then treated with 3 mL of trypsin for fifteen minutes and resuspended in 15 mL of fresh FBS-free media. The cell suspension was subsequently centrifuged at 1200 rpm (4 °C) for 5 min three times, and the pellets were washed twice with 10 mL of dPBS between cycles. The pellets dried upside-down for 10 minutes then stored at -20 °C until analysis.

Determination of Protein Concentration

The cell pellets were homogenized in 5 mL of 0.001% Triton X-100 solution by vortexing followed by sonication (5 x 5 s). 1 mL was removed for protein quantification and the remaining 4 mL were lyophilized in preparation for iron quantification. Protein concentration was determined by the Bradford method using the commercially available Pierce™ BCA Protein Assay Kit # 23225 prepared per the manufacturer's instructions. Protein standards were prepared using human serum albumin (HSA) in 0.001% Triton X-100 solution. As Triton X-100 is a known interfering substance, additional dilutions of the protein standards were done using an identical concentration of the detergent. A calibration curve was constructed by calculating the 590/450 nm absorbance ratio using a micro-plate reader. The protein concentration of the cell lysates were determined as described by Zor and Selinger (see discussion section). A standard protein calibration curve is shown below.

Determination of Iron Concentration

The lyophilized samples were dissolved in 230µL of concentrated nitric acid and heated at 65°C for 6 h. The samples were then diluted to a total volume of 10 mL using 0.1% Triton X-100 and the iron

concentration (ng/g) was determined by ICP-MS. The iron concentration was then related to the protein concentration to account for differences in biomass between separate flasks. Results are expressed as an average of three independent experiments.

RNA Preparation and Reverse Transcription Quantitative Polymerase Chain Reaction Analysis

HeLa cells were incubated with 2.13 for 12 hours than exposed to 1 h hν and allowed to be incubated for multiple time points. Culture medium was removed and washed three times with cold dPBS incubated with TRIzol reagent for 5 min. Cells were pelleted by centrifugation and RNA isolated completed as outlined by TRIzol kit. The concentrations of RNA was determined with a Nanodrop Lite spectrophotometer (Thermo Scientific). Reverse transcription was performed by using 1 μg of RNA and following instructions from the iScript cDNA Synthesis Kit (BioRad, Hercules, CA). Real-time quantitative polymerase chain reaction (RT-qPCR) experiments were completed on a CFX96 quantitative polymerase chain reaction (qPCR) system (BioRad) with Ssoadvanced SYBR Green reagent (BioRad). Primers were designed through (http://primerdepot.nci.nih.gov/). Transcription levels were quantified with the Ct value normalized to alpha tubulin (*TUBA1A2*).

Protein Preparation and Western Blots

HeLa cell lysates were prepared in a RIPA buffer. After protein concentration determination by Bradford Reagent, protein samples were subjected to gel electrophoresis by using Nupage 4–12% (wt/vol) Bis-Tris gradient gel (ThermoFisher). Western blots were developed and imaged using a ChemiDoc Touch Imaging System (BioRad).

4.7 Chapter 4 References

95. Gao, M.; Monian, P.; Jiang, X., Metabolism and iron signaling in ferroptotic cell death. *Oncotarget* **2015,** *6* (34), 35145-35146.

96. Hoong, C. Synthesis, Design, and Cytotoxicity of Organoferrous Anticancer Agents. University of California San Diego, 2017.

97. Milani, P.; Gagliardi, S.; Cova, E.; Cereda, C., SOD1 Transcriptional and Posttranscriptional Regulation and Its Potential Implications in ALS. *Neurology Research International* **2011,** *2011*, 9.

98. Rosen, D. R.; Siddique, T.; Patterson, D.; Figlewicz, D. A.; Sapp, P.; Hentati, A.; Donaldson, D.; Goto, J.; O'Regan, J. P.; Deng, H.-X.; Rahmani, Z.; Krizus, A.; McKenna-Yasek, D.; Cayabyab, A.; Gaston, S. M.; Berger, R.; Tanzi, R. E.; Halperin, J. J.; Herzfeldt, B.; Van den Bergh, R.; Hung, W.-Y.; Bird, T.; Deng, G.; Mulder, D. W.; Smyth, C.; Laing, N. G.; Soriano, E.; Pericak–Vance, M. A.; Haines, J.; Rouleau, G. A.; Gusella, J. S.; Horvitz, H. R.; Brown, R. H., Mutations in Cu/Zn superoxide dismutase gene are associated with familial amyotrophic lateral sclerosis. *Nature* **1993,** *362* (6415), 59-62.

99. Sea, K.; Sohn, S. H.; Durazo, A.; Sheng, Y.; Shaw, B. F.; Cao, X.; Taylor, A. B.; Whitson, L.; Holloway, S. P.; Hart, P. J.; Cabelli, D. E.; Gralla, E. B.; Valertine, J. S., Insights into the Role of the Unusual Disulfide Bond in Copper-Zinc Superoxide Dismutase. *J Biol Chem* **2015,** *290* (4), 2405-2418.

100. Imai, H.; Matsuoka, M.; Kumagai, T.; Sakamoto, T.; Koumura, T., Lipid Peroxidation-Dependent Cell Death Regulated by GPx4 and Ferroptosis. In *Apoptotic and Non-apoptotic Cell Death*, Nagata, S.; Nakano, H., Eds. Springer International Publishing: Cham, 2017; pp 143-170.

101. Conrad, M.; Friedmann Angeli, J. P., Glutathione peroxidase 4 (Gpx4) and ferroptosis: what's so special about it? *Mol Cell Oncol* **2015,** *2* (3), e995047.

102. Singh, M.; Sharma, H.; Singh, N., Hydrogen peroxide induces apoptosis in HeLa cells through mitochondrial pathway. *Mitochondrion* **2007,** *7* (6), 367-373.

103. Blachly-Dyson, E.; Baldini, A.; Litt, M.; McCabe, E. R. B.; Forte, M., Human Genes Encoding the Voltage-Dependent Anion Channel (VDAC) of the Outer Mitochondrial Membrane: Mapping and Identification of Two New Isoforms. *Genomics* **1994,** *20* (1), 62-67.

104. Rahmani, Z.; Maunoury, C.; Siddiqui, A., Isolation of a novel human voltage-dependent anion channel gene. *European Journal of Human Genetics* **1998,** *6* (4), 337-340.

105. Messina, A.; Oliva, M.; Rosato, C.; Huizing, M.; Ruitenbeek, W.; van den Heuvel, L. P.; Forte, M.; Rocchi, M.; De Pinto, V., Mapping of the Human Voltage-Dependent Anion Channel Isoforms 1 and 2 Reconsidered. *Biochemical and Biophysical Research Communications* **1999,** *255* (3), 707-710.

106. Amodeo, G. F.; Scorciapino, M. A.; Messina, A.; De Pinto, V.; Ceccarelli, M., Charged Residues Distribution Modulates Selectivity of the Open State of Human Isoforms of the Voltage Dependent Anion-Selective Channel. *PLOS ONE* **2014,** *9* (8), e103879.

107. Shoshan-Barmatz, V.; De Pinto, V.; Zweckstetter, M.; Raviv, Z.; Keinan, N.; Arbel, N., VDAC, a multi-functional mitochondrial protein regulating cell life and death. *Molecular Aspects of Medicine* **2010,** *31* (3), 227-285.

108. Reina, S.; Palermo, V.; Guarnera, A.; Guarino, F.; Messina, A.; Mazzoni, C.; De Pinto, V., Swapping of the N-terminus of VDAC1 with VDAC3 restores full activity of the channel and confers anti-aging features to the cell. *FEBS Letters* **2010,** *584* (13), 2837-2844.

109. Wang, Y.-Q.; Chang, S.-Y.; Wu, Q.; Gou, Y.-J.; Jia, L.; Cui, Y.-M.; Yu, P.; Shi, Z.-H.; Wu, W.-S.; Gao, G.; Chang, Y.-Z., The Protective Role of Mitochondrial Ferritin on Erastin-Induced Ferroptosis. *Frontiers in Aging Neuroscience* **2016,** *8* (308).

110. Esworthy, R. S.; Doan, K.; Doroshow, J. H.; Chu, F.-F., Cloning and sequencing of the cDNA encoding a human testis phospholipid hydroperoxide glutathione peroxidase*. *Gene* **1994,** *144* (2), 317-318.

111. Seiler, A.; Schneider, M.; Forster, H.; Roth, S.; Wirth, E. K.; Culmsee, C.; Plesnila, N.; Kremmer, E.; Radmark, O.; Wurst, W.; Bornkamm, G. W.; Schweizer, U.; Conrad, M., Glutathione peroxidase 4 senses and translates oxidative stress into 12/15-lipoxygenase dependent- and AIF-mediated cell death. *Cell Metab* **2008,** *8* (3), 237-48.

112. Imai, H., New Strategy of Functional Analysis of PHGPx Knockout Mice Model Using Transgenic Rescue Method and Cre-LoxP System. *J Clin Biochem Nutr* **2010,** *46* (1), 1-13.

113. Friedmann Angeli, J. P.; Schneider, M.; Proneth, B.; Tyurina, Y. Y.; Tyurin, V. A.; Hammond, V. J.; Herbach, N.; Aichler, M.; Walch, A.; Eggenhofer, E.; Basavarajappa, D.; Rådmark, O.; Kobayashi, S.; Seibt, T.; Beck, H.; Neff, F.; Esposito, I.; Wanke, R.; Förster, H.; Yefremova, O.; Heinrichmeyer, M.; Bornkamm, G. W.; Geissler, E. K.; Thomas, S. B.; Stockwell, B. R.; O'Donnell, V. B.; Kagan, V. E.; Schick, J. A.; Conrad, M., Inactivation of the ferroptosis regulator Gpx4 triggers acute renal failure in mice. *Nature Cell Biology* **2014,** *16*, 1180.

114. Nakagawa, Y., Role of Mitochondrial Phospholipid Hydroperoxide Glutathione Peroxidase (PHGPx) as a Antiapoptotic Factor. *Biological and Pharmaceutical Bulletin* **2004,** *27* (7), 956-960.

115. Imai, H.; Hakkaku, N.; Iwamoto, R.; Suzuki, J.; Suzuki, T.; Tajima, Y.; Konishi, K.; Minami, S.; Ichinose, S.; Ishizaka, K.; Shioda, S.; Arata, S.; Nishimura, M.; Naito, S.; Nakagawa, Y., Depletion of selenoprotein GPx4 in spermatocytes causes male infertility in mice. *The Journal of biological chemistry* **2009,** *284* (47), 32522-32532.

116. Yang, W. S.; SriRamaratnam, R.; Welsch, M. E.; Shimada, K.; Skouta, R.; Viswanathan, V. S.; Cheah, J. H.; Clemons, P. A.; Shamji, A. F.; Clish, C. B.; Brown, L. M.; Girotti, A. W.; Cornish, V. W.; Schreiber, S. L.; Stockwell, B. R., Regulation of ferroptotic cancer cell death by GPX4. *Cell* **2014,** *156* (1-2), 317-331.

Chapter 5 Ferroptosis Inducing Endoperoxide Tethered to 1-Benzoylferrocene and 1,1`-Dibenzoylferrocene Cytotoxicity Studies

5.1 Background of biological activity endoperoxides

Endoperoxide biological activity was discovered back in 1971 in a natural herb medicine *Artemisia annua* L that was originally a traditional Chinese medicine.[117, 118] The endoperoxide *A. annua L*, was considered to be the active constituent of its antimalarial and anticancer activity. The 2015 Nobel Prize in Medicine was awarded for Youyou Tu for purifying and discovering artemisinin antimalarial activity and developing it as a treatment. [119-122] The semisynthetic derivates dihydroartemisinin, artemether, arteether, and artesunate proved to have biological activity but as anticancer compounds.[119, 123-125] Endoperoxides are also reported to be biologically important to convert arachidonic acid to PG endoperoxides PGG2 and PGH2 by the action of COX for nonsteroidal anti-inflammatory drugs (NSAIDs). [126]

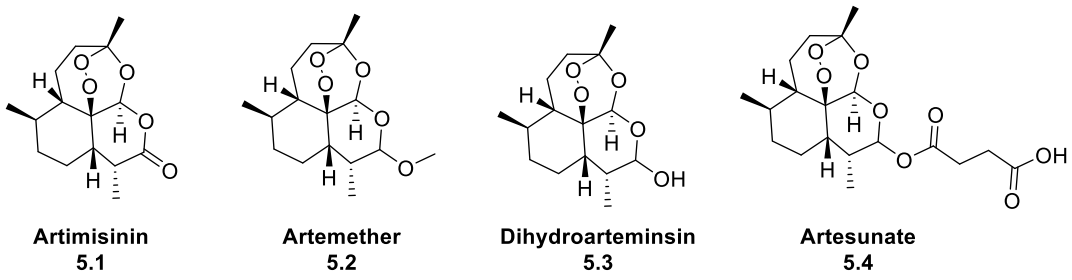

Figure 5.1: Previously synthesized endoperoxides with reported antimalarial and anti-cancer activity

Recently, Woerpel and Stockwell synthesized and studied the endoperoxide, $FINO_2$ (Figure 5.2). It was reported that $FINO_2$ induced ferroptosis in BJ-hTERT and CAKI-1 cells lines with IC_{50} values of 20 μM and 18 μM respectively. [127] $FINO_2$ was reported to oxidize ferrous to ferric iron, which is an initiator of ferroptosis but it does not bind to GPx4 as previous ferroptosis inducers have reported.[91, 92, 101]

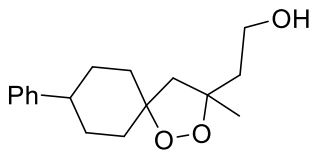

$FINO_2$

5.5

Figure 5.2: Previously reported compound $FINO_2$ chemical structure

5.2 Cytotoxicity studies of $FINO_2$ and tether 1-Benzoylferrocene and 1,1`-Dibenzoylferreocene derivatives

Incorporation of $FINO_2$ endoperoxide to 1-benzoylferrocene and 1,1`-dibenzoylferrocene was synthesized to produce a family of photoactivated iron-peroxide agents (PIPAs). This generation of compounds was hypothesized to be more potent due to the ferrous iron-oxidizing behavior of $FINO_2$ and light activates free iron(II) releasing capacity of **2.6** and **2.13** (Figure 5.3). The endoperoxide adduct would then initiate Fenton chemistry and increase ROS concentrations, which could induce higher cell death after light activation. Collaborator Alexander Braddock, of the Theodorakis lab, completed the synthesis of PIPAs, from compounds **2.3** and **2.10** (Figure 5.4).

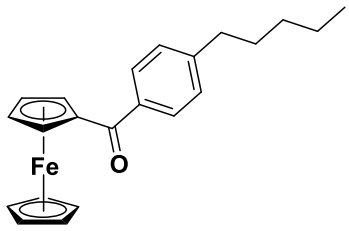

2.6

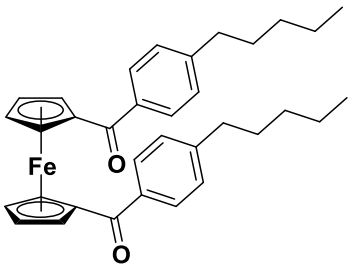

2.13

Figure 5.3: Compounds 2.6 and 2.13 chemical structures

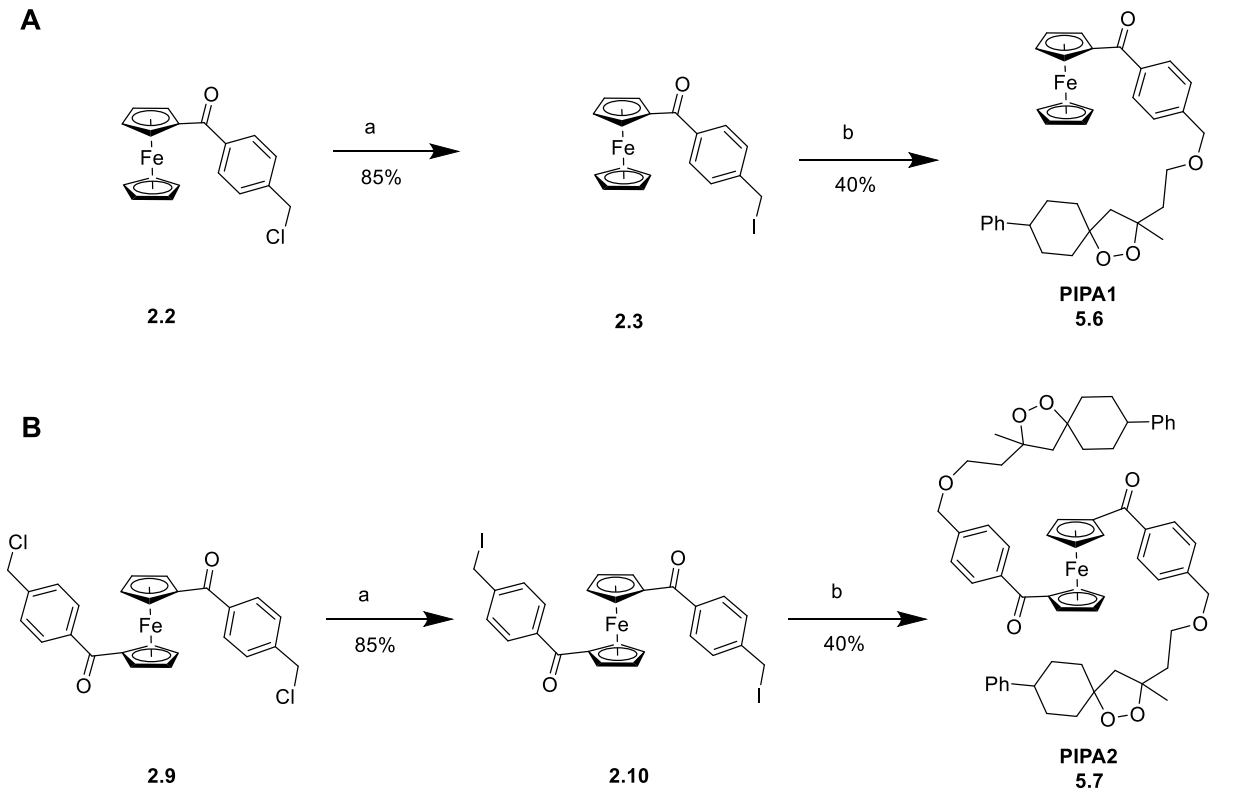

Figure 5.4: Synthesis of PIPA1 and PIP2 compounds completed by Alexander Braddock. A) a. NaI, acetone, 25 ºC, overnight; b. NaH, $FINO_2$, DMF, 25 ºC, overnight B) a. NaI, acetone, 25 ºC, overnight; b. NaH, , $FINO_2$, DMF, 25 ºC, overnight

5.2.1 Cytotoxicity of FINO2 and PIPA1

$FINO_2$ proved to be biologically active in both HeLa and CaOV3 cell lines and surprisingly have increased cytotoxicity upon photoactivation that was not previously reported (Figure 5.5).[128] $FINO_2$ displayed dark and light cytotoxicity in the HeLa cell line at 9.92 μM, and 7.15 μM. In CaOV3 cell line dark and light cytotoxicity was reported at 18.21 μM and 9.23 μM. CaOV3 had the highest PDT efficacy, difference of dark and light cytotoxicity to determine specificity and effectiveness of a PDT, of 1.97. This difference of light and dark cytotoxicity is hypothesized to be from light activation of biradical oxygen. Peroxide light activation has been previously reported and used in light-activated teeth whitening and thermally activated chemiluminescence. [127, 129-132] With incubation of **2.13** at 0.4 μM proved to have no significant potency of cytotoxicity, but additionally no harmful effects.

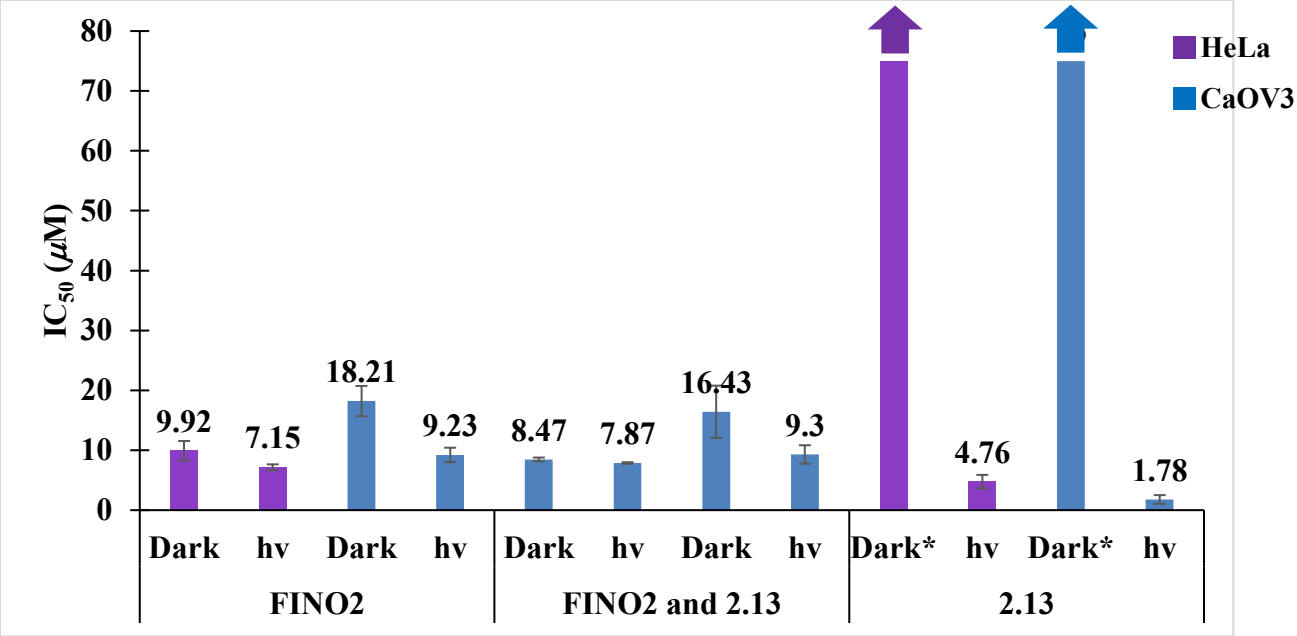

Figure 5.5: Cytotoxicity of FINO2 and FINO2 with 2.13

5.2.2 Cytotoxicity of PIPA1 and PIPA2

PIPA1 and PIPA2 proved to have relatively high potency in cancer cell lines. PIPA1 displayed no dark cytotoxicity up to solubility and 7.66 μM after 3 h photolysis in the HeLa cell line. The PDT efficacy was 9.79, which was similar to compound **2.6**. Although differing from compound **2.6**, in that CaOV3 had limited specificity as a PDT. It is dark, and light cytotoxicity was 5.92 μM and 3.07 μM, a difference of 1.92. This difference proved that this generation of compounds has a cell line dependent PDT efficacy. PIPA2 also proved to have limited PDT efficacy both in HeLa and CaOV3 cell line and the same cytotoxic effect as FINO2, which limits its utility as a ferrocene scaffold of $FINO_2$.

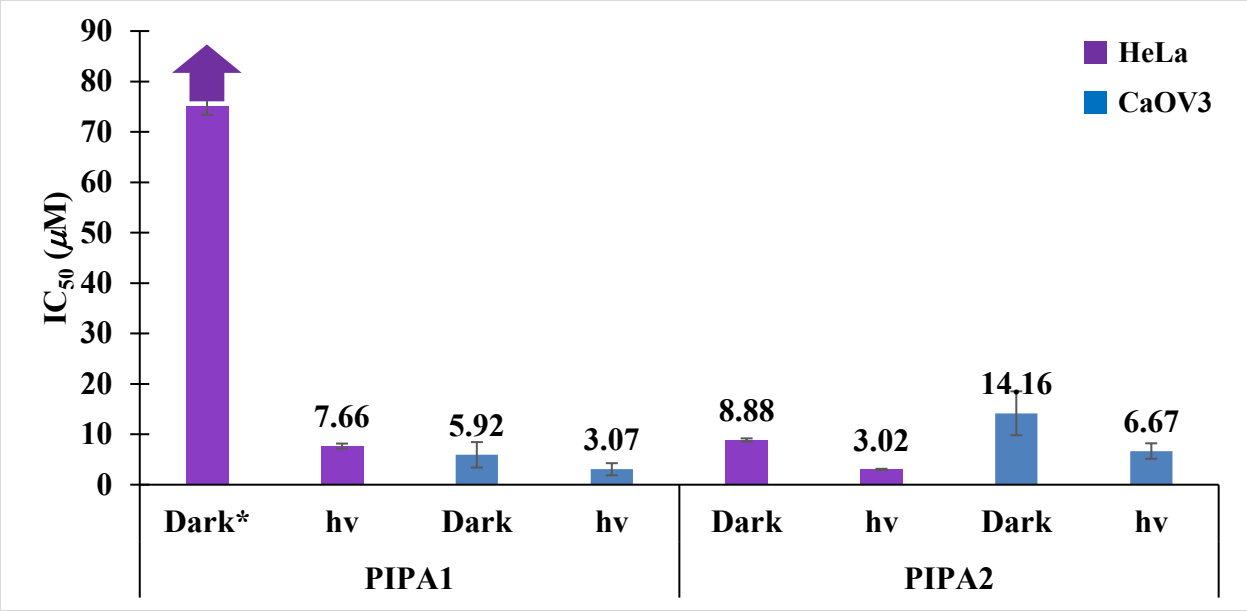

Figure 5.6: Cytotoxicity of PIPA1 and PIPA2 in HeLa and CaOV3

In agreement with previous studies, $FINO_2$ ferrocene derivatives were found to have potent cytotoxicity, but not reported to have PDT efficacy. PIPA1 was noted to be the best PDT of the endoperoxide generation with the best PDT specificity, as it had no dark toxicity in HeLa cell line. The cytotoxicity of PIPA1 was similar to compounds **2.6** and **2.13** in the HeLa cell line. Unfortunately, PIPA1 PDT efficacy was not seen in CaOV3 nor any cell line with PIPA2 derivative. As this work shows promise, future studies should be to optimize PIPAs by limiting dark cytotoxicity in all cell lines.

5.3 Acknowledgements

Olsen, Pauline; Braddock, Alexander; O'Connor, Joseph. Alexander Braddock synthesized the material for the studies completed. The dissertation author was the primary investigator and author of this material..

5.4 Chapter 5 References

117. Firestone, G. L.; Sundar, S. N., Anticancer activities of artemisinin and its bioactive derivatives. *Expert Rev Mol Med* **2009,** *11*, e32.

118. Ho, W. E.; Peh, H. Y.; Chan, T. K.; Wong, W. S., Artemisinins: pharmacological actions beyond anti-malarial. *Pharmacol Ther* **2014,** *142* (1), 126-39.

119. Zhang, J.-F., Zhou, K.D., Zhou, Y.Q., Fu, L.S., Wang, H.S., and Song, S.Y. , *A detailed chronological record of project 523 and the discovery and development of qinghaosu (artemisinin)*. Yangcheng Evening News Publishing Company: Guangzhou, China: , 2006.

120. Tran, T.; Qiao, Y.; You, H.; Cheong, D. H. J., Chapter 25 - Chronic Inflammation in Asthma: Antimalarial Drug Artesunate as a Therapeutic Agent. In *Immunity and Inflammation in Health and Disease*, Chatterjee, S.; Jungraithmayr, W.; Bagchi, D., Eds. Academic Press: 2018; pp 309-318.

121. Reddy, V. P., Chapter 5 - Organofluorine Pharmaceuticals. In *Organofluorine Compounds in Biology and Medicine*, Reddy, V. P., Ed. Elsevier: Amsterdam, 2015; pp 133-178.

122. NJ., W., Qinghaosu (artemisinin):the price of success. *Science* **2008,** *320* (5874), 330-4.

123. Huang, X. J.; Ma, Z. Q.; Zhang, W. P.; Lu, Y. B.; Wei, E. Q., Dihydroartemisinin exerts cytotoxic effects and inhibits hypoxia inducible factor-1alpha activation in C6 glioma cells. *J Pharm Pharmacol* **2007,** *59* (6), 849-56.

124. Li LN, Z. H., Yuan SJ, Tian ZY, Wang L, Sun ZX, Artesunate attenuates the growth of human colorectal carcinoma and inhibits hyperactive Wnt/beta-catenin pathway. *Int J Cancer* **2007,** *121* (6), 1360-5.

125. T., E., Molecular pharmacology and pharmacogenomics of artemisinin and its derivatives in cancer cells. *Curr Drug Targets* **2006,** *4*, 407-21.

126. Birmingham, B.; Buvanendran, A., 40 - Nonsteroidal Anti-inflammatory Drugs, Acetaminophen, and COX-2 Inhibitors. In *Practical Management of Pain (Fifth Edition)*, Benzon, H. T.; Rathmell, J. P.; Wu, C. L.; Turk, D. C.; Argoff, C. E.; Hurley, R. W., Eds. Mosby: Philadelphia, 2014; pp 553-568.e5.

127. Abrams, R. P.; Carroll, W. L.; Woerpel, K. A., Five-Membered Ring Peroxide Selectively Initiates Ferroptosis in Cancer Cells. *ACS Chem Biol* **2016,** *11* (5), 1305-12.

128. Gaschler, M. M.; Andia, A. A.; Liu, H.; Csuka, J. M.; Hurlocker, B.; Vaiana, C. A.; Heindel, D. W.; Zuckerman, D. S.; Bos, P. H.; Reznik, E.; Ye, L. F.; Tyurina, Y. Y.; Lin, A. J.; Shchepinov, M. S.; Chan, A. Y.; Peguero-Pereira, E.; Fomich, M. A.; Daniels, J. D.; Bekish, A. V.; Shmanai, V. V.; Kagan, V. E.; Mahal, L. K.; Woerpel, K. A.; Stockwell, B. R., FINO2 initiates ferroptosis through GPX4 inactivation and iron oxidation. *Nat Chem Biol* **2018,** *14* (5), 507-515.

129. Kearns, D. R., Selection rules for singlet-oxygen reactions. Concerted addition reactions. *Journal of the American Chemical Society* **1969,** *91* (24), 6554-6563.

130. Baroudi, K.; Hassan, N. A., The effect of light-activation sources on tooth bleaching. *Niger Med J* **2014,** *55* (5), 363-368.

131. Hayward, R.; Osman, Y.; Grobler, S. R., A clinical study of the effectiveness of a light emitting diode system on tooth bleaching. *Open Dent J* **2012,** *6*, 143-147.

132. Wang, W.; Zhu, Y.; Li, J.; Liao, S.; Ai, H., Efficacy of cold light bleaching using different bleaching times and their effects on human enamel. *Dental Materials Journal* **2013,** *32* (5), 761-766.

Chapter 6 First Monometal Cobaltocenium to Exhibit Anticancer Activity

6.1 Background of cobalt(III) and cobaltocenium biological discoveries

Cobalt(III) was not seen as a biologically active metal until discovery in metalloenzyme, vitamin B_{12}, back in 1948.[133] Since the discovery of vitamin B_{12}, cobalt (III) displayed cytotoxicity in a variety of inhibitors mechanisms, such as DNA replication, topoisomerase II, and Heme oxygenase-1.[134-139] Additionally, cobalt (III) has been utilized as a cationic scaffold for localization of compounds within cells, and it has been shown to accumulate within nucleus. As DNA is negatively charged and utilized as an indicator for DNA health.[140-142]

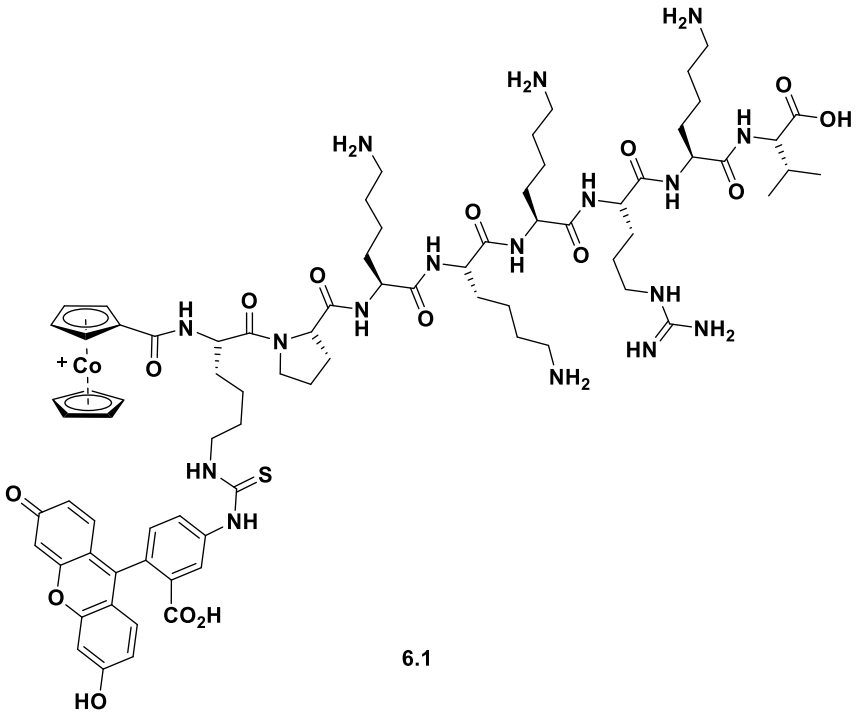

6.1

Figure 6.1: Previously reported cobaltocenium peptide compound

Lipophilic cobaltocenium similarly has been used for imaging in the cell with peptide linked to a fluorescent probe, unsurprisingly within the nucleus (Figure 6.1**)**.[143, 144] Cobaltocenium has also been utilized as a scaffold to induce membrane permeability similarly to ferrocene. Cytotoxicity was reported against cancer with cobaltocenium and well-known toxic metals such as mercury(I) and gold(I) (Figure

6.2).[145, 146] The cobaltocenium itself with a carboxylic acid substitution displayed no significant cytotoxicity.[145]

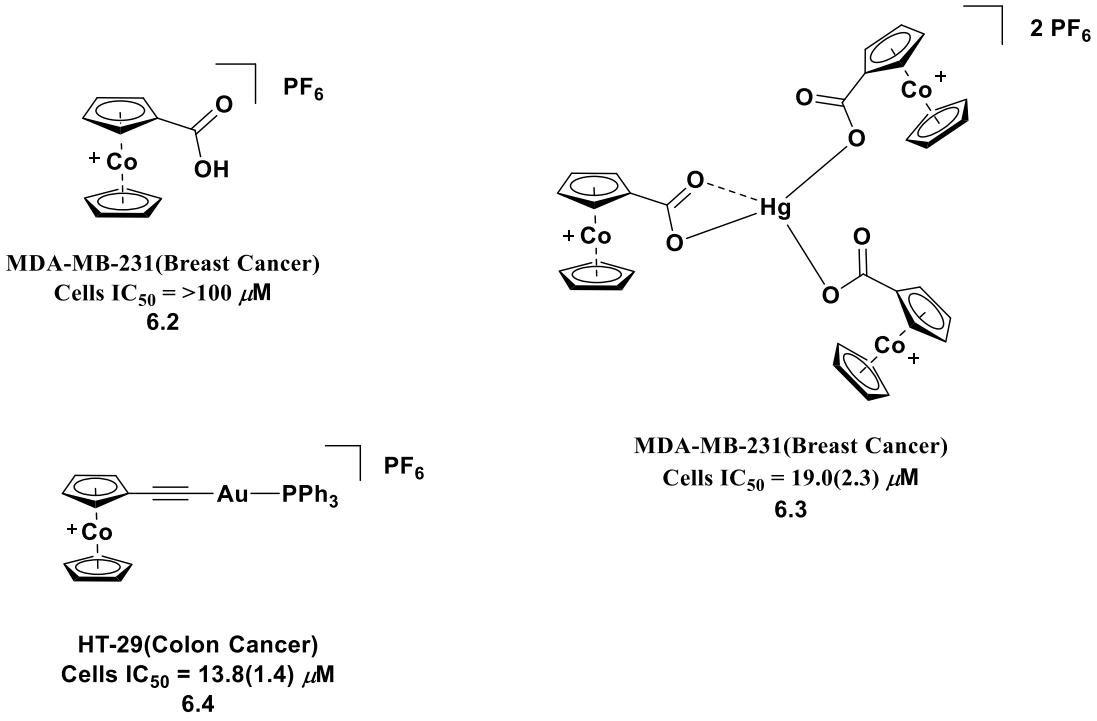

Figure 6.2: Previously reported cobaltocenium cytotoxicity[145, 146]

6.2 Cytotoxicity of Cobaltocenium

Lab member Pengjin Qin synthesized a trisubstituted cobaltocenium complex bearing a methyl, trimethylsilane (TMS), and a sulfone functional group, as shown in Figure 6.3. This compound is hypothesized to have biological activity due to its added substituents.

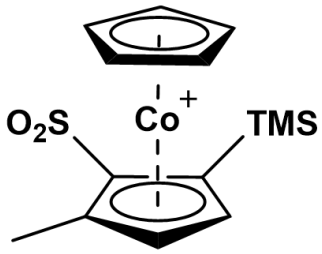

6.5

Figure 6.3: Chemical structure of cobaltocenium studied in HeLa cell line

This complex was tested in the HeLa cell line and proved to be the first monometal cobaltocenium complex to possess cytotoxicity with an IC_{50} value of 54.19 ± 3.10 μM with an R^2 value of 0.989 (Figure 6.4). It is hypothesized that the complex is toxic due to the sulfone and/or trimethyl silane addition. Sulfones have been proven to possess antimicrobial and anticancer activity[147, 148]. Silyation functional groups have proven to improve the lipophilicity and cytotoxicity of complexes .[149-152] Silabolin® a Russian drug with a silyation function group exhibits low toxicity, high anabolic potency, and long duration of action.[152]

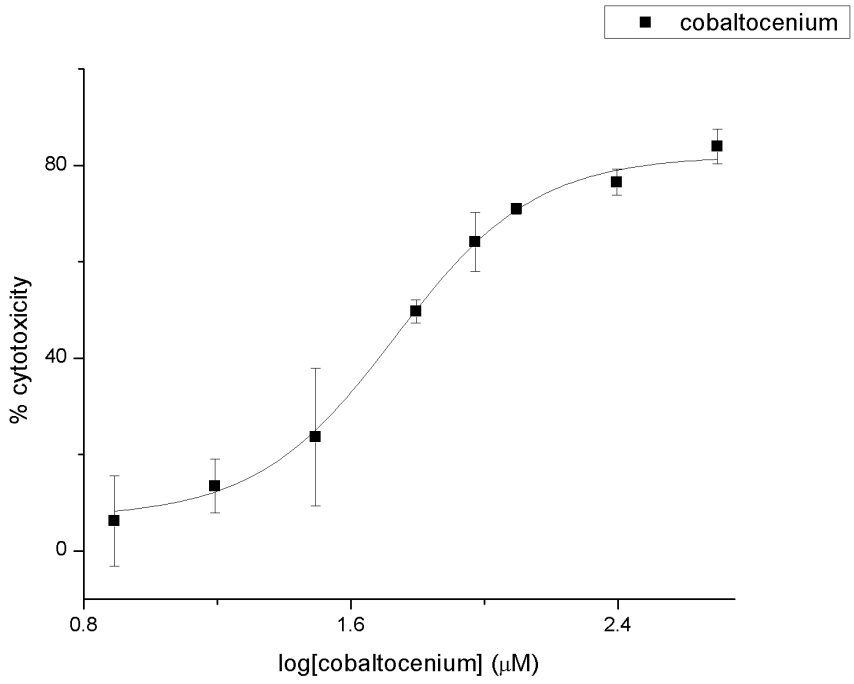

Figure 6.4: Cytotoxicity graph of the first cobaltocenium complex to contain anticancer activity

This study supports previous studies that cobaltocenium shows promise as a scaffold for biological activity. The cytotoxicity of cobaltocenium proved to be less potent than other iron containing metallocenes previously reported in previous chapters. Ultimately it was the first monometal cobaltocenium to report anticancer cytotoxicity and proves as a promising scaffold for future studies.

6.3 Acknowledgements

Olsen, Pauline; Qin, Pengjin; O'Connor, Joseph. Pengjin synthesized and characterized the material for the biological studies. The dissertation author was the primary investigator and author of this material.

6.4 Chapter 6 References

133. Dodson, G.; Glusker, J. P.; Sayre, D., *Structural Studies on Molecules of Biological Interest-A Volume in Honour of Dorthy Hodgkins*. Oxford University Press Clarendon, Oxford, 1981; p 610.

134. Jayaraju, D.; Gopal, Y. N. V.; Kondapi, A. K., Topoisomerase II Is a Cellular Target for Antiproliferative Cobalt Salicylaldoxime Complex. *Archives of Biochemistry and Biophysics* **1999,** *369* (1), 68-77.

135. Hall, I. H.; Bastow, K. F.; Warren, A. E.; Barnes, C. R.; Bouet, G. M., Cytotoxicity of cobalt complexes of furan oximes in murine and human tissue-cultured cell lines. *Applied Organometallic Chemistry* **1999,** *13* (11), 819-828.

136. Sastri, C. V.; Eswaramoorthy, D.; Giribabu, L.; Maiya, B. G., DNA interactions of new mixed-ligand complexes of cobalt(III) and nickel(II) that incorporate modified phenanthroline ligands. *Journal of Inorganic Biochemistry* **2003,** *94* (1-2), 138-145.

137. Jungwirth, U.; Kowol, C. R.; Keppler, B. K.; Hartinger, C. G.; Berger, W.; Heffeter, P., Anticancer Activity of Metal Complexes: Involvement of Redox Processes. *Antioxidants & Redox Signaling* **2011,** *15* (4), 1085-1127.

138. Zhang, Q.; Qian-Ling Zhang; Jin-Gang Liu; Hui Chao; Gen-Qiang Xue; Ji, L.-N., DNA-binding and photocleavage studies of cobalt(III) polypyridyl complexes: [Co(phen)2IP]3+ and [Co(phen)2PIP]3+. *Journal of Inorganic Biochemistry* **2001,** *83* (1), 49-55.

139. Zhang, Q.-L.; Liu, J.-G.; Liu, J.; Xue, G.-Q.; Li, H.; Liu, J.-Z.; Zhou, H.; Qu, L.-H.; Ji, L.-N., DNA-binding and photocleavage studies of cobalt(III) mixed-polypyridyl complexes containing 2-(2-chloro-5-nitrophenyl)imidazo [4,5-f][1,10]phenanthroline. *Journal of Inorganic Biochemistry* **2001,** *85* (4), 291-296.

140. Abeysinghe, R. D.; Ellis, B. L.; Porter, J. B., Platelet labelling with indium-hydroxypyridinone and indium-hydroxypyranone complexes. *Eur J Nucl Med* **1994,** *21* (10), 1141-7.

141. Mathias, C.; Welch, M., *J. Nucl Med* **1979,** *20*, 659.

142. Sinzinger, J. S. G. K. H., Synthesis of cobalt-55/57-complexes for radiolabelling of platelets as a potential PET imaging agent. *J. Labelled Cpd. Radiopharm* **2001,** *44*, 395-403.

143. Noor, F.; Wustholz, A.; Kinscherf, R.; Metzler-Nolte, N., A Cobaltocenium–Peptide Bioconjugate Shows Enhanced Cellular Uptake and Directed Nuclear Delivery. *angew Chem Int Ed* **2005,** *44*, 2429-2432.

144. Noor, F.; Kinscherf, R.; Bonaterra, G. A.; Walczak, S.; Wolfl, S.; Metzler-Nolte, N., Enhanced cellular uptake and cytotoxicity studies of organometallic bioconjugates of the NLS peptide in Hep G2 cells. *Chembiochem* **2009,** *10* (3), 493-502.

145. Vanicek, S.; Kopacka, H.; Wurst, K.; Vergeiner, S.; Oehninger, L.; Ott, I.; Bildstein, B., Cobaltocenium Carboxylate Transition Metal Complexes: Synthesis, Structure, Reactivity, and Cytotoxicity. *Z. Anorg Allg Chem* **2015,** *641* (7), 1282-1292.

146. S. Vanicek; H. Kopacka; K. Wurst; S. Vergeiner; S. Kankowski; J. Schur; Bildstein, B.; Ott, I., Cobaltoceniumethynyl gold(I) as an unusual heterodinuclear bioorganometallic fragment to study the biological properties of alkynyl gold complexes. *Dalton Trans* **2016,** *45*, 1345-1348.

147. Muralikrishna, A.; Venkatesh, B. C.; Padmavathi, V.; Padmaja, A.; Kondaiah, P.; Krishna, N. S., Synthesis, antimicrobial and cytotoxic activities of sulfone linked bis heterocycles. *European Journal of Medicinal Chemistry* **2012,** *54*, 605-614.

148. Romero, A.; Ramos, E.; Ares, I.; Castellano, V.; Martinez, M.; Martinez-Larranaga, M. R.; Anadon, A.; Martinez, M. A., Fipronil sulfone induced higher cytotoxicity than fipronil in SH-SY5Y cells: Protection by antioxidants. *Toxicol Lett* **2016,** *252*, 42-9.

149. Hausheer, F. H.; Kanter, P.; Cao, S.; Haridas, K.; Seetharamulu, P.; Reddy, D.; Petluru, P.; Zhao, M.; Murali, D.; Saxe, J. D.; Yao, S.; Martinez, N.; Zukowski, A.; Rustum, Y. M., Modulation of platinum-induced toxicities and therapeutic index: mechanistic insights and first- and second-generation protecting agents. *Semin Oncol* **1998,** *25* (5), 584-99.

150. Van Hattum, A. H.; Pinedo, H. M.; Schluper, H. M.; Hausheer, F. H.; Boven, E., New highly lipophilic camptothecin BNP1350 is an effective drug in experimental human cancer. *Int J Cancer* **2000,** *88* (2), 260-6.

151. Keir, S. T.; Hausheer, F.; Lawless, A. A.; Bigner, D. D.; Friedman, H. S., Therapeutic activity of 7-[(2-trimethylsilyl)ethyl)]-20 (S)-camptothecin against central nervous system tumor-derived xenografts in athymic mice. *Cancer Chemother Pharmacol* **2001,** *48* (1), 83-7.

152. Shishkina, A. A.; Ivanenko, T. I.; Zarubina, N. A.; Volzhina, O. N.; Angarskaya, V. G.; Pivnitskii, K. K., Experimental and clinical study of the anabolic preparation silabolin. *Pharmaceutical Chemistry Journal* **1986,** *20* (2), 143-148

Chapter 7 First NMR Evidence of a Monomeric Carbene Cu(I)-Hydride Species and Postulated Rearrangement of Pinacolborane

7.1 Background on Copper Hydride

Wurtz discovered the first copper(I)-hydride species in 1844, but it did not gain interest as a catalyst until Stryker's reagent $[(Ph_3P)CuH]_6$, was reported in 1971.[153, 154] Copper(I) hydride has been studied in a wide range of organic reactions; such as hydrosilylation of ketones and aldehydes along with the regioselective conjugated reduction of carbonyl derivatives, including unsaturated ketones, aldehydes, and esters. [154-156] Although heavily studied mechanistically, isolation of the copper hydride monomers is still sought after.[157, 158]

Phosphine and carbene-ligated copper hydride complexes have been postulated as key intermediates in a wide range of synthetic organic transformations.[159] In 2004, *N*-heterocyclic carbene (NHC) ligands were used to stabilize dimeric copper-hydride complexes for the isolation and structural characterization of compound **7.1** (Figure 7.1).[160] Unfortunately, it was noted that 7.1 underwent slow decomposition, even at 40 °C. In 2011, utilizing the more σ-donating and bulkier menthyl-cyclic alkyl amino carbene (CAAC) ligand, the first room temperature stable copper-hydride dimer, **7.2**, was isolated.[161] By enlarging the NHC ring from a 5-membered ring to a 6- or 7-membered ring, dimeric copper-hydrides $[(6\text{- and } 7\text{-NHC})CuH]_2$, **7.3** and **7.4**, were also reported to be stable at room temperature.[162] These dimers feature reactivity reminiscent of what is expected for their corresponding monomers.

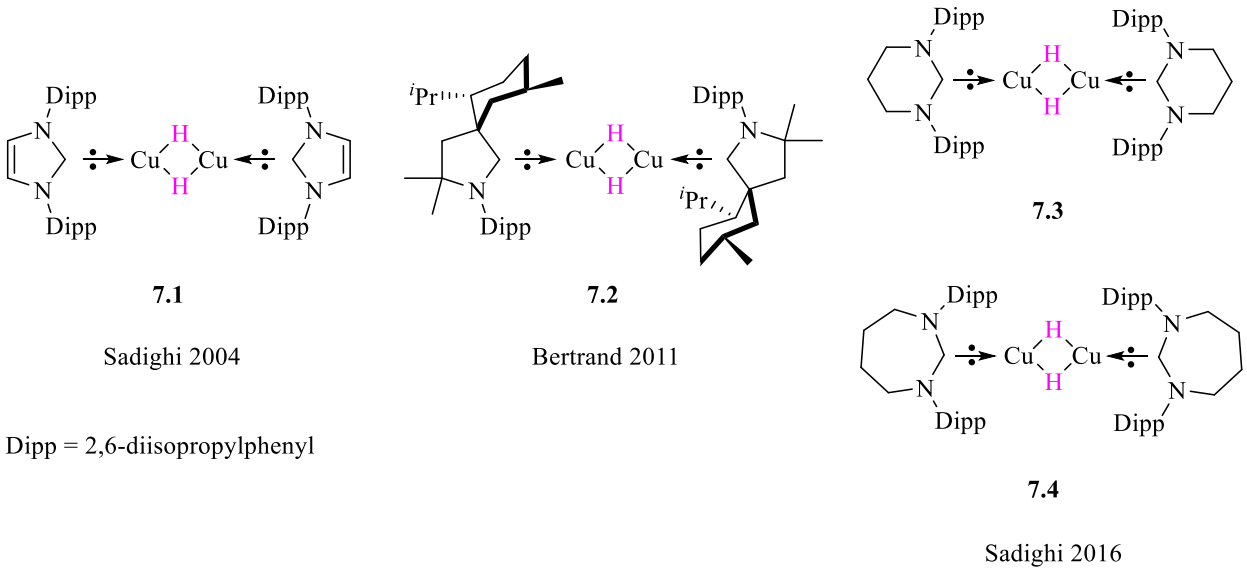

Figure 7.1: Previous reported and structurally characterized carbene copper(I)-hydride dimers.

7.2 Rearrangement and NMR Spectroscopy of the Copper Hydride

In an approach to stabilize a monoligated copper-hydride monomer, it was hypothesized that much more sterically encumbering NHC ligands, such as 1,3-bis(2,6-bis(diphenylmethyl)-4-methylphenyl)-imidazole-2-ylidene (IPr*) or 1,3-bis[2,6-bis[di(4-tert-butylphenyl)methyl]-4-methylphenyl]imidazol-2-ylidene (IPr**), could provide kinetic and steric protection thereby allowing for spectroscopic and solid-state crystallographic characterization.[163, 164]

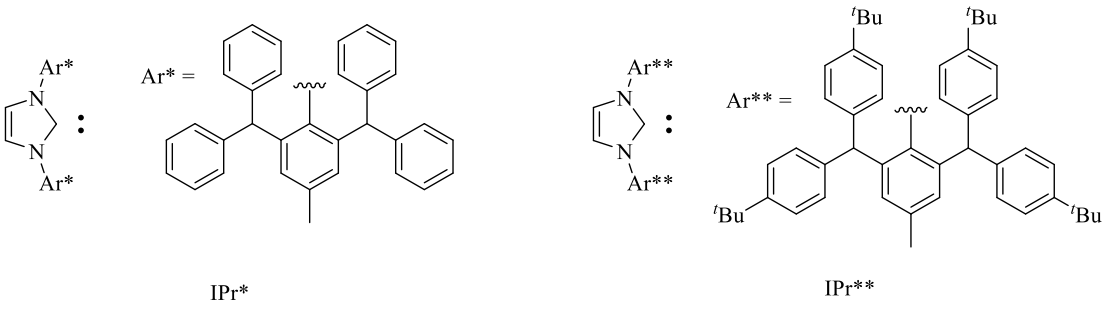

Figure 7.2: Previously reported sterically demanding NHC ligands, IPr* (left) and IPr (right).**

A salt metathesis reaction between (IPr*)CuCl with potassium phenolate produced (IPr*)CuOPh (**7.6**). Addition of 1 equivalent of pinacolborane to a THF solution of **7.6** resulted in the formation of a deep orange solution along with copious amounts of a bright yellow solid precipitate (Scheme 7.1).

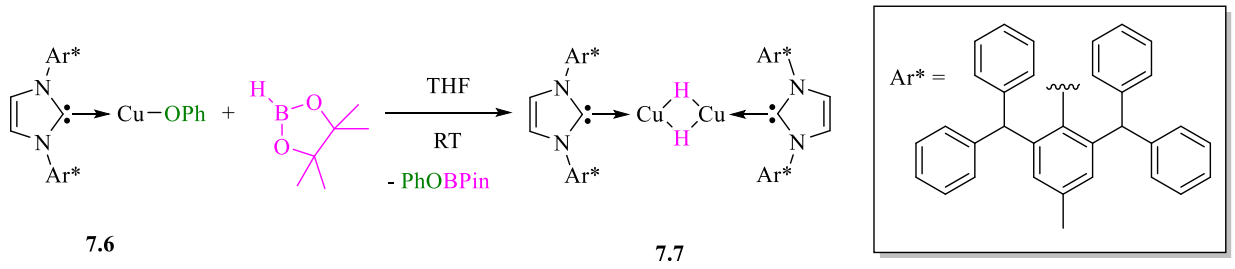

7.6 **7.7**

Scheme 7.1: Synthesis of dimeric [(IPr*)CuH]$_2$.

This yellow solid, **7.7** was extremely moisture sensitive, and the ^{11}B {^1H} NMR spectrum of the supernatant revealed the presence of PhOBPin.[165] The $^{13}C\{^1H\}$ NMR in C_6D_6 spectrum showed a notable shift of the carbene signal from 181.2 ppm (**7.6**) to 194.3 ppm (**7.7**) which resolves as a triplet ($^2J_{CH}$ = 6.4 Hz). The intense yellow color of the precipitate suggested the dimeric species [(IPr*)CuH]$_2$ was isolated. A single crystal X-ray diffraction study confirmed the connectivity (IPr*)CuH dimer **7.7**, which was crystallized from diffusion of pentane into a saturated benzene solution at 5 ^oC. The Ar* complex **7.7** shows a nearly linear arrangement of the C1-Cu1-Cu2-C2 framework with non-coplanar NHC rings. The Cu1-Cu2 (2.3144(10) Å) and C-Cu (1.900(3) Å) distances are comparable to those reported previously in the literature.[158, 160-162] Interestingly this resonance the hydride was significantly downfield shifted at 3.91 ppm in the ^1H NMR spectrum compared to previously reported Cu(I)-H dimers **7.1-3**.[160-162]

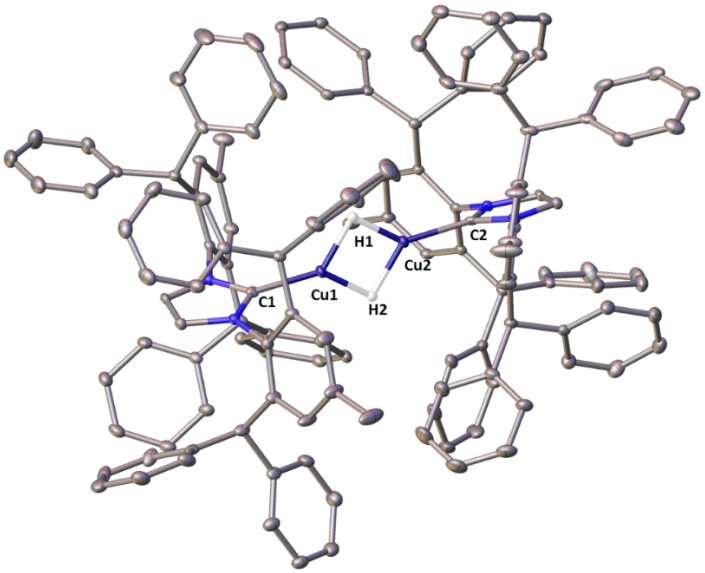

Figure 7.3. Molecular structure of 7.7 in the solid state. Ellipsoids are set at 25 % probability. Ligand hydrogen atoms and solvent molecules have been omitted for clarity. Selected distances [Å]: C1-Cu1 1.900(3); Cu1-H1 1.71(5); Cu1-H2 1.59(5); Cu1-Cu2 2.3144(10). Atoms Cu2, C2, and H2 are symmetry generated.

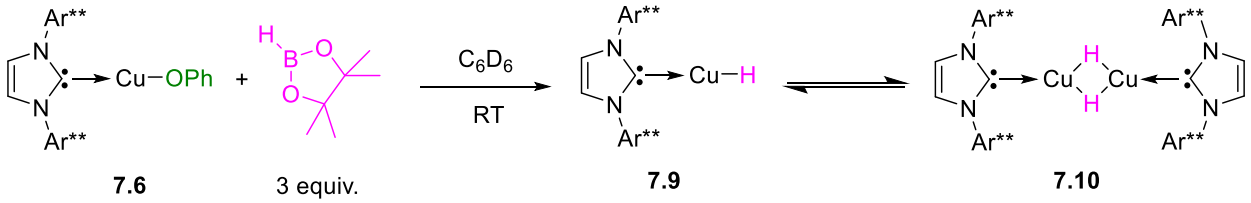

Scheme 7.2: Immediate reactions of 7.6 with pinacolborane.

At another attempt to isolate the monomeric copper(I) hydride IPr** was used as it provided additional extensive steric and kinetic protection of other highly reactive species.[166] The initial reaction of (IPr**)Cu-OPh complex **7.6** (Scheme 2) with three equivalents of HBPin led to a colorless solution (Scheme 7.2). Monitoring through ^{13}C NMR spectroscopy, two carbene signals were noticed immediately, a singlet at δ 192 ppm and a doublet at 185 ppm (Figure 7.4). Erik Romero studied the system by the ^{1}H-^{13}C -HMBC NMR and correlated the carbene resonance in ^{13}C NMR to distinctive proton signals at δ 4.26 (**7.10**), and 2.14 ppm (**7.9**) (Figure 7.6). This was the first spectroscopic evidence reported for monomeric and dimeric copper(I) hydrides. No previous phosphine or carbene polynuclear copper-hydride clusters $(LCuH)_n$ have reported a solution-phase equilibrium with the corresponding copper(I) hydride monomers (LCuH).

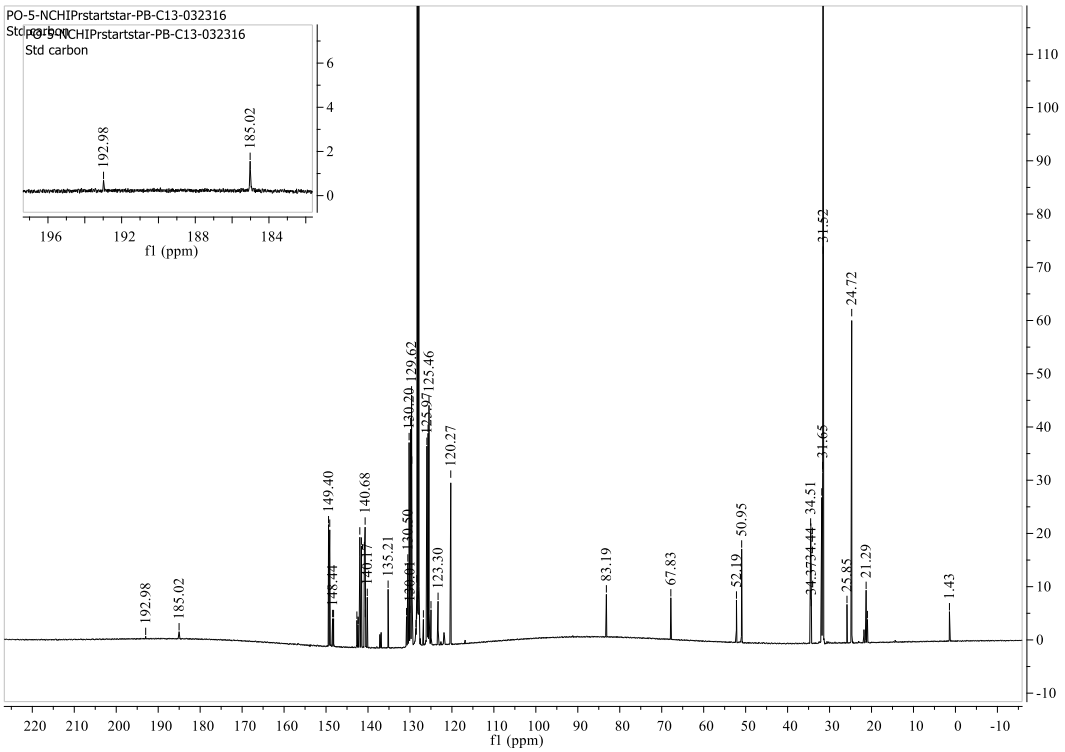

Figure 7.4: Crude ^{13}C NMR spectrum (C_6D_6) showing two species and carbene resonances of species 7.9 and 7.10.

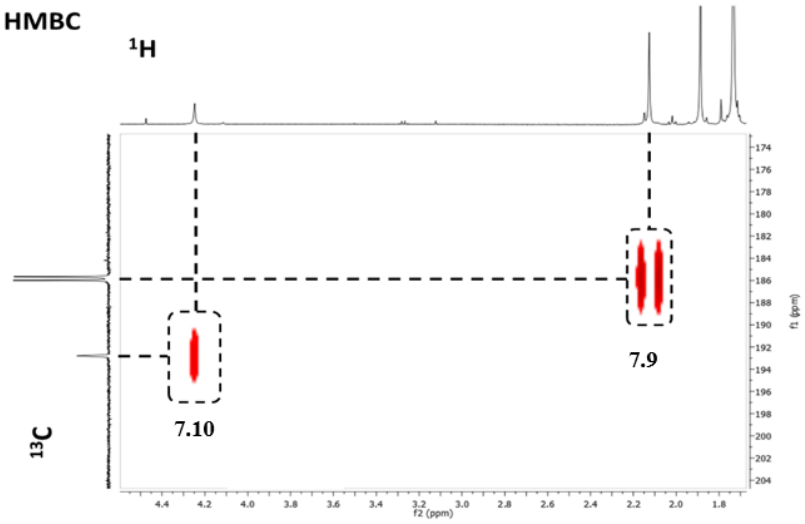

Figure 7.5: The selected region of the ^{1}H-^{13}C HMBC spectrum of 7.9 and 7.10 in C_6D_6, completed by Erik Romero.

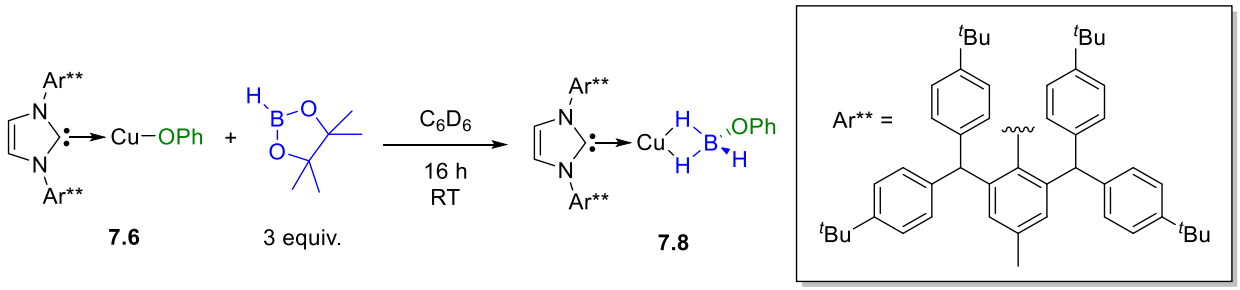

Scheme 7.3: Reactions of 7.6 with pinacolborane overnight.

From the same reaction overnight, colorless needles in nearly quantitative yield crystallized. These were studied by X-ray crystallographic analysis. This revealed the formation of complex **7.8** featuring the phenoxide group at boron without pinacol (Figure 7.6) Further study of compound **7.8** displayed a resonance at -12.5 ppm in ^{11}B NMR spectroscopy that resolved as a broad quartet ($J_{B\text{-}H}$ = 81.5 Hz) which confirmed the rearrangement of pinacolborane to the new $LCuH_2BHOPh$ species. The mechanism leading to **7.8** is not readily apparent but has never been reported from previously isolated phosphine or carbene copper(I) hydride species. Interestingly, the IPr* ligand did not display this type of reactivity with pinacolborane but was in its dimeric form. Notably, the IPr** ligand was the first monomeric copper(I) hydride species observed by NMR spectroscopy which suggest that rearrangement to compound **7.8** may be accessed from a monomeric Cu-H species. This reaction presents an avenue for studying the mechanism of this unprecedented reaction.

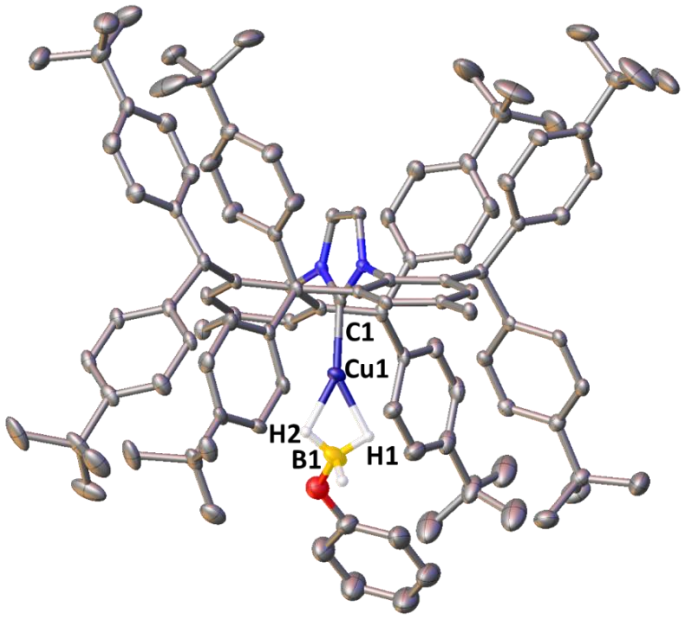

Figure 7.6: Molecular structure of 7.8 in the solid state. Hydrogen atoms other than those on boron have been omitted for clarity. Thermal ellipsoids are set at 25% probability. Selected distances [Å]: C1-Cu1 1.884(5); Cu1-B1 2.058(7); C1-Cu1-B1 178.6(3).

In conclusion, bulky IPr* NHC ligand cannot support the monomeric copper(I)-hydride and therefore dimerizes immediately to form complex **7.10**. While IPr** proved to have an equilibrium of monomer and dimer species in solution which led to LCuH borane stabilized species, **7.8**. This work strongly supports the hypothesis that copper hydride aggregates dissociate in solution and react as their corresponding monomers. [157, 158]

7.3 Acknowledgements

As it appears in Angewandte Chemie International Edition 2017. Romero, Erik A.; Jazzar, Rodolphe; Solieilhavoup, Michele; Gembicky, Milan; Bertrand, Guy. Volume 56, page 4024-4027. The dissertation author was the secondary investigator and author of this paper.

7.4 Chapter 7 References

153. Wurtz, A., Sur l'Hydrure de Cuivre. *Ann. Chim. Phys.* **1844,** *11*, 250.

154. Mahoney, W. S. B., D. M.; Stryker, J. M., Selective hydride-mediated conjugate reduction of α,β-unsaturated carbonyl compounds using [(Ph3P)CuH]6. *J. Am. Chem. Soc.* **1988,** *110*, 291.

155. Albert, C. F.; Healy, P. C.; Kildea, J. D.; Raston, C. L.; Skelton, B. W.; White, A. H., Lewis-base adducts of Group 11 metal(I) compounds. 49. Structural characterization of hexameric and pentameric (triphenylphosphine)copper(I) hydrides. *inorg chem* **1989,** *28*, 1300.

156. Bezman, S. A.; Churchill, M. R.; Osborn, J. A.; Wormald, J., Preparation and crystallographic characterization of a hexameric triphenylphosphinecopper hydride cluster. *J. Am. Chem. Soc.* **1971,** *93*, 2063.

157. Deutsch, C.; Krause, N.; Lipshutz, B. H., CuH-Catalyzed Reactions. *Chem. Rev.* **2008,** *108*, 2916.

158. Jordan, A. J.; Lalic, G.; Sadighi, J. P., Coinage Metal Hydrides: Synthesis, Characterization, and Reactivity. *Chem Rev* **2016,** *116* (15), 8318-72.

159. F. Lazreg; F. Nahra; Cazin, C. S. J., *Coord. Chem. Rev.* **2015,** *293-4*, 48-79.

160. Mankad, N. P.; Laitar, D. S.; Sadighi, J. P., Synthesis, Structure, and Alkyne Reactivity of a Dimeric (Carbene)copper(I) Hydride. *Organometallics* **2004,** *23*, 3369.

161. Frey, G. D.; Donnadieu, B.; Soleilhavoup, M.; Bertrand, G., Synthesis of a room-temperature-stable dimeric copper(I) hydride. *Chem Asian J* **2011,** *6* (2), 402-5.

162. Jordan, A. J. W., C. M.; Bacsa, J.; Sadighi, J. P. , Synthesis and Reactivity of New Copper(I) Hydride Dimers. *Organometallics* **2016,** *35*, 613.

163. Berthon-Gelloz, G.; Siegler, M. A.; Spek, A. L.; Tinant, B.; Reek, J. N.; Marko, I. E., IPr* an easily accessible highly hindered N-heterocyclic carbene. *Dalton Trans* **2010,** *39* (6), 1444-6.

164. Weber, S. G. L., C.; Rominger, F.; Straub, B. F. , Synthesis of an extremely stericall shielding N-heterocyclic carbene ligand. *Arkivok* **2012,** *iii*, 226.

165. Romero, E. A.; Peltier, J. L.; Jazzar, R.; Bertrand, G., Catalyst-free dehydrocoupling of amines, alcohols, and thiols with pinacol borane and 9-borabicyclononane (9-BBN). *Chem Commun (Camb)* **2016,** *52* (69), 10563-5.

166. Liu, L. R., D. A.; Munz, D.; Bertrand, G. , *Chem Asian J* **2016,** *1*, 147.